2010-09

Development and Testing of a Field Ionized Ion Thruster for Microsatellite Applications

Shrank, Bryan P.

Monterey, California. Naval Postgraduate School

NAVAL POSTGRADUATE SCHOOL

MONTEREY, CALIFORNIA

THESIS

DEVELOPMENT AND TESTING OF A FIELD IONIZED ION THRUSTER FOR MICROSATELLITE APPLICATIONS

by

Bryan P. Shrank

September 2010

Thesis Co-Advisors: Marcello Romano
Oscar Biblarz

THIS PAGE INTENTIONALLY LEFT BLANK

26 Sep 2014

SUBJECT: Change in distribution statement for *Development and Testing of a Field Ionized Ion Thruster for Microsatellite Applications* – September 2010.

1. Reference: Shrank, Bryan P. *Development and Testing of a Field Ionized Ion Thruster for Microsatellite Applications*. Monterey, CA: Naval Postgraduate School, September 2010. UNCLASSIFIED [Distribution authorized to U.S. Government Agencies only; Premature Dissemination; 13 September 2010.].

2. Upon consultation with NPS faculty, the School has determined that this thesis may now be released to the public and that its distribution is unlimited, effective September 26, 2014.

University Librarian
Naval Postgraduate School

THIS PAGE INTENTIONALLY LEFT BLANK

REPORT DOCUMENTATION PAGE		Form Approved OMB No. 0704-0188

Public reporting burden for this collection of information is estimated to average 1 hour per response, including the time for reviewing instruction, searching existing data sources, gathering and maintaining the data needed, and completing and reviewing the collection of information. Send comments regarding this burden estimate or any other aspect of this collection of information, including suggestions for reducing this burden, to Washington headquarters Services, Directorate for Information Operations and Reports, 1215 Jefferson Davis Highway, Suite 1204, Arlington, VA 22202-4302, and to the Office of Management and Budget, Paperwork Reduction Project (0704-0188) Washington DC 20503.

1. AGENCY USE ONLY *(Leave blank)*	2. REPORT DATE	3. REPORT TYPE AND DATES COVERED
	September 2010	Master's Thesis

4. TITLE AND SUBTITLE
Development and Testing of a Field Ionized Ion Thruster for Microsatellite Applications

5. FUNDING NUMBERS

6. AUTHOR(S) MAJ Bryan P. Shrank

7. PERFORMING ORGANIZATION NAME(S) AND ADDRESS(ES)
Naval Postgraduate School
Monterey, CA 93943-5000

8. PERFORMING ORGANIZATION REPORT NUMBER

9. SPONSORING /MONITORING AGENCY NAME(S) AND ADDRESS(ES)
N/A

10. SPONSORING/MONITORING AGENCY REPORT NUMBER

11. SUPPLEMENTARY NOTES The views expressed in this thesis are those of the author and do not reflect the official policy or position of the Department of Defense or the U.S. Government. IRB Protocol number _____.

12a. DISTRIBUTION / AVAILABILITY STATEMENT
~~Distribution authorized to U.S. Government Agencies only; (Premature Dissemination); (13 September 2010); Other requests for this document must be referred to President, Code 261, Naval Postgraduate School, Monterey, CA 93943-5000 via the Defense Technical Information Center, 8725 John J. Kingman Rd., STE 0944, Ft. Belvoir, VA 22060-6218.~~
Approved for public release; distribution is unlimited

12b. DISTRIBUTION CODE
A

13. ABSTRACT (maximum 200 words)

Development of a miniaturized ion thruster would enable microsatellites to sustain orbits over a long period of time with a high efficiency while minimizing mass and volume. The advent of carbon nanotube technology has made the development of a field ionized ion thruster possible.

An interagency effort between the Naval Postgraduate School and the Nanotechnology Lab at NASA Ames Research Center into the development of a field ionized ion thruster is undertaken. A test apparatus is designed and constructed in order to allow testing of carbon nanotube samples grown on a silicon substrate with a 200 μm by 200 μm hole as the ionizing element of a new design for an ion thruster.

Field emission tests show measured geometric electric field enhancement factors for our samples ranging from 1428 to 5229. Two of seven experiments show successful ionization of argon gas in a flow. A measured current of 2.1×10^{-5} Amps is achieved from a 14 μm sample with a 113 μm gap distance and an applied voltage of 1000 Volts.

Characterization of the Drag Coefficient of the sample orifice is also conducted to allow for determination of the mass flow rate and maximum expected current in future tests.

14. SUBJECT TERMS	15. NUMBER OF PAGES
Space Propulsion; Microsatellite; Nanosatellite; Cubesat; Ion Thruster; Carbon Nanotube; Carbon Nanotube Pillar Array.	165
	16. PRICE CODE

17. SECURITY CLASSIFICATION OF REPORT	18. SECURITY CLASSIFICATION OF THIS PAGE	19. SECURITY CLASSIFICATION OF ABSTRACT	20. LIMITATION OF ABSTRACT
Unclassified	Unclassified	Unclassified	UU

NSN 7540-01-280-5500 Standard Form 298 (Rev. 8-98)
Prescribed by ANSI Std. Z39.18

THIS PAGE INTENTIONALLY LEFT BLANK

DEVELOPMENT AND TESTING OF A FIELD IONIZED ION THRUSTER FOR MICROSATELLITE APPLICATIONS

Bryan P. Shrank
Major, United States Army
B.S. Mechanical Engineering, United States Military Academy, 1998

Submitted in partial fulfillment of the
requirements for the degree of

MASTER OF SCIENCE IN ASTRONAUTICAL ENGINEERING

from the

NAVAL POSTGRADUATE SCHOOL
September 2010

Author: Bryan P. Shrank

Approved by: Marcello Romano
Thesis Co-Advisor

Oscar Biblarz
Thesis Co-Advisor

Knox T. Millsaps
Chairman, Department of Mechanical and Aerospace Engineering

THIS PAGE INTENTIONALLY LEFT BLANK

ABSTRACT

Development of a miniaturized ion thruster would enable microsatellites to sustain orbits over a long period of time with a high efficiency while minimizing mass and volume. The advent of carbon nanotube technology has made the development of a field ionized ion thruster possible.

An interagency effort between the Naval Postgraduate School and the Nanotechnology Lab at NASA Ames Research Center into the development of a field ionized ion thruster is undertaken. A test apparatus is designed and constructed in order to allow testing of carbon nanotube samples grown on a silicon substrate with a 200 μm by 200 μm hole as the ionizing element of a new design for an ion thruster.

Field emission tests show measured geometric electric field enhancement factors for our samples ranging from 1428 to 5229. Two of seven experiments show successful ionization of argon gas in a flow. A measured current of 2.1 x 10^{-5} Amps is achieved from a 14 μm sample with a 113 μm gap distance and an applied voltage of 1000 Volts.

Characterization of the Drag Coefficient of the sample orifice is also conducted to allow for determination of the mass flow rate and maximum expected current in future tests.

THIS PAGE INTENTIONALLY LEFT BLANK

TABLE OF CONTENTS

THIS PAGE INTENTIONALLY LEFT BLANK

LIST OF FIGURES

LIST OF TABLES

LIST OF ACRONYMS AND ABBREVIATIONS

C_d	Coefficient of Drag
CNT	Carbon Nanotube
CPA	Carbon Nanotube Piller Array
CVD	Chemical Vapor Deposition
DS1	Deep Space 1
e_i	Ionization Energy
e_l	Energy loss per ion
g_e	Acceleration due to Earth's gravity
$I_{\max}$	Maximum Current
$I_{measured}$	Measured Current
I_{SP}	Specific Impulse
k_{Ar}	Specific heat ratio of argon
LabVIEW	Laboratory Virtual Instrument Engineering Workbench
m	Ion Mass
MATLAB	Matrix Laboratory
NASA	National Aeronautics and Space Administration
R	Gas constant
SEM	Scanning Electron Microscope
SERT	Space Electric Rocket Test
T	Temperature
u_e	Exhaust velocity of ions
η	Efficiency
α	Constant, function of specific heat ratio
μ_{Ar}	Mass of argon ion

THIS PAGE INTENTIONALLY LEFT BLANK

ACKNOWLEDGMENTS

The list of people I wish to acknowledge is endless. Countless people have assisted me throughout the course of my thesis. Those included in this section were invaluable, and critical to our success.

I would like to first thank my thesis advisors, Professor Marcello Romano and Professor Oscar Biblarz, for their guidance and unceasing faith in my ability.

I would like to thank my NASA family for their support and help. A special thanks to Dr. Darrell Niemann without whom I would never have been able to begin my work. To the rest of the crew: Jovi Gacusan, Bryan Ribaya, Setha Yim, Jay Longson, Sunny Nguyen, and Dr. Cattien Nguyen, your help was invaluable and you have my undying gratitude for the hours spent in the lab helping the soldier out. You have impressed me with your intelligence and kindness.

Thank you to the staff and faculty at NPS who helped in whatever capacity I needed: Dr. Jim Newman for pointing me towards this thesis, Dan Sakoda for providing help with producing prototype parts and for being a sounding board, Dr. Chris Brophy for assisting me with the methods to experimentally determine mass flow rates, and John Mobley for not only machining my parts but helping me to be a better designer as well.

To my peers and fellow warfighters, thank you for the time spent balancing the rest of my life between thesis and everything else. I have enjoyed my time at the Naval Postgraduate School because of the time we have spent together.

Finally, and most importantly, I want to say thank you to my loving wife Randi and my three beautiful girls: Kylie, Lauren, and Juliana. I am in awe of your strength and am blessed to have you as my family. Thank you for your support through all of the trips and time spent working on my thesis, and for pretending to care when I came home every day talking about ion propulsion. You are my rock.

THIS PAGE INTENTIONALLY LEFT BLANK

I. INTRODUCTION

A. BACKGROUND

Ion thrusters have the capability to provide constant thrust with a high specific impulse (I_{SP}) for years. This application makes the ion thruster the perfect choice for long duration and inter-planetary missions. The National Aeronautics and Space Administration (NASA) has experimented with ion thrusters since the 1950s. NASA successfully employed an electron collision ion thruster on the Deep Space 1 (DS1) mission that continued to operate for 678 days [1]. NASA currently has three ion thrusters on the 8 year Dawn mission to conduct a flyby of Mars and a stop on the asteroids Vesta and Ceres. Dawn launched on 27 September 2007 and is still currently enroute to Mars [2].

Cubesats were initially developed with academia in mind. The standard cubesat is a ten centimeter cube, known as a 1U (or one unit) form factor. It is very common to stack two (2U) or three (3U) of these cubes together to make a satellite with greater capability. These small satellites give universities a medium with which they can teach the design process for a real satellite in enough time that they may actually see their creation launched into space. However, industry and the government have both realized the great potential these small satellites possess and have quickly surged onto the cubesat scene. With this increased interest comes a desire to maximize the capability of these satellites across a breadth of various applications. The need for propulsion now takes on a higher priority, and many forms of propulsion are currently being developed such as pulse plasma thrusters and cold gas thrusters.

The small amount of propellant mass required to operate ion engines for such a long time also makes the ion engine an attractive option for use in cubesats. A small continually applied thrust could counteract the effects of atmospheric drag, enabling a cubesat to stay in a prescribed orbit.

Unfortunately, the main problem with using current ion engine technology in a cubesat is that the engine can not be reasonably scaled down enough to fit into an appropriately sized form factor. The electron collision chamber is too large and the power requirement is too massive to employ in a cubesat.

One possible way to miniaturize an ion engine is to change its method of ionization. An ion engine that uses field ionization would be vastly smaller than its electron collision counterpart. Field ionization does not require a large ionization chamber because it ionizes atoms by passing it through a very high electric field as opposed to subjecting it to electron bombardment. Advancements in carbon nanotube technology have made the miniaturization of ion thrusters feasible in both size and power.

B. THE SCIENCE BEHIND ION THRUSTERS

There are several ways to ionize a gas. The methods vary, but the basic principle and end result are the same. A gas atom loses an electron through some action, making it a positively charged ion. This newly formed ion will be attracted to a negatively charged accelerator surface. Harnessing this attraction gives us a force that can be used to propel an object through space.

1. Selecting the Appropriate Fuel

Originally, metals like mercury and cesium were used for ion engines because they have very low ionization energies and a high molar mass. Both of these traits are highly desired in ion thrusters. Lower ionization energies require less external work be applied in order to ionize the atoms, and high molar mass correlates to a higher power efficiency. However, the alkali metals are very difficult to gasify. Additionally, cesium and mercury are not only toxic, but have proven to be very messy because their natural state is in metallic form which can coat and clog the inside of the ionization chamber.

The next place to turn to was the noble gases, which naturally exist in a stable state. Ionized noble gases can be accelerated as they search for an

electron to return them to their natural state. While they require higher ionization energies than the metals, they can still be ionized relatively affordably. The most common gas used in ion thrusters is xenon. Xenon is one of the easiest monatomic gases to ionize, making it a prime candidate for ion thrusters. Other gases that ionize relatively easily are krypton and argon. While the ionization energy of radon is lower than xenon's, radon is not preferred because it is radioactive and very expensive to produce.

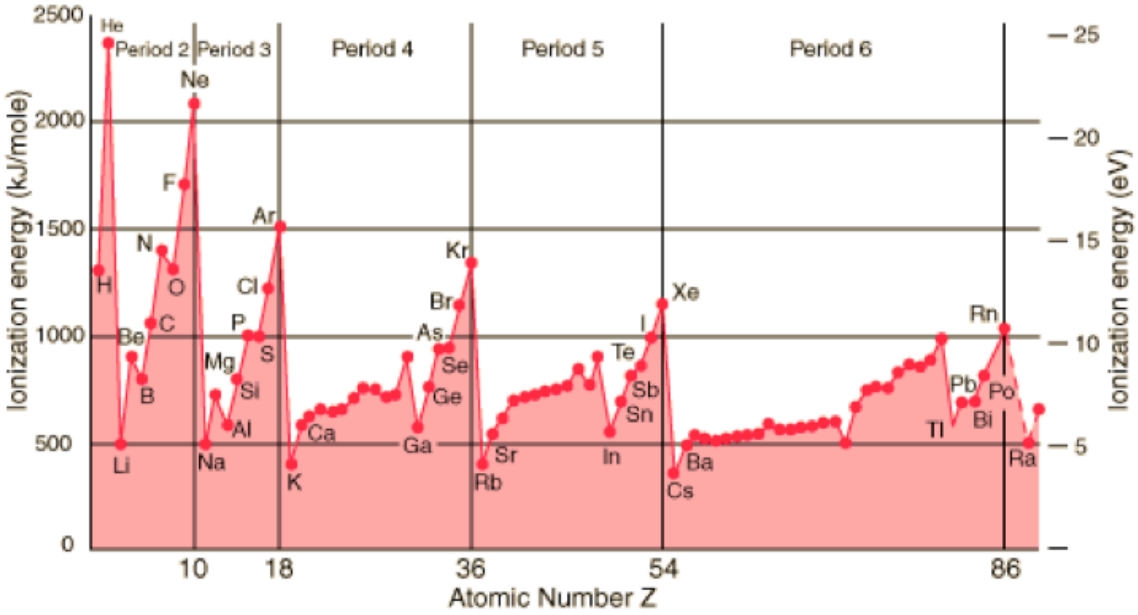

Figure 1. Ionization Energy Chart for the Elements (From [3]).

Ionization power efficiency, η, is a measure of the power available in the ion beam to the total electrical power required to create it:

$$y = hdkd \qquad \eta = \frac{\text{beam power}}{\text{total electrical power}}. \tag{1}$$

However, if beam interception neutralization power is ignored and we look at the equation in terms of energy per ion instead of power, the equation becomes:

$$\eta \cong \frac{\text{exhaust kinetic energy}}{\text{exhaust kinetic energy + charging energy}}. \tag{2}$$

Mathematically, this is represented as

$$\eta \cong \frac{\frac{1}{2} m u_e^2}{\frac{1}{2} m u_e^2 + e_i + e_l} \tag{3}$$

where m is the mass of the ion, u_e is the exhaust velocity of the ions, e_i is the ionization energy, and e_l is the energy loss per ion. Since the ionization energy is significantly less than the energy loss ($|e_i| = e_l$) in most circumstances, the equation can be manipulated even further to

$$\eta \cong \frac{\frac{1}{2} m g_e^2 I_{SP}^2}{\frac{1}{2} m g_e^2 I_{SP}^2 + e_l} \tag{4}$$

where g_e is the acceleration due to Earth's gravity and I_{SP} is the specific impulse. Now, this equation shows that for any given specific impulse, higher masses will give greater power efficiency [4].

When discussing the use of gasses other than xenon, such as krypton or argon, the natural question is why. It has just been shown that higher masses are more efficient. Why use something with a smaller mass? There are two main reasons. The first is cost. Xenon is expensive to produce in large amounts. Krypton and argon are significantly less expensive. The second reason is more interesting. As can be seen in Figure 2, as high I_{SP} levels in the range of 5000-6000 seconds are approached, the efficiencies begin to level out. If we assume that we could operate at those I_{SP} levels, a reasonable assumption for an ion thruster, then the difference is negligible and krypton and argon become very attractive options.

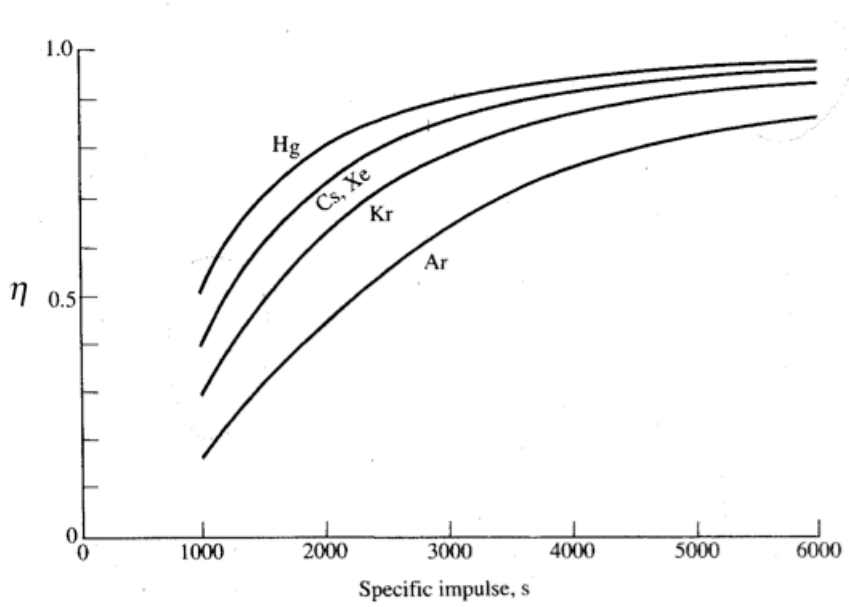

Figure 2. Efficiency of ion thrusters with 100 eV loss per ion (From [4]).

2. Surface Ionization

In metals, electrons will move around freely, but at the surface they are bound by a potential well, a sort of barrier. This barrier is known as the Fermi Level. The work function (ϕ) is a measure of the energy required for an electron to break through the Fermi Level measured in electron Volts (eV). The ionization energy (I_e) of an atom is similar, except that the ionization energy is a measure of the energy required to free an electron from an atom in free space. In general, the ionization energy is greater than the work function ($I_e > \phi$). However, if an electric field is applied, the characteristics of the barrier change. The barrier can be weakened, allowing an electron to tunnel through [5], [6].

Tungsten has a work function of approximately 4.5 eV, while cesium has an ionization energy of approximately 3.89 eV [5]. Since tungsten's work function is higher than cesium's ionization energy ($\phi_W > I_{e\_Cs}$), it is the perfect candidate to ionize cesium. When cesium atoms flow across charged and

heated tungsten they release an electron through adsorption, creating a positively charged cesium ion. Figure 3 shows an example of the surface ionization.

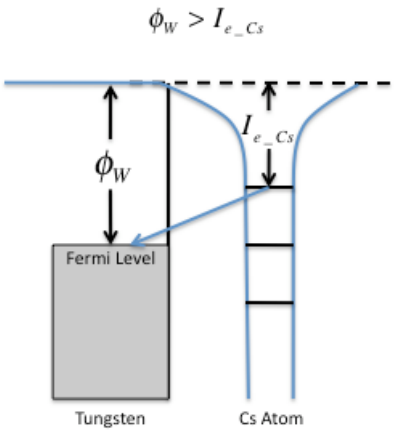

Figure 3. Cesium/Tungsten surface ionization.

The first spaceflight proven approach to ion thrusters used this method of ionization. In a cesium ion motor, cesium is heated to its gaseous state then sent through a porous tungsten metal ionizer. These newly created ions are drawn towards a negatively charged accelerator grid. As the ions pass through, a device shoots electrons at the exiting ions right after they pass through the accelerator grid in order to neutralize them and prevent them from turning back towards the engine. Figure 4 shows a typical cesium ion engine.

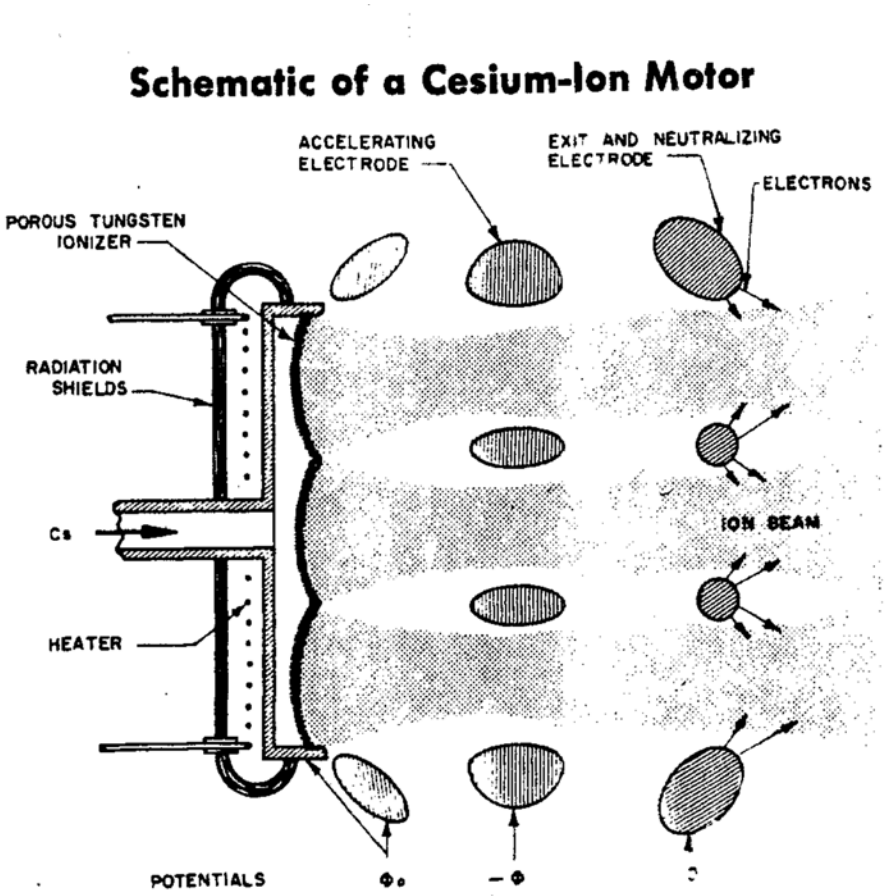

Figure 4. Cesium Ion Motor (From [7]).

NASA worked on these types of engines in the 1950s and 1960s. The Space Electric Rocket Test (SERT I) was the first successful flight test of the engine in July 1964. The first successful orbital test took place aboard the ATS-4 spacecraft on 10 August 1965. This vehicle had two cesium ion contact engines [8].

NASA determined that cesium and mercury were not practical materials to work with based on spaceflights and tests performed. The metal tended to build up on the hardware, reducing its effectiveness. These materials are also toxic, making them a hazard to the scientists working on them. This pushed NASA to look for different ways to build ion thrusters [9].

3. Electron Collision

Current designs for ion thrusters use electron collision. Electron collision thrusters bombard a gas atom with electrons that are emitted from a heated cathode [10]. As the electrons collide into the gas atoms they knock off an electron. A relatively large chamber with magnets or RF fields to increase the electron path is required to maximize ionization. The newly created particles are drawn towards negatively charged acceleration grids. Once they pass through the grids they are sprayed with electrons in order to neutralize the ion. The electron collision thruster is the design currently used by NASA on the Dawn spacecraft. A typical electron collision thruster is shown in Figure 5.

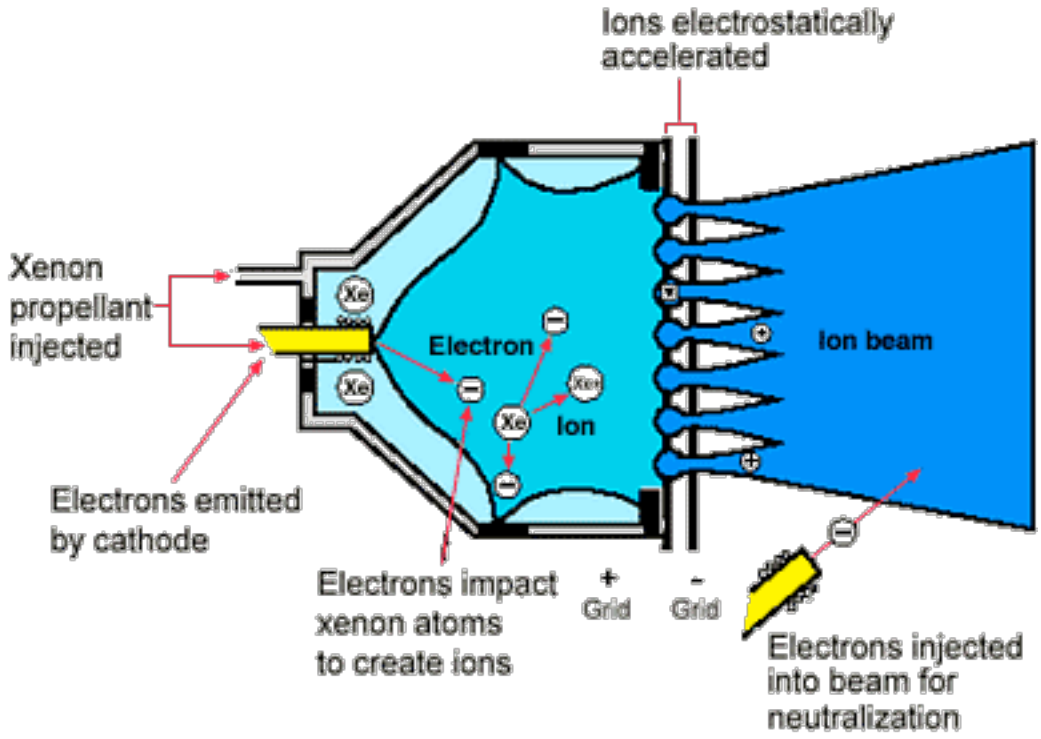

Figure 5. Electrostatic Ion Engine (From [11]).

4. Field Ionization

There are many parallels between surface ionization and field ionization. Surface ionization involves ionizing a gas by having that atom come in contact with a charged, heated surface that allows an electron to escape from the atom into the metal through the process of adsorption. In field ionization, a highly charged positive electric field provides the energy necessary for an atom to release its valence electron. The applied charge enables the electron to tunnel through the barrier into the metal providing the charge. Figure 6 shows an example of an electron tunneling into the metal. An ion thruster using this form of ionization would then have accelerator grids and a neutralizer similar to the other forms of ion thrusters.

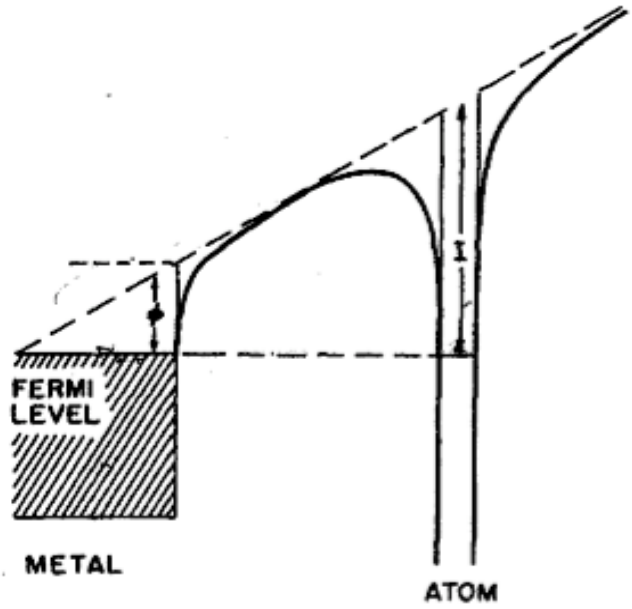

Figure 6. The valence electron tunnels with field ionization (From [12]).

The main difficulty in using this type of ionization for an ion thruster is the very high amount of electric field that must be generated in order to actually ionize a gas. In space applications, power is a rationed commodity, especially in nanosatellites. This is where the advent of new technology in carbon nanotubes comes in perfectly.

C. THESIS APPROACH

This thesis discusses the development and testing of a carbon nanotube pillar array as the ionizing element of a field ionized ion thruster. This cutting edge technology has the potential to revolutionize the world of ion thrusters, providing a more efficient thruster that can be scaled to any size.

The thesis will first discuss the science of how carbon nanotubes can ionize a gas and how they could be employed in an ion thruster. Then, the design and development of the test apparatus used during the course of the experiments will be laid out as well as the methods for how the test samples were developed.

The conduct of all of the tests will be discussed. All of the samples tested showed high enhancement factors, the key characteristic of carbon nanotubes that makes field ionization possible with such a low applied electric field.

Two of the seven experiments successfully proved that a carbon nanotube pillar array can ionize argon gas in a flow, the first step in building a prototype for a working field ionized ion thruster. The data from these tests indicate an average current of 5.00×10^{-5} Amps was detected through the ionization of argon flowing through only one relatively large hole. The potential is great for much higher currents that show a high propellant utilization factor once samples are developed with multiple, smaller holes.

Finally, recommendations will be made for how the process can be improved as the march towards a field ionized ion thruster continues.

II. FIELD IONIZATION USING CARBON NANOTUBES

A. CARBON NANOTUBES AND CARBON NANOTUBE PILLAR ARRAYS

1. Carbon Nanotubes

Carbon nanotubes (CNT) have enabled the development of many new technologies. CNTs are pillars of pure carbon with a highly ordered structure at the atomic level. Nanotubes can be developed in either single-walled or multi-walled structures. The multi-walled structures can be formed in either a construction of concentric single-walled structures (Russian Doll) or in a single rolled sheet resembling a rolled newspaper (Parchment model) [13], [14]. Examples of single-walled and multi-walled structures are shown in Figure 7.

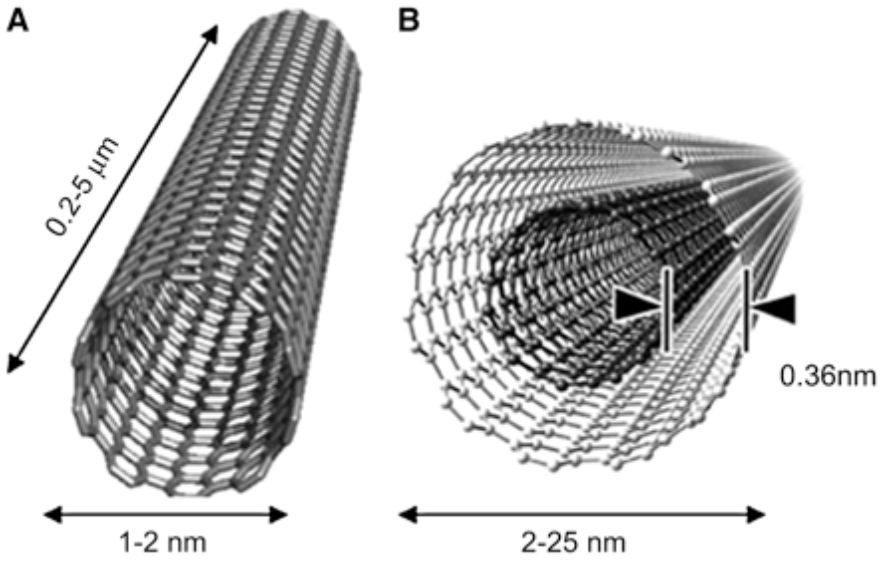

Figure 7. (A) Single-walled and (B) multi-walled carbon nanotubes (From [15]).

Carbon nanotubes possess unique characteristics that make them ideal for use. CNTs are one of the stiffest and strongest substances known to man. Tests have shown an elastic modulus of up to 0.95 TPa and a tensile strength of

up to 150 GPa. They have a density of approximately 1.4 g/cm^3 and a specific strength of up to 48000 kN-m/kg. To put this in perspective, the specific strength of high carbon steel is 154 kN-m/kg. CNTs have excellent thermal conductivity along the tube and a thermal stability of up to 2800 °C in a vacuum. CNTs are also excellent conductors, with the capability of carrying electrical current densities of up to 1000 times that of copper [13], [14], [16]-[19].

2. Carbon Nanotube Pillar Arrays

In order to develop tall, vertically aligned CNTs, it is useful to grow them in pillar arrays. A carbon nanotube pillar array (CPA) resembles a “forest” of CNTs in a nice ordered alignment. Van der Waals forces present in dense growth encourage the CNTs to “grow” in a vertical direction, providing the nice, tall nanotubes useful for conducting emission and ionization. Figure 8 shows a carbon nanotube pillar array. This sample was used in Experiment 3.

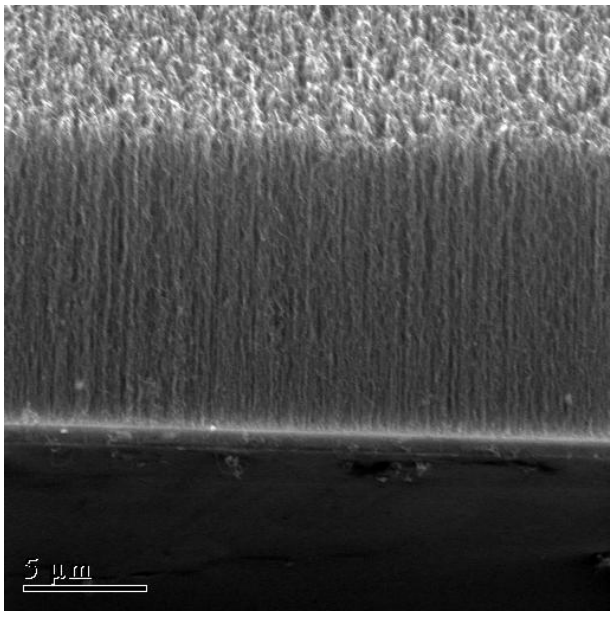

Figure 8. A carbon nanotube pillar array at 4000x magnification.

The characteristics of CPAs are similar to CNTs, but there are some minor differences. CNTs have higher amplification factors by themselves than when they are in a tight array. This amplification factor will be discussed further later in this chapter.

3. Chemical Vapor Deposition

One of the best methods for growing CNTs, and the method used for this thesis, is chemical vapor deposition (CVD). For CVD, a metal catalyst is deposited on a substrate and then heated to approximately 750 °C. While heated, a process gas (such as hydrogen) and a gas containing carbon (such as ethylene) are introduced. Carbon breaks away from the carbon-containing gas and deposits on the metal catalyst [13], [14]. This is how the nanotubes are formed. The length of time the substrate is exposed to the two gases under the extreme heat determines the length of the carbon nanotubes. Growth of approximately 10 μm can be achieved with as little as 30 seconds of exposure.

B. FIELD IONIZATION USING CARBON NANOTUBES

1. Geometry and Enhancement Factors

The highly charged electric field in carbon nanotubes is created as a result of the geometry of the tubes themselves. Depending on nanotube packing, an extremely sharp tip will have a very high amplification factor at its crest. This allows the possibility of using a relatively small voltage to create the electric fields on the order of 10^{10} V/m necessary to effectively ionize gases. Figure 9 is a graphical representation of a field ionization tip.

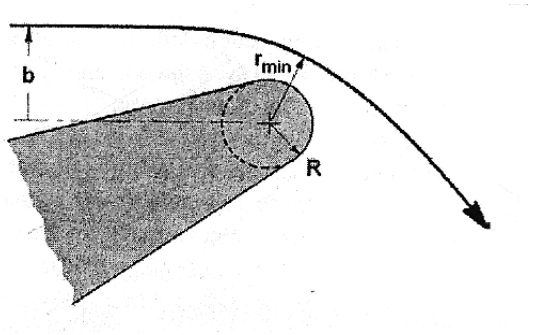

Figure 9. A gas molecule following the trajectory specified by the impact parameter b to pass through the radius of closest approach $r_{\min}$ near a field ionization tip, modeled as a sphere of radius R (From [20]).

The geometry of the tip truly plays a large role. There is a critical value b^* for what the impact parameter b can be and still ionize a gas. This value is defined as [20]:

$$b^* \equiv \left(\frac{2\alpha V_o^2 R^2}{E_o} \right)^{\frac{1}{4}} \tag{5}$$

$\alpha =$ Static Polarizability

$V_o =$ Applied Voltage

$E_o =$ Effective Potential Energy of Molecule

The Fowler-Nordheim equation represents the field-emitted electron current density, $J_{FN}(s)$, from this geometry. Included in the equation is the field enhancement factor β. The field enhancement factor is a unitless ratio of the local normal surface electric field to the applied field. Both equations are listed below [21]:

$$J_{FN} = \frac{A\left(\beta\left(\frac{V}{d}\right)\right)^2}{\phi_w t^2} \exp\left(\frac{-Bv\phi_w^{\frac{3}{2}}}{\beta\left(\frac{V}{d}\right)} \right) \quad \text{A/m}^2 \tag{6}$$

$$\beta(s) \equiv \frac{E_n}{\left(\frac{V}{d}\right)} \tag{7}$$

$A, B =$ Constants

$v, t =$ Functions due to the inclusion of image charge effects

$\frac{V}{d} =$ Applied field

$E_n =$ Local normal surface electric field

$\phi_w =$ Work function of the metal

$\beta =$ Field enhancement factor

2. Field Ionized Ion Thruster

CNT technology offers the first feasible platform for an ionized thruster. Ideally, a porous base would allow a gas to flow up through the positively charged CNT field and ionize as it reaches the tips. Since this field would be positively charged, the ions would be immediately repelled towards a negatively charged accelerator grid and then neutralized once past the grid. The major benefit here is that the ion chamber is miniaturized. The whole ionization and acceleration process can take place in a very small area without the requirement for a large ionization chamber. This makes it an ideal candidate for use in cubesats or other small satellites looking to minimize space. A sample model of a field ionized thruster is shown in Figure 10.

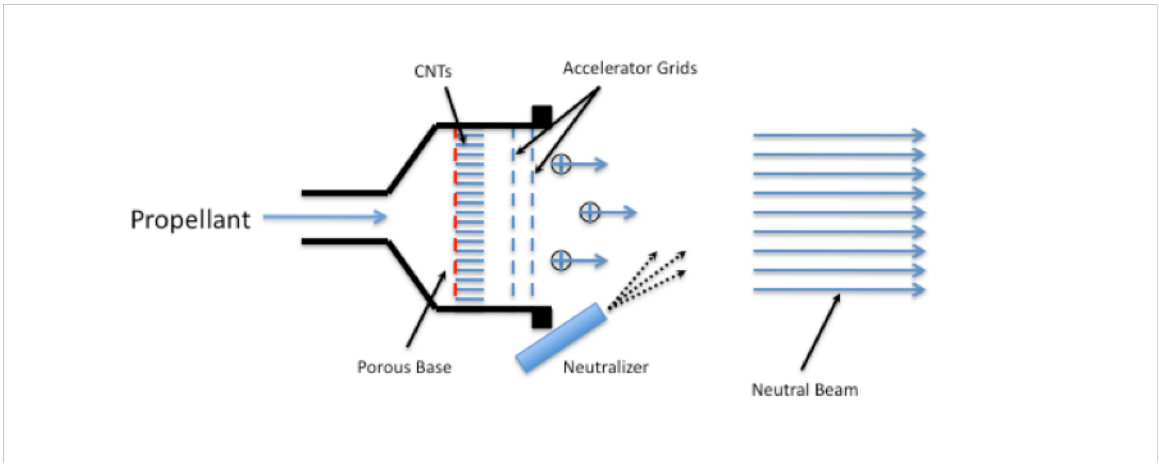

Figure 10. Field Ionized Ion Thruster.

III. TEST APPARATUS

The test device was a critical component of this research. The development of the test samples is the main focus of this thesis, but they would mean nothing if they were not tested. Previous research conducted by Troy Hicks [13] proved that CPAs could ionize Argon in a static environment. The next step was to develop a device capable of allowing samples to be tested under vacuum with an actual gas flow in order to determine the ionization ratio.

The device was built at NASA Ames Research Center in the Nanotechnology Laboratory, as this was where all of the test samples were developed. Through a mutual agreement between NASA and the Naval Postgraduate School, the author was able to work in the Nanotechnology Laboratory developing samples and learning the procedures and characteristics of carbon nanotube growth under the guidance of Dr. Darrell Niemann and his staff.

A. TEST STAND

Developing a test stand was the first step in the design of the test apparatus. A freestanding device that could be used solely for these tests was necessary since each test required significant vacuum down times. Having a separate test device also ensured that the tests could take place without having to compete for lab time with other researchers in the nanotechnology lab.

1. Design Considerations

The table had specific design requirements. It had to be sturdy and capable of holding the heavy test device. The table also had to be capable of withstanding the vibrations induced by the turbopump it would hold. It needed to be large enough to allow for workspace and future expandability without being too cumbersome. Finally, it also needed to be affordable.

2. Parts

Aluminum extrusions were cut to order by Misumi USA, Inc. for the table's framework. These bars are made of high rigidity aluminum, making them very sturdy. They are specifically designed to be constructed into worktables and supporting structures. The majority of the bars are 40 mm by 40 mm and were cut to a specified length. Two of the bars are 40 mm by 80 mm with a specific function to support the weight of the vacuum and test apparatus. Table 1 displays all items ordered to construct the test stand.[1]

Misumi Part Number	Part Description	Quantity
GFS8-4040-1180	High Rigidity Aluminum Frame	1
GFS8-4040-2134	High Rigidity Aluminum Frame	4
GFS8-4040-1444	High Rigidity Aluminum Frame	6
GFS8-4040-702	High Rigidity Aluminum Frame	4
GFS8-4040-834	High Rigidity Aluminum Frame	15
GFS8-4080-834	High Rigidity Aluminum Frame	2
GFS8-4040-340	High Rigidity Aluminum Frame	3
HBLFS8-C	Brackets for Aluminum Frame	130
HNTU8-8	Nuts for Aluminum Frame	278
CBM8-20	Hexagon Socket Cap Screws	270
CBM8-25	Hexagon Socket Cap Screws	14
L8NR8	Nut	6
NFJNF12-80	Adjuster Pads	4

Table 1. Parts list for the test stand.

Another critical component of the test stand was the table plate. The design required a structure that could hold a Varian Turbo-V 250 turbopump as well as support the rest of the test apparatus. The design was rendered in SolidWorks by the author and machined out of aluminum at the Naval Postgraduate School by Mr. John Mobley. The plate assembly consists of two identical pieces that mate together around the neck of the Varian turbopump to

[1] Table 1 shows all items that were eventually used to make the table. The GFS8-4040-1180 was originally ordered with a 1220 mm length but was cut down to the appropriate size.

hold it in place. The plate is then bolted down to the table. The drawings for the table plate are in Appendix A. The final machined plate is shown in Figure 11.

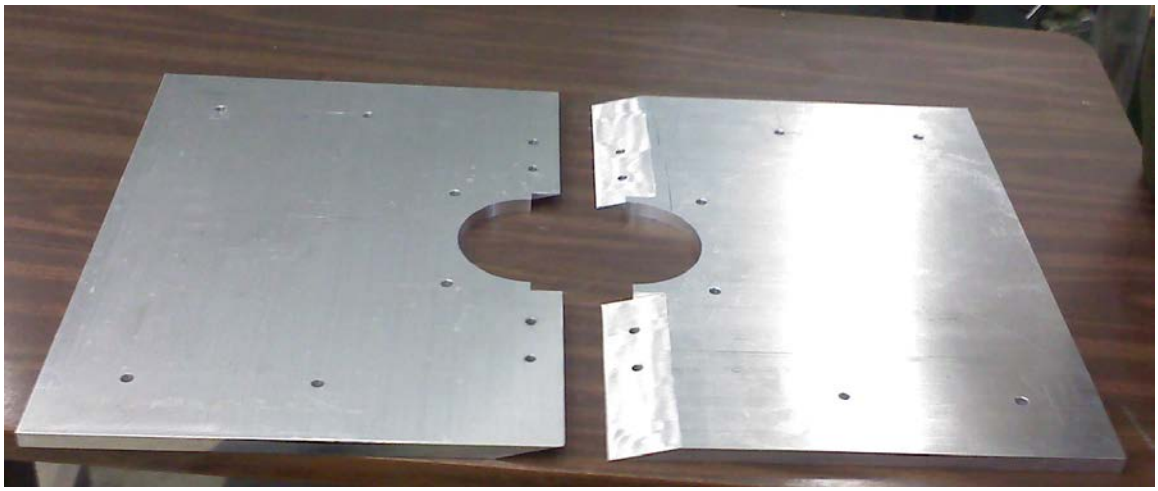

Figure 11. Table Plate.

3. Construction

Construction of the table stand took place as soon as all of the necessary parts arrived. Actual assembly required a level, an allen wrench and an adjustable wrench for the frame. A manual tap was used to create the threading necessary for the adjustable feet. A picture of the test stand is displayed in Figure 12.

Figure 12. Test stand.

B. TEST DEVICE

The actual test apparatus configuration was originally designed by Dr. Darrell Niemann and Lieutenant Commander A.J. McCoy, USN. The parts ordered for the apparatus were based on this design. After several rounds of testing, the configuration was changed slightly for experiment 6 in order to better determine the mass flow rate. All stock components for the vacuum were purchased from either MDC Vacuum Products or Duniway Stockroom. Table 2 is a list containing all vacuum parts purchased for this device. Table 3 lists all vacuum parts NASA-Ames had on hand and where they were purchased.

MDC Vacuum Part	Part Description	Quantity
407006	6-Way Cross, 6" Sphere	1
409007	Cluster Flange, 6"x3-2.75"	1
312055	Angle Valve, .5" UHV	1
400000	Flex Coupling, 1.33"	1
402011	Nipple Reducer, 2.75"x.75", Rotatable	1
404044	Reducing Tee, 2.75"x1.33"	1

Duniway Part	Part Description	Quantity
SPBN-200-600	6" flange blots and plate nuts [set of 25]	4
SBX-24-125	6" flange blots for tapped flanges [set of 25]	2
SPAN32-075-133	1.33" flange blots and plate nuts [set of 25]	1
SPBN28-125-275	2.75" flange blots and plate nuts [set of 25]	1
N/A	12 point socket (1/4 socket)	1
N/A	12 point socket (5/16 socket)	1
G600	10 pack of 6" copper gaskets	1
G275	10 pack of 2.75" copper gaskets	1
G133	10 pack of 1.33" copper gaskets	1
VP-600-400	6" view port	1
F274-000-N	2.75" blank	3
F600-000-N	6" blank	3

Arvi Mfg. Part	Part Description	Quantity
N/A	Custom machining of test base	1
N/A	Custom machining of gate (cathode)	3

McMaster-Carr Part	Part Description	Quantity
91435A140	High-temp insulating polyimide flat washer, No. 2 screw size, package of 10	1
9464K17	Viton O-Ring, AS568A-012, package of 100	1

Ted Pella, Inc. Part	Part Description	Quantity
16399	PELCO SEM Clip replacement clip, package of 10	1

Ceramco, Inc. Part	Part Description	Quantity
N/A	Ceramic #2-56 socket cap screw, 1/4"	10
N/A	Ceramic #2-56 socket cap screw, 1/2"	10
N/A	Ceramic #2-56 washer	10

Table 2. Purchased vacuum parts list.

MDC Vacuum Part	Part Description	Quantity
405002	4-Way Cross, 2.75"	2
640002	Medium CurrentFT, 2.75", 2 connections, solid (electrical feedthrough)	1
Duniway Part	**Part Description**	**Quantity**
N/A	6" Stainless Steel manual gate valve	1
BPG-400-CFF	Inficon BPG-400 Combi Gauge	2
TERRA-970	Terranova Model 970 Vacuum Gauge Controller	2
VLVE-1000	Bakeable variable leak valve, dead volume= 20 cc	1
N/A	Varian Turbo-V 250 turbopump	1
N/A	Varian Turbo-V 250 turbopump controller	1
N/A	Varian 600DS Dry Scroll pump	1

Table 3. Vacuum parts available at NASA Ames Research Center

1. Pumps

The vacuum system has two pumps. Both were purchased by NASA Ames. The first pump is the roughing vacuum. It is a Varian Dry Scroll pump and is capable of vacuuming down to 10^{-2} Torr within five minutes. This was paired with a Varian Turbo-V 250 turbopump. During the initial vacuum test, the two pumps vacuumed down to a pressure of 4.7×10^{-10} Torr over a period of two weeks. The system is easily capable of pressures down to 10^{-7} within two hours and 10^{-8} within 12 hours.

2. Sample Holder

In order to perform the flow rate tests, a test base was developed to hold the sample in place. This test base had to be able to fit 1-inch-by-1-inch samples, since this was the average sample size we were using at the time of development. The base needed to be able to fit inside the reducing tee into which it would. A recessed trench around the hold was necessary in order to allow for an o-ring, ensuring a tight fit. Finally, the test base needed to have enough threaded holes to allow for screws that could hold down the sample and

the cathode, as well as allow for future expansion. The design was rendered in SolidWorks and the drawings are available in Appendix A. Arvi Manufacturing machined the test base out of 304 stainless steel and welded it into the reducing tee. The finished test base is displayed in Figure 13.

Figure 13. Test base welded into the reducing tee.

The cathode was designed as a straight bar that would fit over the sample since it would be used for current collection only. Arvi Manufacturing machined three samples of the cathode out of 304 stainless steel based on the design developed using SolidWorks. The drawing is available in Appendix A. After we received the bar, we conducted a test fit and found that the cut-outs for the screws did not perfectly match the screw holes by approximately 0.5 mm on each side. This was remedied by using a drill to deepen the cut-out. Final

manufacturing of the cathode involved hand polishing using finer and finer grits and eventually polishing paste until it was as flat as possible. Figure 14 shows the cathode fitted onto the test base immediately after it was drilled for test fitting. Note the ceramic screws and ceramic and polyimide (Kapton) washers used to isolate the separate charges for the substrate and the cathode.

Figure 14. Test fit of cathode and blank sample on the test base.

3. Complete Test Apparatus Construction

Construction of the main portion of the vacuum system took two days to complete. Initial vacuum testing did not include the sample holder. Figure 15 shows the configuration of the test device during the initial vacuum test conducted May 28, 2010 to June 11, 2010. This configuration achieved a chamber pressure of 4.7x10-10 Torr.

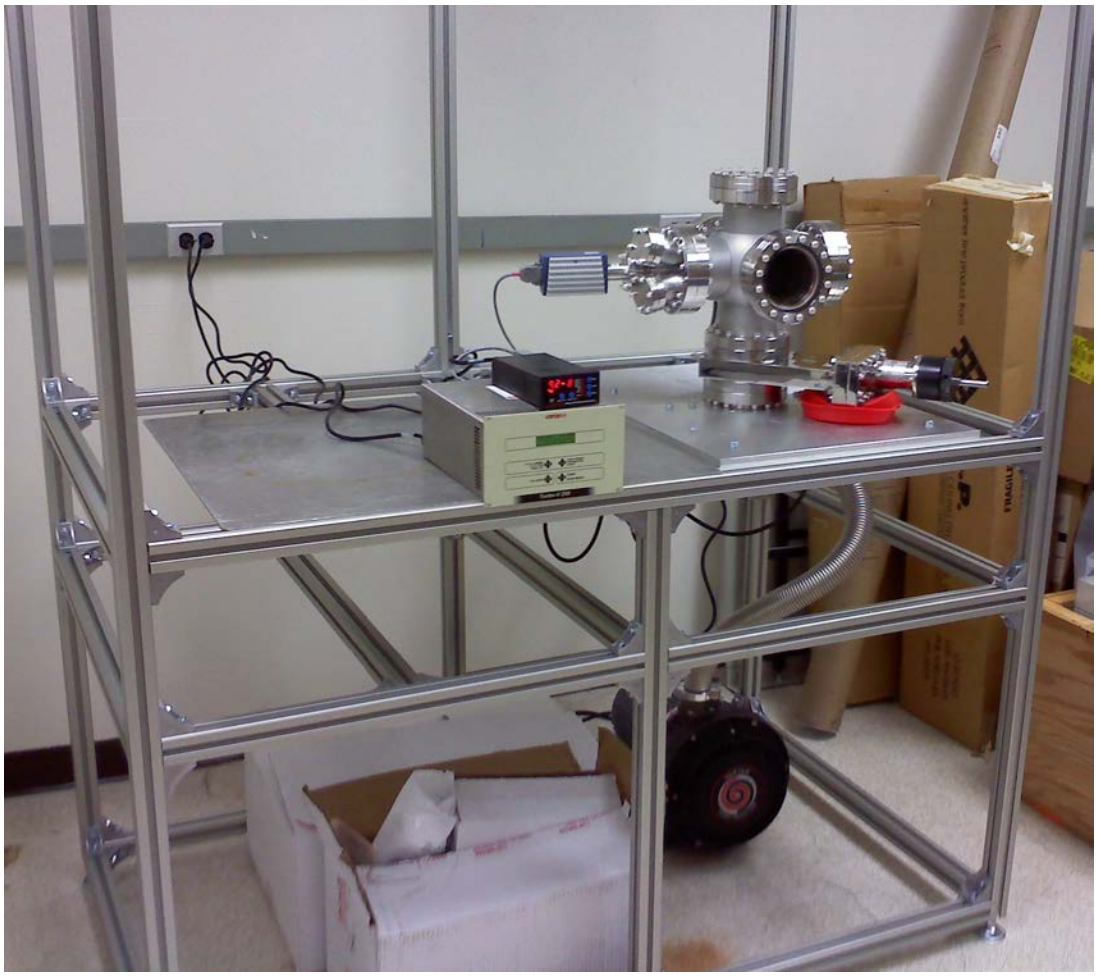

Figure 15. Initial vacuum test configuration.

After the successful vacuum test, the electric feedthrough, valves, and sample holder were mounted and another test was conducted. This time the vacuum achieved a chamber pressure of 1.5×10^{-8} Torr over the course of three days. On June 18, 2010, the test apparatus was erected in full configuration, complete with leak valve, in preparation for the first experiment. This configuration, shown in Figure 16, was used for experiments 1-5.

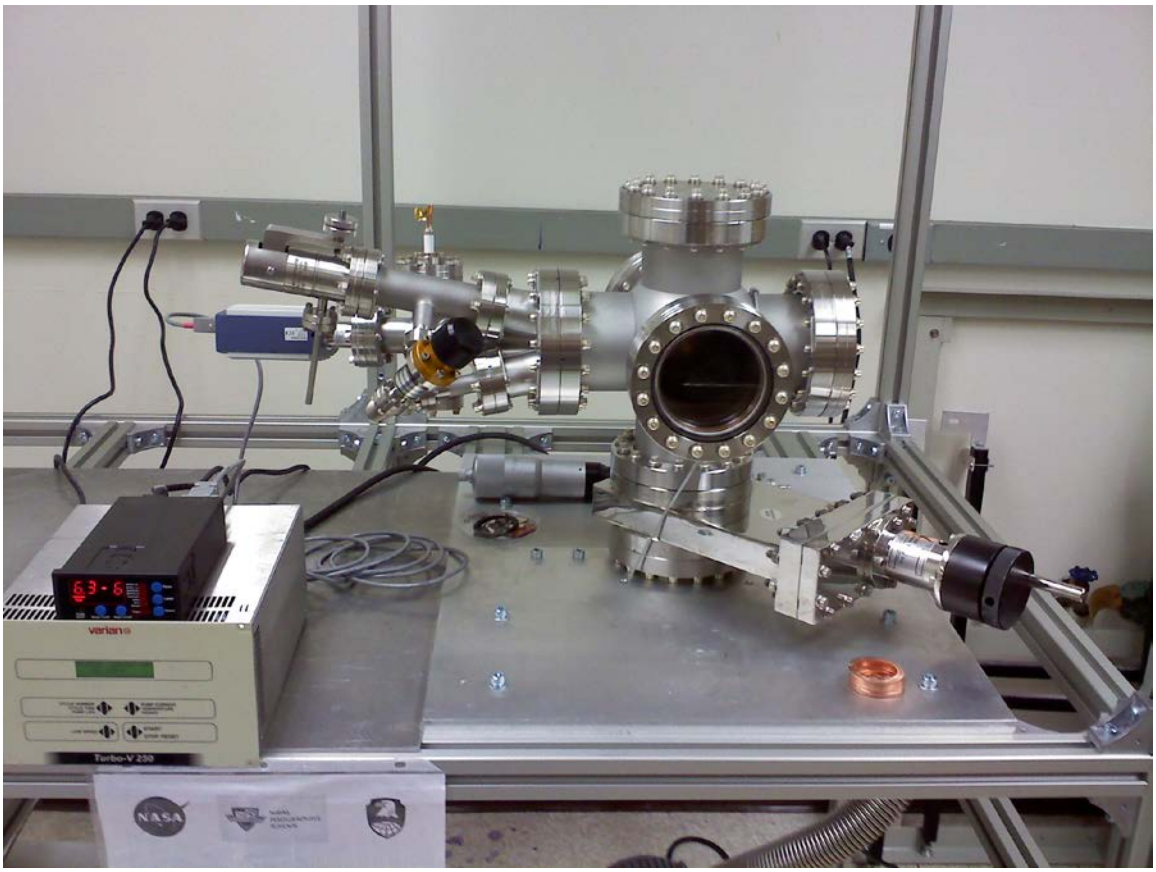

Figure 16. Test configuration for experiments 1-5.

Measuring a flow rate is difficult during these types of tests because of the extremely low flows of argon in the apparatus. During the course of the first five experiments, it became apparent that measuring the mass flow rate was not easy to accomplish accurately in the current configuration. A second four-way cross was added along with a second pressure gauge behind the test sample, so the back pressure could be measured as well. Additionally, the window on the six-way cross was moved to a position that allowed better viewing of the sample under vacuum. The final experiment configuration, to include the power source and computer test console, is shown in Figure 17.

Figure 17. Final test configuration.

C. OPERATION

1. Loading Samples

Loading samples into the test apparatus was an extremely delicate operation. It is very easy to brush up on, and therefore ruin, a sample. Additionally, an extra set of hands was very useful when mounting the test base back onto the chamber because it was easy for the mount to slip while mounting the screws, causing the heads of the ceramic screws to shear off.

Due to these experiences, various measures were instituted to allow for better loading. The method used for setting the gap distance and charge isolation was changed from using washers of known thickness to stand off the cathode from the test sample to strips of Kapton tape applied directly to the

sample substrate and allowing the cathode to rest directly on the tape. Since the thickness of the tape was measureable, it was easy enough to determine the gap distance between the carbon nanotubes and the cathode by subtracting the height of the tubes from the thickness of the tape. This allowed the sample to be loaded without scratching the sample while trying mounting the cathode. Figure 18 shows the Kapton tape applied directly to a test sample.

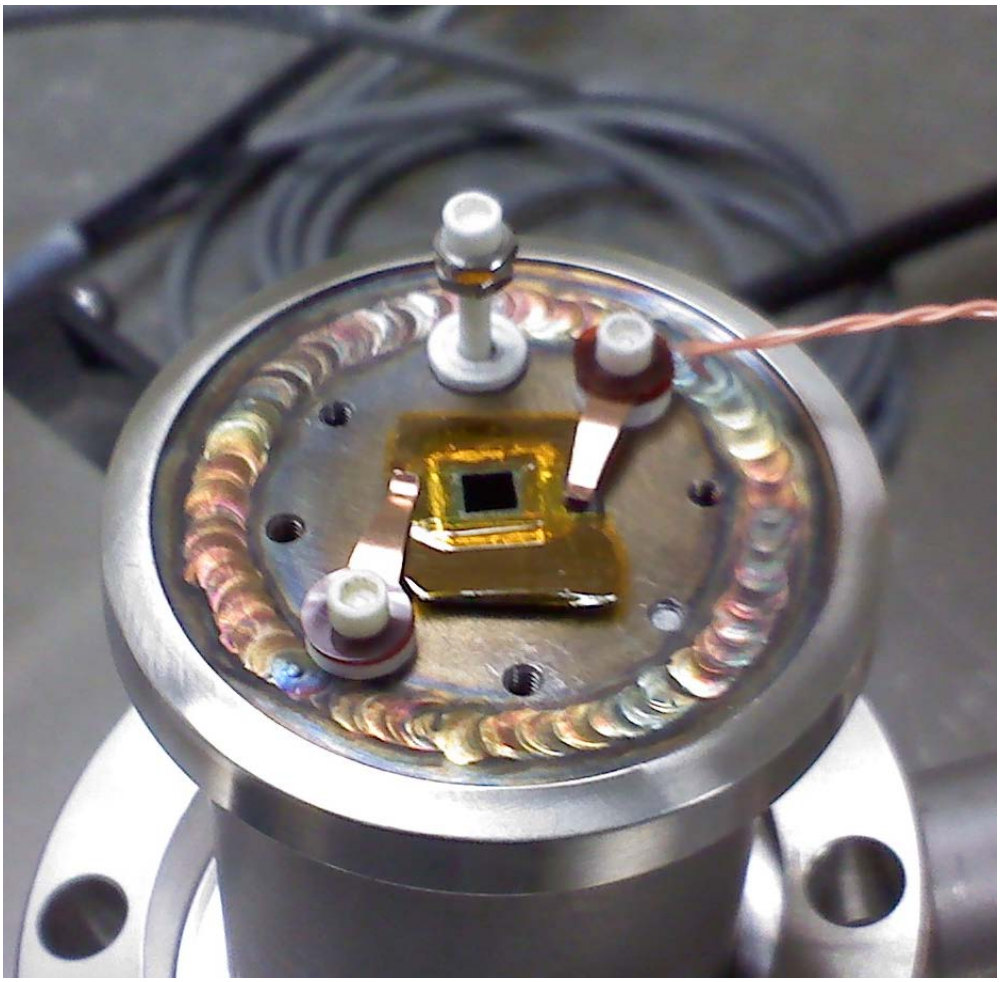

Figure 18. Kapton tape used as a standoff for charge isolation.

Additionally, whenever possible, another person would help with the physical connection of the test base assembly to the chamber. One person

would hold the assembly while the other would feed the wires back into the chamber and then screw in the bolts to hold it in place. Figure 19 shows this process.

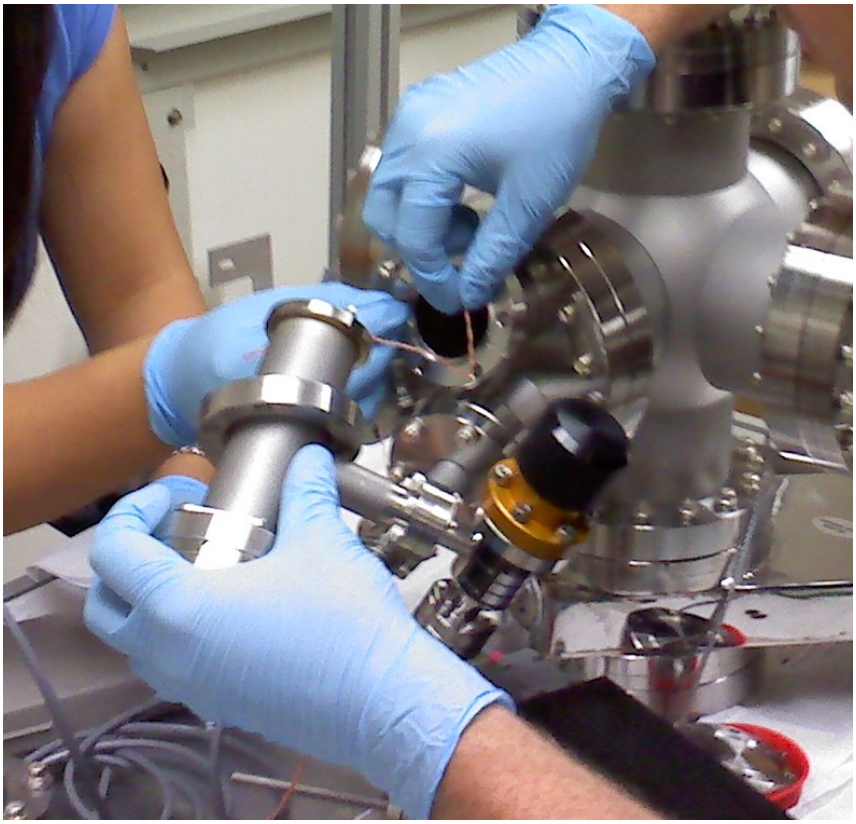

Figure 19. Affixing the test base assembly to the chamber.

2. Operation

Basic operation involved mounting the sample and letting the vacuum pump down until chamber pressure measured on the order of 10^{-7} or 10^{-8} Torr. The first tests conducted on a sample were the Fowler-Nordheim characterization tests. This required the sample to be put in field emission mode. A negative charge was applied to the substrate and a positive charge was applied to the bar by placing the appropriately charged alligator clips to the

electrode leads on the electric feedthrough. This enabled determination of the beta and gamma enhancement factors for that particular sample.

The power source used was a Keithley 237 High Voltage unit. This device has a voltage source and measurement device as well as a current source and measurement device. The Keithley is capable of measuring very low currents down to the order of 10 fA and voltage to 10 μV [12]. It has a maximum voltage capacity of 1100 V. For experiment 7 only, it was determined that more voltage was required for ionization then the Keithley could provide. The power source was switched to a Matsusada AU15R2. This power source is capable of providing 15 kV and 2 mA, but does not possess the sensitive measuring capability and quick current shutoff capability of the Keithley.

Control of both power sources was provided through the use of a Laboratory Virtual Instrument Engineering Workshop (LabVIEW) program. This program not only controlled the power supply but also saved and displayed the data in real-time during conduct of the test.

Once the field emission tests were complete, dry ionization runs were conducted just to determine if there was any leakage current. In order to switch to ionization mode, the alligator clips were switched on the electrode leads so that the substrate was now positively charged and the bar was negatively charged.

When the dry runs were complete, argon was released into the chamber until the desired chamber pressure was reached. The valve, allowing vacuum to the backside of the test sample, was then closed so that all argon had to flow through the test sample only. Measuring the change in chamber pressure for a set time allowed for a rough determination of the mass flowrate of argon through the sample. Once the mass flowrate was calculated, the actual ionization tests began.

Initial ionization runs always consisted of a linear step of voltage up to a set value, usually 1100 V. This was used to determine what voltage level was

capable of causing the argon to ionize. When a voltage level was determined, a run at that fixed level was conducted. During the fixed level runs, the mass flowrate would be adjusted from the existing rate to nothing and back again to see if the current truly changed. If the measured current went to zero with no flow, and then showed a current again when the flow was turned back on, it would indicate that ionization truly did occur at that voltage.

THIS PAGE INTENTIONALLY LEFT BLANK

IV. DEVELOPMENT OF TEST SAMPLES

A. CARBON NANOTUBE GROWTH

The process of growing carbon nanotubes in any given desired pattern can be a tedious process. However, the basics of growth are rather simple. As discussed in Chapter II, the process used to develop CPA samples for this thesis was chemical vapor deposition. The entire process used for growing samples will be discussed.

1. Sputtering

The substrate used for this thesis was silicon. Silicon is relatively easy to work with and can be conductive if using the appropriate composition. This is good for conducting the charge to the base of the carbon nanotubes. Unfortunately, CNTs will not grow directly on silicon, so a catalyst must be applied to the silicon substrate. Aluminum was used for this purpose.

A process known as sputtering was used in order to deposit the layers of metal onto the silicon substrate. The sputtering machine was an IBS/e Ion Beam Sputtering/Etching System made by South Bay Technology, Inc. A picture of this system is shown in Figure 20. The machine directs two ion beam sources at the target metal (i.e. aluminum) that needs to be applied to the substrate. The target metal is positioned directly across from the substrate. As the ion beam impacts the target metal, material is separated from the target and deposited onto the substrate [22], [23]. The process for conducting sputtering operations is detailed in Appendix B.

Figure 20. Ion Beam Sputtering/Etching System (From [23]).

2. CPA Growth

Initially, the author practiced sputtering and growing CPAs on both silicon and molybdenum substrates to gain familiarity with the process. Table 4 displays a list of all sample growth conducted during the practice phase. Note that in all cases, aluminum was used as the adhesion layer. The author also practiced using photolithography to imprint a pattern for growth onto a silicon chip. Since the pattern process is a long, tedious process, attempts to make imprinted patterns were abandoned due to time constraints and focus was turned towards growing on pre-etched silicon substrates.

Date	Substrate	Sputter Material	Sputter Thickness (nm)	Recipe	Growth (μm)	Notes
9-Apr-10	Si	Al/Fe	10/2.5	F, w/ 50 SCCM H2O	200	Training run.
13-Apr-10	Mo	Al/Fe	10/2.5	F	250	Training run.
13-Apr-10	Mo	Al/Fe	10/2.5	F, w/ 30 SCCM H2O	500	Training run.
15-Jun-10	Si	Al/Fe/Cr/Mo	10/2.5/10/15	n/a	n/a	Lithography training.
16-Jun-10	Si	Al/Fe	10/2.5	F	250	Training run on drilled hole.

Table 4. Practice growth results.

For the test samples, the initial growth was simply done on a pre-etched silicon substrate with 10 nm of aluminum for an adhesion layer and 2.5 nm of iron as the catalyst layer. This initial sample configuration is shown in Figure 21.

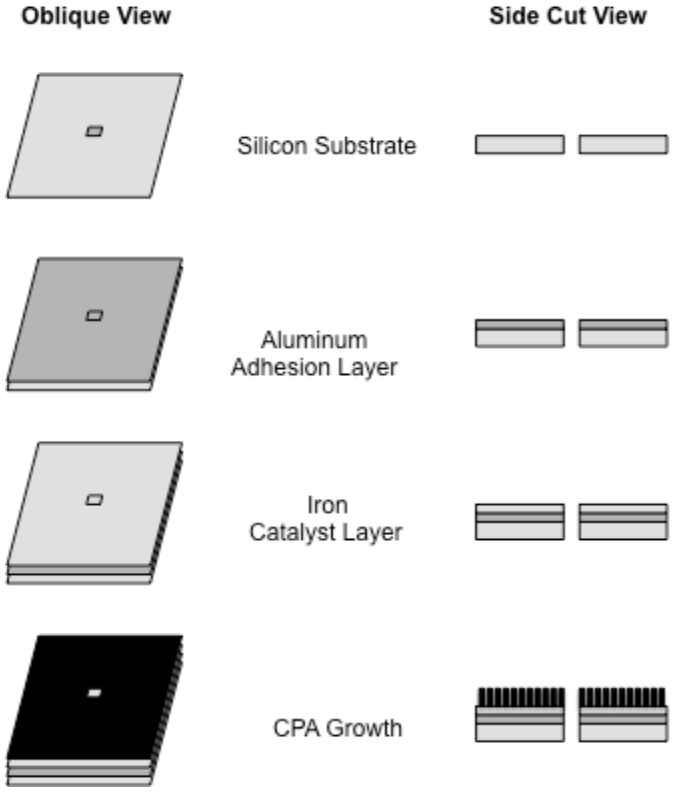

Figure 21. Initial sample configuration for CPA sputter and growth process.[2]

After an initial failure with Experiment 1 due to disturbing growth while mounting the samples to a larger piece of silicon, it was determined that there needed to be room on the growth substrate to be able to work without ruining and sample growth. This working area needed to be conductive, as well to ensure the applied charge would actually reach the carbon nanotubes. In order to do this, a conductive, non-catalytic layer was added as a border around the hole, providing plenty of room to work without having to disturb CNT growth. First, the

[2] Inspiration for displaying the growth process in this manner was derived from the thesis written by Troy Hicks [13].

silicon wafer was handled the same as before. The base layers of 10 nm of aluminum and 2.5 nm of Iron were sputtered onto the silicon wafer. Then, a mask was applied over the desired CNT growth area around the hole. For this purpose, a cut piece of the adhesive portion of a Post-it® note was used. Then, 10 nm of molybdenum were sputtered on as an adhesion layer followed by 15 nm of chromium. Finally, the mask was removed, remaining adhesive was cleaned off using acetone and water, and the sample was put into the furnace for growth. Although this increased overall processing time to make each sample, the benefit was well worth it. The new samples were much easier to work with. The process is shown in Figure 22.

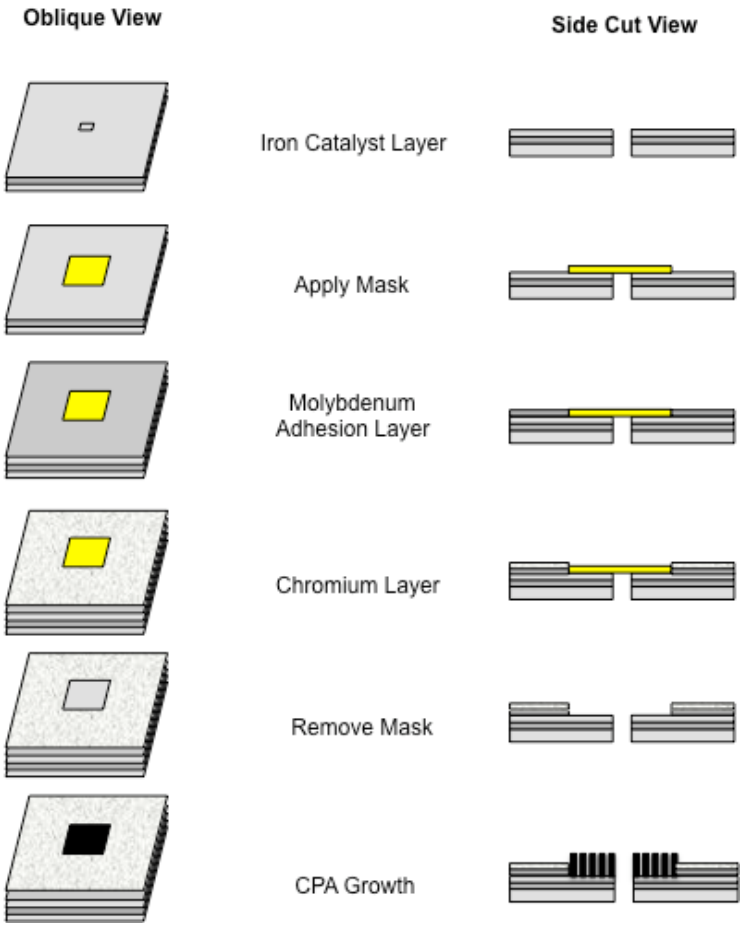

Figure 22. Altered sample configuration for CPA growth allowing for a conductive, non-catalytic layer to enable handling.

For the actual test samples, the basic recipe used for growing the CPAs was slightly modified. The recipe used for the practice runs was what the NASA Ames Nanotechnology Lab refers to as recipe F. This recipe grows very nice, large samples. The author achieved an average growth of 250 μm using the standard, unmodified recipe. This involved 10 minutes of "growing" time where the catalyst is exposed to ethylene and hydrogen in a 750 °C environment. This type of length was too long for our needs however. For the test samples, the growing time was reduced to 0.5 minute. This achieved growth results of anywhere from 10 μm to 70 μm. The modified recipe F is shown in Table 5. The test sample results are shown in Table 6. The entire CVD process used for growing the CPAs is available in Appendix C.

Time (min)	Argon (SCCM)	Hydrogen (SCCM)	Ethylene (SCCM)	Furnace (°C)
15	500	0	0	0
5	0	201	0	0
11	0	100.5	0	750
0.5	0	100.5	455.6	750
5	500	0	0	750
30	500	0	0	0

Table 5. Modified Recipe F for 0.5 min growth.

Date	Sample	Substrate	Sputter Material	Sputter Thickness (nm)	Recipe	Growth (μm)	Notes
17-Jun-10	1	Si	Al/Fe	10/2.5	F, w/ 1 min growth	8.5	Destroyed while loading
18-Jun-10	1a	Si	Al/Fe	10/2.5	F, w/ 1 min growth	70	Experiment 1
23-Jul-10	2	Si	Al/Fe/Cr/Mo	10/2.5/10/15	F, w/ 0.5 min growth	10	Experiment 2
24-Jul-10	3	Si	Al/Fe/Cr/Mo	10/2.5/10/15	F, w/ 0.5 min growth	14	Experiment 3
7-Aug-10	4	Si	Al/Fe/Cr/Mo	10/2.5/10/15	F, w/ 0.5 min growth	24	Experiment 4
7-Aug-10	5	Si	Al/Fe/Cr/Mo	10/2.5/10/15	F, w/ 0.5 min growth	25.5	Experiment 5
14-Aug-10	6	Si	Al/Fe/Cr/Mo	10/2.5/10/15	F, w/ 0.5 min growth	26	Experiment 7
14-Aug-10	7	Si	Al/Fe/Cr/Mo	10/2.5/10/15	F, w/ 0.5 min growth	26	Destroyed while handling
14-Aug-10	8	Si	Al/Fe/Cr/Mo	10/2.5/10/15	F, w/ 0.5 min growth	62.2	Experiment 6

Table 6. Test sample growth results.

3. Growth Verification

When a sample was complete with the growth process, it was taken to the scanning electron microscope (SEM) for measurement and assessment of its vertical alignment. The SEM available at NASA Ames was a Hitachi S-4000. Samples were viewed at a 45-degree tilt to allow for proper height measurement. All apparent height measurements were multiplied by $\sqrt{2}$ to get the true height of the nanotubes. The process for operation of the SEM is in Appendix D.

B. SUBSTRATE MANIPULATION

The test base was sized for a 1" x 1" silicon wafer. Unfortunately, the pre-etched wafers were only 1 cm x 1 cm. This created a bit of a problem for how to load the sample. Creating a new modification assembly to accommodate the smaller samples would not be practical given the time constraints imposed. Instead, the author chose to manufacture an appropriately sized 1" x 1" silicon base for each sample and then mate them together with epoxy. This solved the size issue, but a hole still needed to be made in the new base.

1. Drilling Through Silicon Wafers

The author approached Jay Longson, a research scientist in the Nanotechnology Lab, about possibly drilling through silicon to make the holes. After breaking a few samples, a combination of wet drilling with a Dremel® at its slowest speed and a diamond-tipped bit proved to be successful. The entire process is explained in Appendix E.

2. Tapping Out Pre-Etched Holes in Silicon Wafers

The pre-etched 200 μm x 200 μm holes in the small silicon wafers came with a nitride layer covering the holes. Initially, a very fine needle was used to

penetrate this layer under a Zeiss Axiovert 100-A tabletop microscope in order to open the hole so gas could flow through it. The microscope is shown in Figure 23.

Figure 23. Tabletop microscope used for penetrating the nitride layer.

There were two major problems with the “poking it out” method. First, it is not easy to clean off a nitride layer around a hole using only a needle under a microscope. This is akin to removing all shards of glass from a window frame using a spear. It is also easy to start scratching into the silicon itself. Figure 24 shows the uneven clearing of the hole. This affects growth and the amount of surface area available for ionization. The other major problem was conductivity. The nitride layer also prohibited conductivity from the drilled silicon base to the small silicon wafer. This forced the use of conductive epoxy that lapped over the edge of the small wafer to ensure conduction of the charge to the CPA. The amount of epoxy that lapped over the edge provided an easy path for the sample to potentially short circuit.

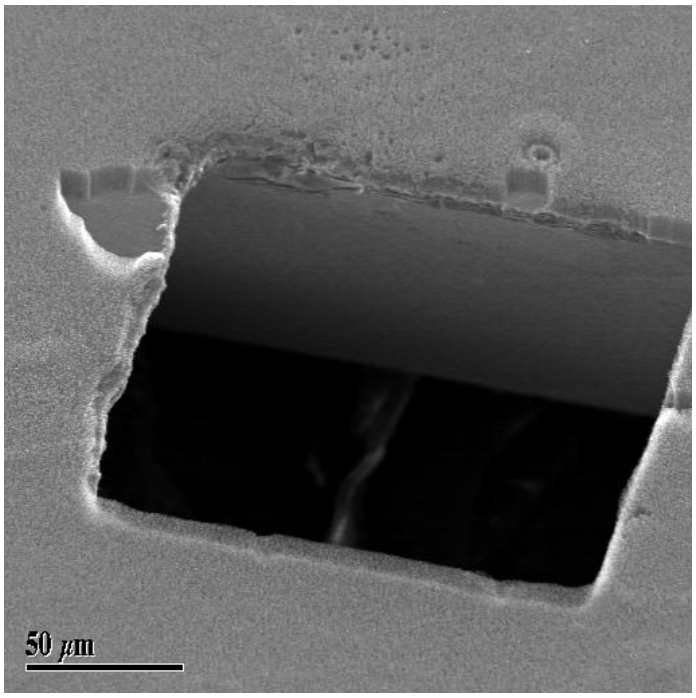

Figure 24. Sample grown on a needle-penetrated nitride layer. Note the jagged edges and non-uniform growth along the edges of the hole.

3. Acid Etching of Pre-Etched Holes in Silicon Wafers

In order to prevent the problems associated with penetration of the nitride layer, another approach was used. This time the pre-etched wafers were soaked in a bath of hydrofluoric acid (HF) and phosphoric acid. Initial attempts to have the wafers sit in the HF for only 5 minutes at a time did not work. The phosphoric acid seemed to have little effect as well. We chose to just leave the samples in HF and periodically revisit to see if the layer was still present. After approximately one hour, the nitride layer was finally removed. The wafers were pulled out of the HF and rinsed with water.

The HF bath worked extremely well. The growth on the new wafers was nice and orderly as can be seen in Figure 25. The silicon wafer was now conductive as well, since the nitride was gone. This meant that the conductive epoxy no longer had to lap over the top edge.

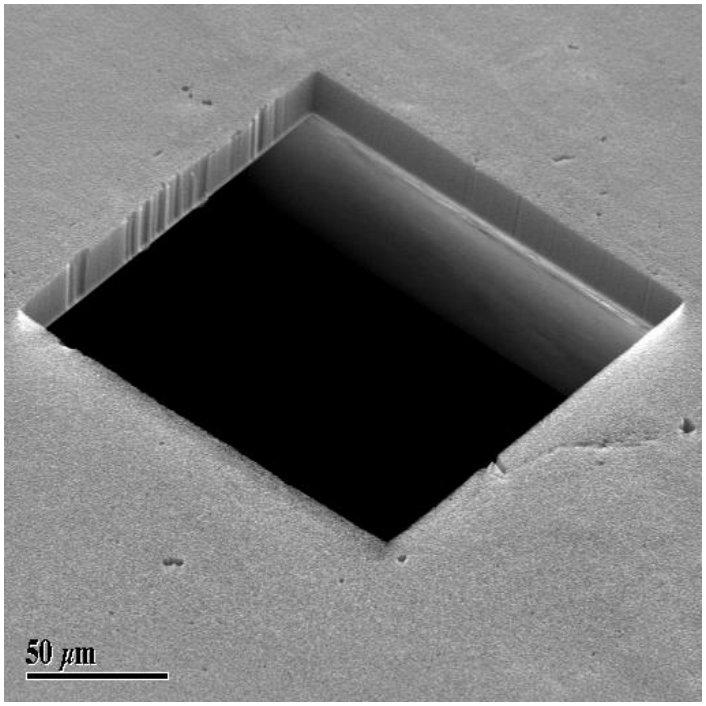

Figure 25. Sample growth on a silicon substrate etched with HF to remove the nitride layer. Note how clean and uniform the growth is along the edge.

4. Mating Silicon Wafers

Silver conductive epoxy was used to mate the two silicon layers together. The silver epoxy served three purposes: adhesion, conduction, and sealing. The epoxy had to ensure that the gas would only flow through the hole and not through the adhesion.

The silver epoxy came in two tubes. Equal amounts from each tube were mixed together to form the epoxy. The epoxy was applied using a piece of chromium wire to make the application as clean as possible. Figure 26 shows this process.

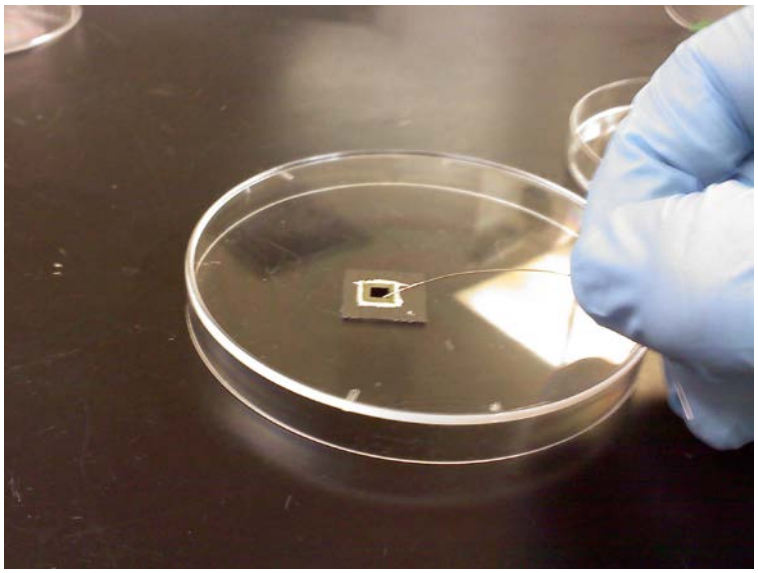

Figure 26. Application of silver epoxy to mate two silicon plates using chromium wire.

After application, the epoxy was cured by placing the sample on a 65 °C hot plate for 10 minutes.

When the nitride layer was etched away with the HF there was no longer a need to put the epoxy on the outside. It was now possible to put a thin ring of epoxy around the drilled hole, providing the necessary sealing, adhesion and conduction without risking a possible short circuit. Figure 27 shows an example of one of these samples.

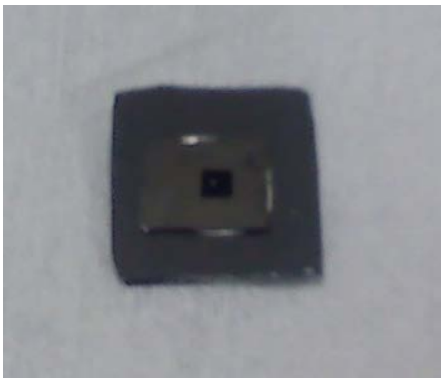

Figure 27. Sample with epoxy applied underneath the small wafer rather than on the outside. Note the seepage caused by the compression of the two layers.

V. TEST RESULTS

A. EXPERIMENT 1

1. Preparation

There was difficulty in loading the first sample. The cathode slipped of the washers used for gap distance standoff during emplacement and scratched the surface of the carbon nanotubes. This ruined the sample. Another sample was quickly manufactured but instead of using the washers as the gap distance standoff, two strips of Kapton tape were placed across the sample and the cathode was allowed to rest on top of the tape, making this the new standoff distance. The thickness of a single strip of tape was measured at approximately 63.5 μm in the SEM.[3]

Figure 28 shows an image of the experiment 1 sample prior to testing. This sample measured approximately 70 μm in height.

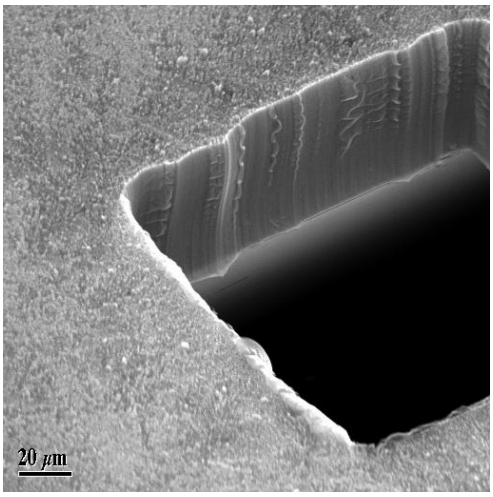

Figure 28. Experiment 1 prior to testing. This image is at 545x magnification.

[3] A thin layer of molybdenum was coated onto the Kapton tape in order to allow it to be viewed in the SEM.

2. Test Execution and Results

Initial vacuum pressure in the chamber prior to beginning testing on July 9, 2010 was 1.8×10^{-8} Torr. The measured gap distance for this test was approximately 124 μm based on the thickness of the two strips of Kapton tape. Unfortunately, this test never went beyond initial turn-on of the power source. Just prior to the test all connections were checked to ensure there were no short circuits in the system. However, when the charge was applied the system immediately showed a short circuit.

As there was no way to fix this from the outside, the vacuum had to be shut down and the sample was removed to investigate. Upon visual inspection, it was apparent that the CPA blanket pulled up from the substrate to touch the cathode. The point of separation was exactly along the line where the Kapton tape had been applied across the sample. Figure 29 shows an illustration of what happened.

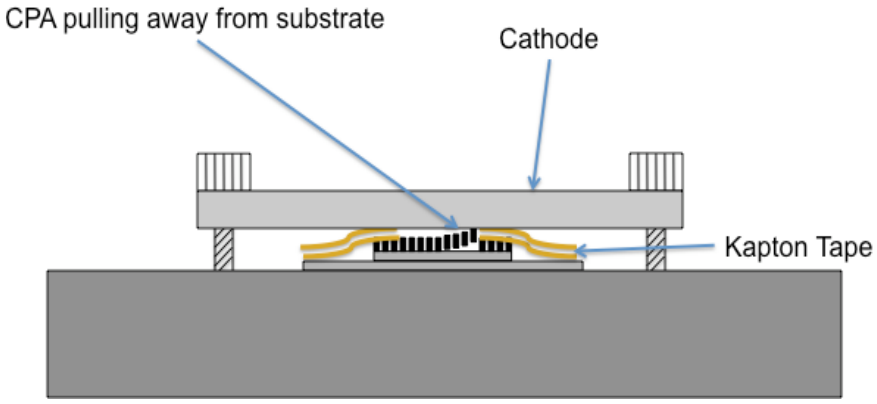

Figure 29. Illustration of CPA pulling away from substrate to create a short circuit.

3. Lessons Learned

The most likely reason that the CPA was able to separate from the substrate is that it was disturbed when the Kapton layers were placed over the

top of them. This prompted the need to create a workable area around the growth for not only mating and handling purposes, but to provide a place to lay down the tape as well.

B. EXPERIMENT 2

1. Preparation

Experiment 2 used sample 2 as its test sample. This time the two layers of Kapton tape were placed over the "working area" created on the surface of the silicon wafer by using the mask and sputtering on an adhesive coat of molybdenum and a conductive, non-catalytic coat of chromium. Figure 30 shows the sample setup for Experiment 2. The sample was placed into the chamber and began vacuuming down on July 24, 2010.

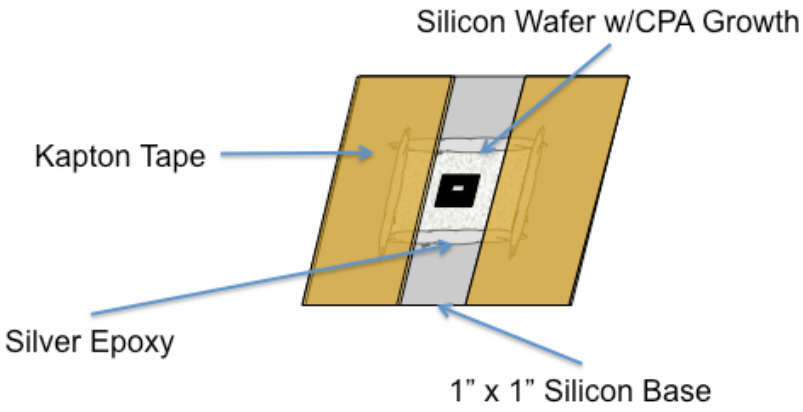

Figure 30. Sample setup for Experiment 2.

2. Test Execution and Results

The first test conducted was to characterize the enhancement factors β and γ by conducting field emission tests on the sample. Five sweeps were conducted on the sample in order to get a good Fowler-Nordheim plot. Test parameters for the field emission tests are shown in Table 7. The results of

those tests are shown in Table 8. The data relating to all Fowler-Nordheim and ionization tests conducted can be found in Appendix F.

Experiment 2	
Fowler-Nordheim Characterization	
Date	29 July 2010
Initial Chamber Pressure	2.40E-8 Torr
Power Source	Keithley 237
CPA Height	10 μm
Gap Distance	117 μm
Compliance Level	2.00E-5 A
Compliance Range	1 μA
Measurements	550
Voltage	Linear stair: 0 V to 550 V

Table 7. Experiment 2 test parameters for Fowler-Nordheim characterization.

Experiment 2		
Enhancement Factors		
Sweep	**Beta**	**Gamma**
1	1.91E+07	2240
2	1.83E+07	2144
3	1.57E+07	1837
4	2.03E+07	2381
5	2.03E+07	2370
Average	**1.88E+07**	**2194.4**

Table 8. Experiment 2 enhancement factor results.

The enhancement factor Beta (β) was determined by first identifying the most vertical portion of the current versus voltage plot where field emission occurs. This area's data was then plotted with 1/V as the x axis and $\ln(I/V^2)$ as the y axis. The slope of the best-fit line through those points determined the beta factor. Gamma was derived from the beta factor based on the gap distance. The MATLAB code for determining the enhancement factors is in Appendix H.

Once we finished characterizing the enhancement factors, we were able to focus on the ionization tests. The test parameters for the first tests are shown in Table 9.

Experiment 2	
Argon Ionization Runs 1-5	
Date	30 July 2010
Initial Chamber Pressure	2.40E-8 Torr
Unobstructed Pressure	2.40E-7 Torr
Obstructed Flow Pressure	1.70E-7 Torr
Power Source	Keithley 237
CPA Height	10 μm
Gap Distance	117 μm
Compliance Level	2.00E-5 A
Compliance Range	1 μA
Measurements	1000
Voltage	Linear stair: 0 V to 1000 V

Table 9. Argon Ionization test parameters for Runs 1-5.

Figure 31 shows the plots from the first runs. The points where the graph peaks out are the compliance level, an automatic shutoff of current if the voltage produces current at this level. This is to protect the system from itself since hitting the compliance level is an indication of a possible short circuit. An interesting phenomenon to notice is that the turn-on voltage was much lower in the first run than in the latter runs. This could be an indication of either conditioning of the system where loose CNTs were separating from the substrate, burning out of various “high spots” across the CPA, or destruction of the CNTs themselves.

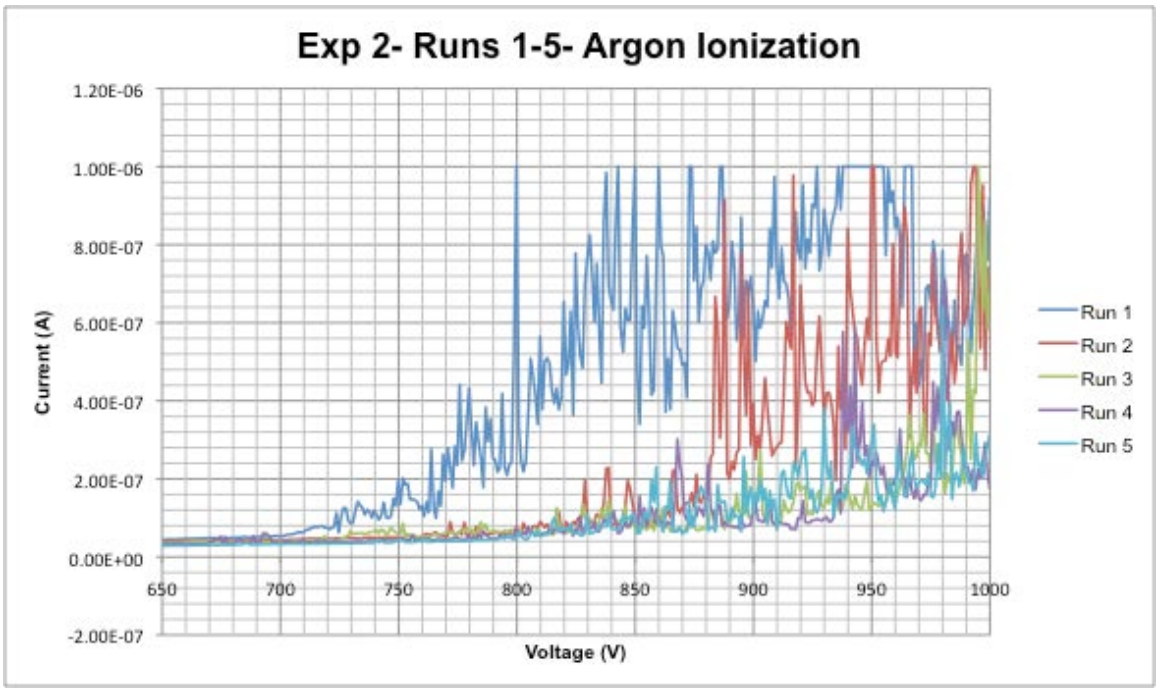

Figure 31. Experiment 2 Argon Ionization Runs 1-5.

A leakage current was also present during the first runs. This was only noticeable in the 10^{-9} to 10^{-10} Amp range, but it was linearly increasing with voltage until either ionization or arcing occurred. Subsequent runs were conducted with no meaningful results, so the sample was pulled out in favor of determining what was causing the leakage current.

A comparison of the sample showed no perceptible damage. A side-by-side comparison of the Experiment 2 sample both before and after testing is shown in Figure 32.

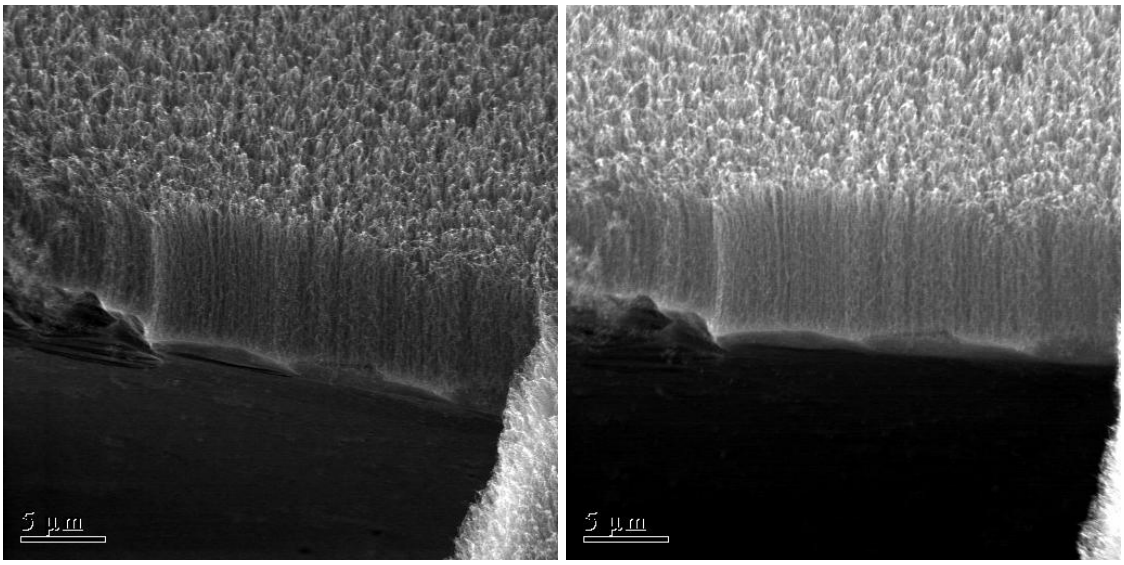

Figure 32. Comparison of the Experiment 2 sample at 3000x magnification. The picture on the left is before testing and the one on the right is after testing.

3. Lessons Learned

The main lesson learned during this experiment was that there appeared to be a leakage current that required looking into prior to continuing further experiments.

C. LEAKAGE CURRENT TESTS

1. Preparation

The leakage current experienced during Experiment 2 indicated a possible problem with the sample setup. In order to try and determine the root cause of the problem, a series of tests were conducted with blank samples to see what was truly happening. First, the sample was replaced with a blank piece of silicon that had another piece of silicon mated to it using silver epoxy. Kapton tape was used as a gap distance standoff similar to the true sample. Figure 32 shows an illustration of this blank test sample.

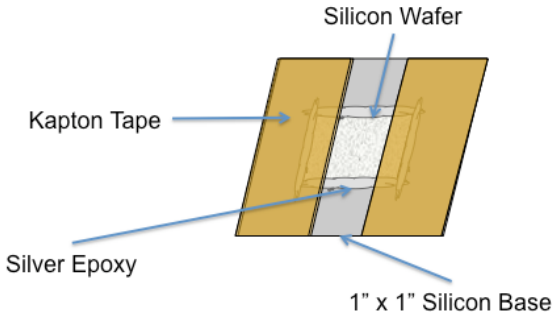

Figure 33. Illustration of blank test sample used for system troubleshooting.

2. Test Execution and Results

The chamber was vacuumed down and voltage was applied to the sample in both field emission and ionization modes. The field emission tests showed minor leakage that remained in the 10^{-10} Amp range, but the ionization modes showed significantly higher leakage current. Figure 34 shows the results of those runs.

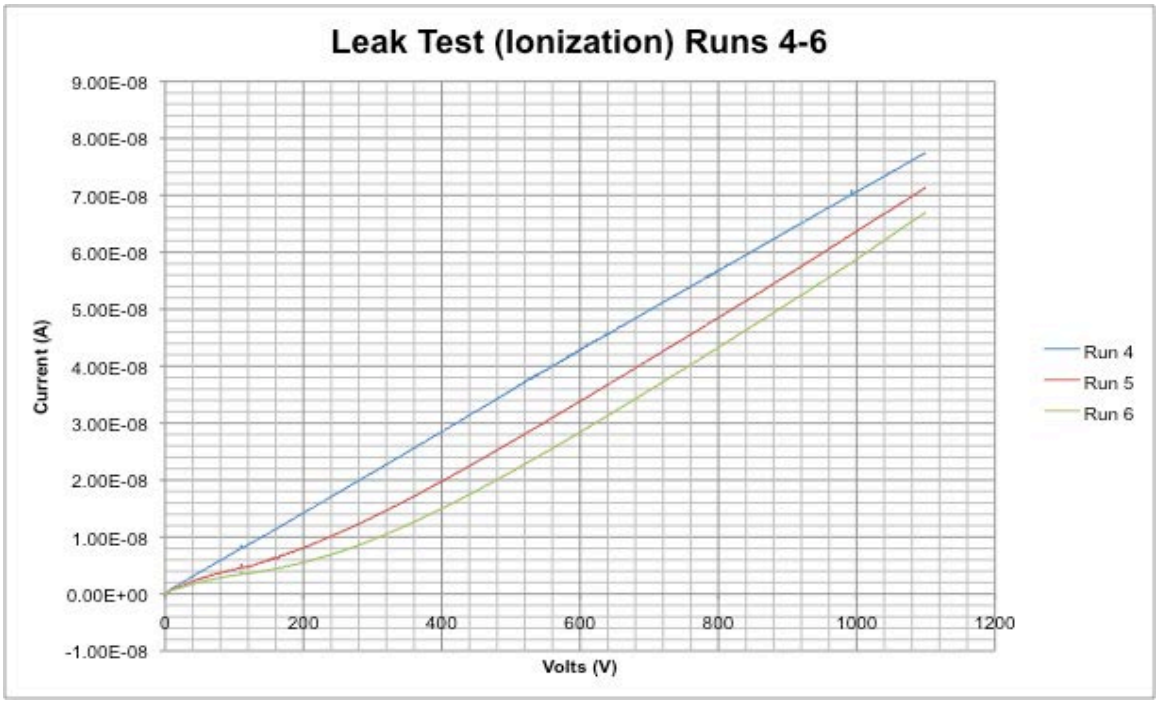

Figure 34. Leak test results when a positive charge was applied to the substrate and a negative charge was applied to the bar.

Figure 34 shows an unmistakable linear trend of current leakage with voltage. It was difficult to actually see what was going on with the sample, however, and constantly removing samples and waiting for the vacuum process to take place became impractical. Instead, open air testing was decided on in order to allow for multiple iterations of testing different possible fixes in a timely manner.

The removal of the sample to open air did introduce some difficulties we had to account for. While in vacuum under no flow conditions, there were no gases to ionize if a charge was applied. However, in open-air testing the air itself is the gas. This did make observation a little easier though, and helped in locating where the sample was arcing.

During Run 10, significant arcing was noticed and visibly confirmed. Further inspection showed that this was occurring at the silver epoxy. The sample was removed and replaced with a blank silicon wafer with a standoff of two strips of Kapton tape. Figure 35 is an illustration of the wafer configuration for the next leakage tests.

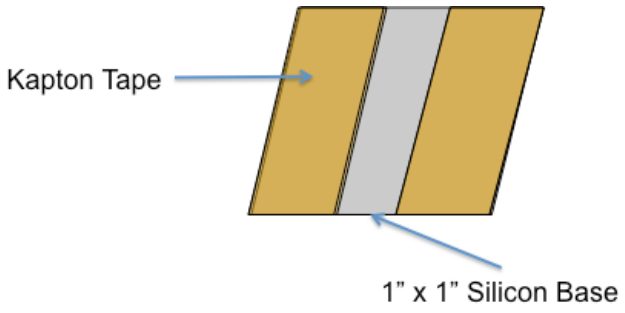

Figure 35. Illustration of the blank test sample used for leakage testing.

Immediate test results showed no change in the behavior of the system. At this point, different test parameters started to be looked at as the possible cause of the leakage. While ceramic screws were specifically chosen for their non-conductive properties, they were some of the only suspects left.

A major isolation campaign began, where anything that could possibly cause leakage was isolated with Kapton tape. Specifically, tape was placed on the bar where it contacted the ceramic screw (see Figure 36), and tape was placed on the screw itself where it made contact. Kapton washers were also placed above and below the electric lead and retaining clip assembly and above the electric lead on the bar. Figure 37 shows an illustration of this assembly.

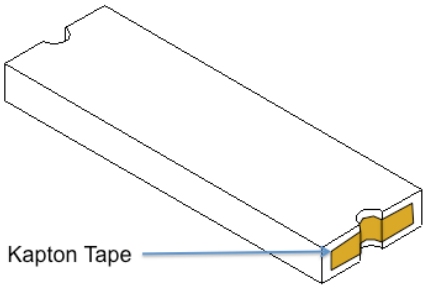

Figure 36. Kapton tape emplacement on the anode/cathode bar.

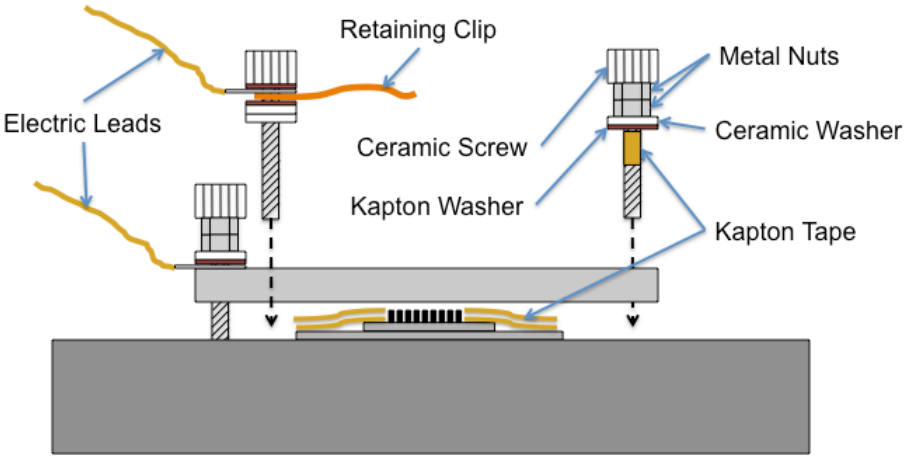

Figure 37. Electric charge isolation procedures.

Unfortunately, tests after this configuration showed no major change in the current leakage problem. Another blank sample was placed on the system with only one piece of tape as the offset layer. During Run 19 this sample arced out at 600 V. Further investigation showed that it arced along the edge of the Kapton

tape. Based on advice from Dr. Niemann, a layer of two strips of Kapton tape was again placed on the sample for standoff, but the layers were offset from each other, and the edges were clean cuts from the inside of the tape using a razor blade to ensure no lint/debris caught on the outer edge of the tape roll could be introduced into the system. It was hoped that offsetting the layers would make it more difficult for the system to arc along the edge of the tape. Figure 38 shows the offset.

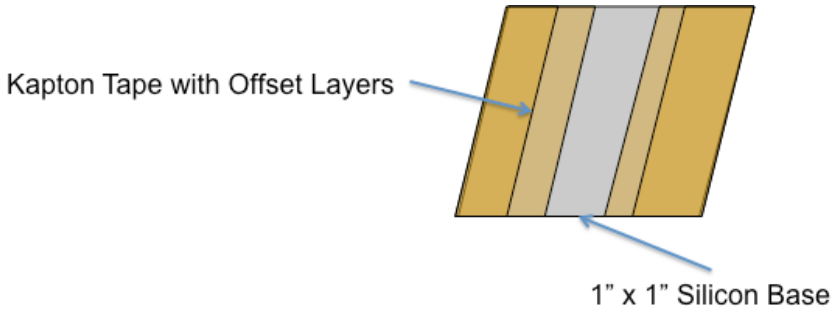

Figure 38. Blank sample with two layers of Kapton tape offset from each other. The exposed edges of the tape were cut from the inside of the roll.

With this final configuration, there was a small arc in Run 20 and a significant amount of arcing in Run 21, but not until 1000 V. When placed back in the vacuum, no arcing was evident for Run 22. Unfortunately, the leakage current problem was not solved at this time.

3. Lessons Learned

The leakage tests did offer a lot of information about the behavior of our system and procedural techniques that needed to be mastered for proper testing. This proved to be invaluable for future experiments.

Among the best lessons learned was the need to minimize the amount of silver epoxy exposed to the system. This affected the mating technique used for all experiments starting with Experiment 4.

The procedure of taping everything to isolate the charges did not seem to solve the problem, but it seemed like a prudent step to take in the future anyway. Staggering the tape and using a fresh cut from the inside of the roll also were good techniques employed throughout the rest of the testing process.

D. EXPERIMENT 3

1. Preparation

The original intention for this experiment was to reload the sample used in Experiment 2 and test again using the lessons learned from the leakage tests. Unfortunately, that sample was scratched during loading, causing the CPAs to touch the bar and short out the system. So, Experiment 3 was set up with Sample 3. A slight modification to the substrate set-up was applied in an effort to minimize the silver epoxy exposed to the system. Figure 39 shows the sample setup just prior to testing.

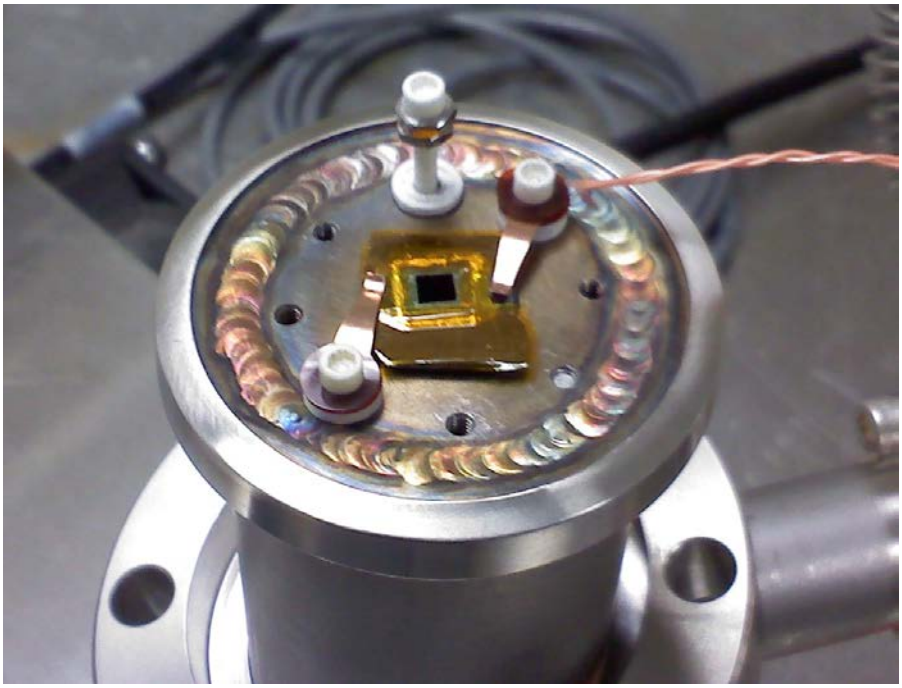

Figure 39. Sample setup for Experiment 3. Note the two small additional strips of Kapton tape used to cover the exposed silver epoxy.

The anode/cathode bar required attention prior to the experiment. All of the arcing that occurred during the leakage test experiments left marks on the bar. This was hand polished away using progressively finer grit sand paper and solutions until the bar was as smooth and flat as possible.

The sample was placed into the chamber and began vacuuming down on August 6, 2010.

2. Test Execution and Results

Nine sweeps were conducted to characterize the CPA enhancement factors for Experiment 3. The parameters for the Fowler-Nordheim tests are shown in Table 10. The results are listed in Table 11.

	Experiment 3	
	Fowler-Nordheim Characterization	
	Date	7 August 2010
	Initial Chamber Pressure	6.80E-8 Torr
	Power Source	Keithley 237
	CPA Height	14 µm
	Gap Distance	113 µm
Runs 1-4	Compliance Level	2.00E-5 A
	Compliance Range	10 µA
	Measurements	550
	Voltage	Linear stair: 0 V to 550 V
Run 5	Compliance Level	2.00E-4 A
	Compliance Range	10 µA
	Measurements	350
	Voltage	Linear stair: 0 V to 350 V
Runs 6-7	Compliance Level	2.00E-4 A
	Compliance Range	100 µA
	Measurements	350
	Voltage	Linear stair: 0 V to 350 V
Runs 8-9	Compliance Level	2.00E-5 A
	Compliance Range	100 µA
	Measurements	350
	Voltage	Linear stair: 0 V to 350 V

Table 10. Experiment 3 test parameters for Fowler-Nordheim characterization.

Experiment 3		
Enhancement Factors		
Sweep	Beta	Gamma
3	4.63E+07	5228
6	4.63E+07	5230
Average	**4.63E+07**	**5229**

Table 11. Experiment 3 enhancement factor results.

Unfortunately, most of the data for the Fowler-Nordheim tests did not save to file. The results show the only two tests that saved properly. However, while the tests showed good behavior and a low turn-on voltage, the enhancement factors are a little inflated. This is most likely a result of the fact that the cutoff voltage was 550 Volts for Sweep 3 and 350 Volts for Sweep 6, and should have been higher. Therefore, the entire portion of the graph that gets measured for the factors is not entirely there.

An additional three tests were conducted in an ionization mode with no flow to check the current leakage. Again, current leakage appeared, stepping from 10^{-10} Amps to 10^{-8} Amps.

As the argon began to flow into the system, we decided to turn it off and check some more no flow ionization runs again. Runs 13 through 16 showed odd behavior, as if it was ionizing something. It is possible that the system was trying to ionize what small amount of residual argon might have remained in the chamber after the pump was turned off. To make sure, a constant voltage of 750 V was applied for Run 17. Unfortunately only Runs 13 and 17 actually saved data.

Table 12 shows the test parameters for the actual conduct of Experiment 3. The initial runs were capped at 900 V. The graph in Figure 40 shows that there was some behavior as the voltage increased, but with each increasing run it took more voltage to make something happen. This is most likely attributed to a conditioning effect, as the uneven portions of the CPA ionize and then either burn off or are pulled away.

Experiment 3	
Argon Ionization Runs 18-20	
Date	7 August 2010
Initial Chamber Pressure	6.80E-8 Torr
Unobstructed Pressure	6.60E-7 Torr
Obstructed Flow Pressure	3.50E-7 Torr
Power Source	Keithley 237
CPA Height	14 μm
Gap Distance	113 μm
Compliance Level	2.00E-5 A
Compliance Range	100 μA
Measurements	900
Voltage	Linear stair: 0 V to 900 V

Table 12. Argon ionization test parameters for Runs 18-20.

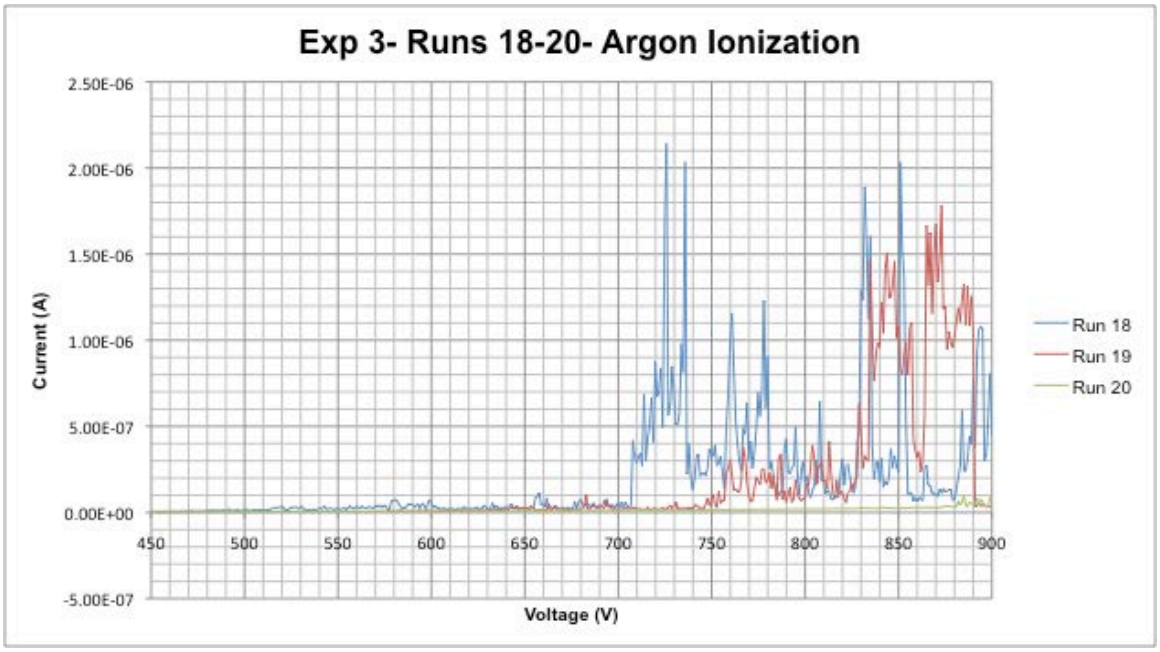

Figure 40. Experiment 3 Argon Ionization Runs 18-20. Note how the behavior exhibited requires more voltage with each successive run.

For Runs 21-24, the voltage was increased to 1100 volts. Most of these runs were relatively uneventful except for Run 23. This particular run exhibited possible ionization around the 1000 volts to 1050 volts range. This behavior is shown in Figure 41.

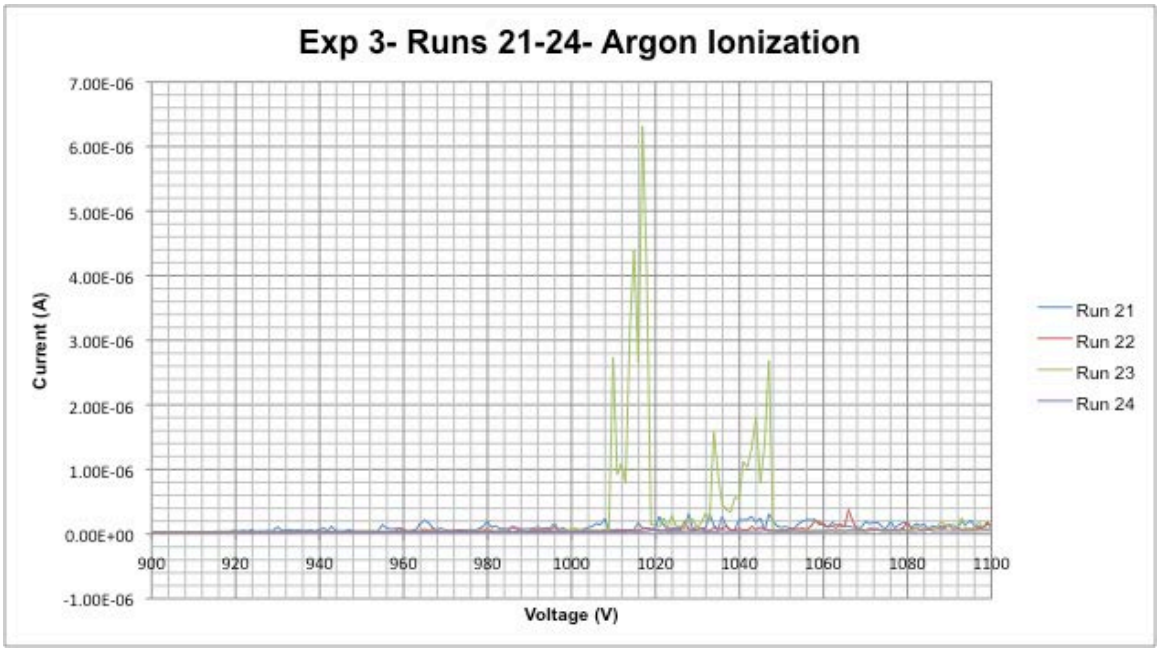

Figure 41. Experiment 3 Argon Ionization Runs 21-24. Note the excitation taking place from 1000 V to 1050 V.

Due to the excitation exhibited during Run 23, a fixed voltage test was conducted for Runs 25 and 26. The parameters for those runs are shown in Table 13. For both of these runs, the intent was to apply a fixed 1000 Volts charge and then vary the flow of gas into the system. If the sample was ionizing at this voltage, it should show ionization when the gas was turned on and nothing when it was turned off. Run 25 showed this behavior exactly. Turning the gas on and off, the sample produced a current of approximately 2.1×10^{-5} Amps each time! In order to produce this, more flow was introduced than previously done before. Chamber pressures due to the flow were on the scale of 10^{-5} Torr as compared to the 10^{-7} Torr ranges used during the linear stair tests. The results of this run are shown in Figure 42.

Experiment 3	
Argon Ionization Runs 25-26	
Date	7 August 2010
Initial Chamber Pressure	6.80E-8 Torr
Unobstructed Pressure	Varied
Obstructed Flow Pressure	Varied
Power Source	Keithley 237
CPA Height	14 μm
Gap Distance	113 μm
Compliance Level	1.00E-4 A
Compliance Range	100 μA
Measurements	2492 (R 25) / 563 (R 26)
Voltage	Fixed Voltage: 1000 V

Table 13. Test parameters for Argon Ionization Runs 25-26.

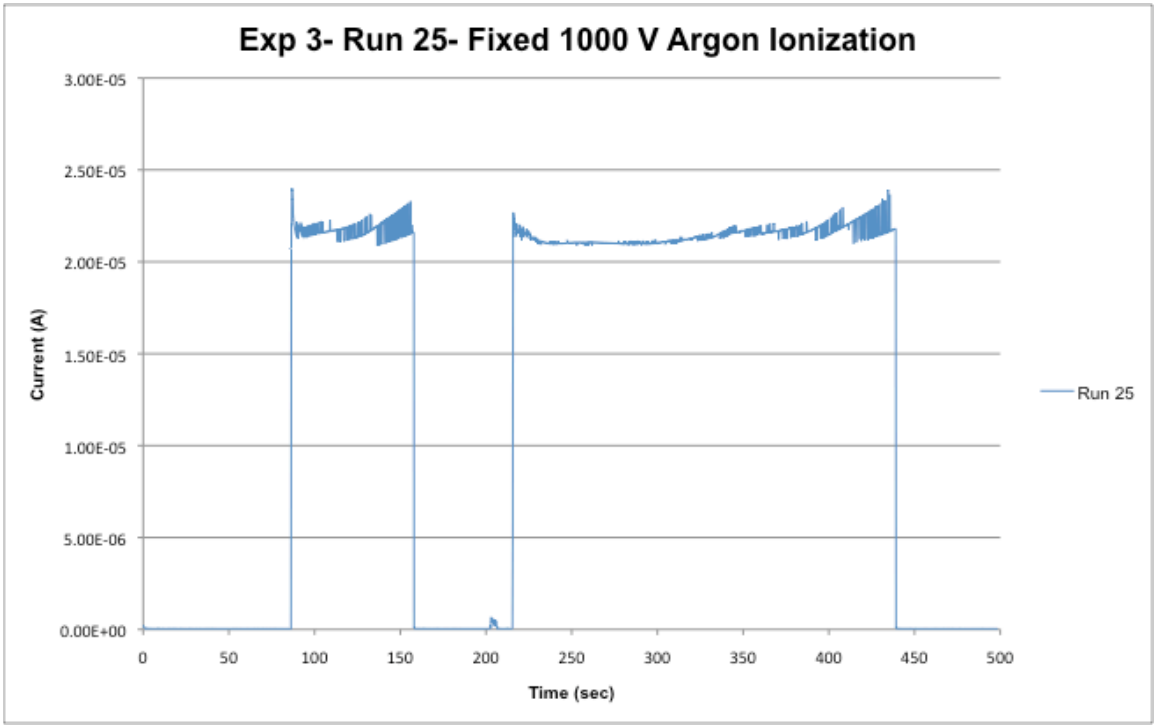

Figure 42. Experiment 3 Argon Ionization Run 25. The peaks occurred when a flow was introduced to the sample at a fixed voltage of 1000 V.

Since Run 25 showed such promising results, another attempt was conducted for Run 26. This time the argon was turned off to allow the chamber to empty and then reintroduced. Careful attempts were made to try and

introduce the flow at an exact pressure. The chamber pressure for the initial unobstructed flow was 5.9 x 10^{-5} Torr and the obstructed flow was 3.4 x 10^{-5} Torr. This time, the sample did show behavior when the gas was turned on, but it immediately jumped to the compliance current level, indicative of a system arcing out. No attempt was made to raise the compliance current any higher to ascertain whether the system was just producing a high current or actually arcing out. This was due to the worry that the sample might be destroyed if it was indeed arcing out. The behavior of Run 26 is shown in Figure 43.

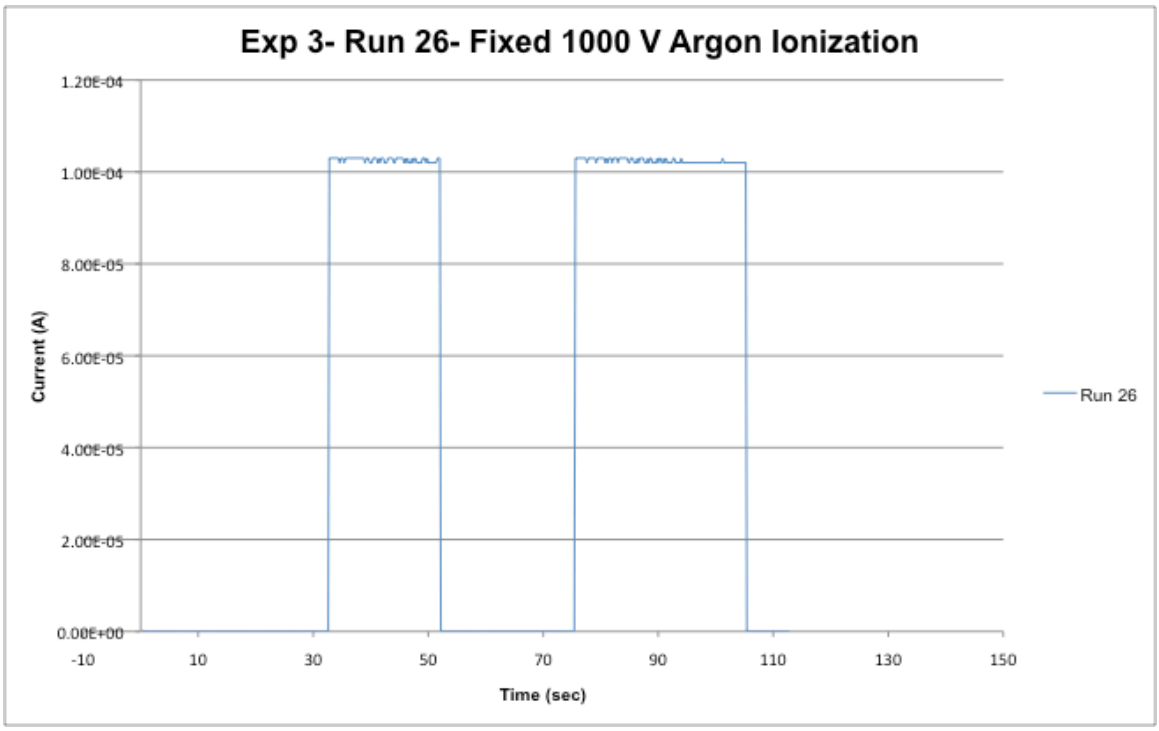

Figure 43. Experiment 3 Argon Ionization Run 26.

Runs 27-29 were linear voltage step tests to 1100 volts. These tests involved varying the flow throughout. Nothing significant was reportable from these tests. Run 30 was an incomplete test. This was intended to be a fixed voltage test at 1050 volts with a variable flow rate. However, during testing the sample exhibited noisy behavior then stopped ionizing. Pressures were fluctuating greatly during this timeframe.

Observation of the sample after testing showed damage around the edges. A side-by-side comparison of the sample before and after testing is shown in Figure 44.

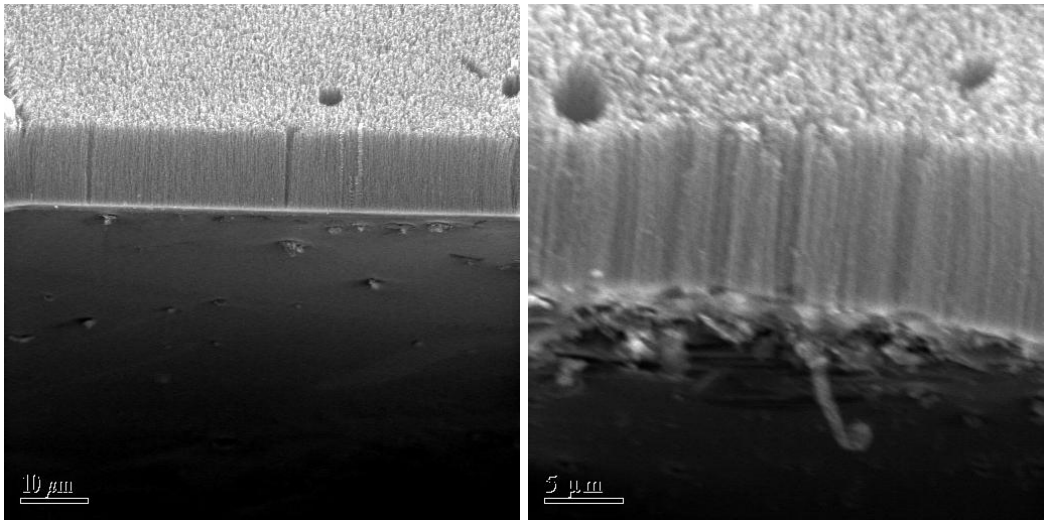

Figure 44. Comparison of the Experiment 3 sample. The picture on the left is prior to testing at a 1300x magnification. The picture on the right is of the same region after testing at a 3000x magnification. Note the significant damage along the edge.

3. Lessons Learned

Experiment 3 showed that ionizing argon in a flow using CPAs for field ionization was possible. This was an important step. One of the major items noted for improvement during this experiment was the measurement of the mass flow rate. The method of trying to determine how much flow was occurring through the hole using only the chamber pressure was later found to be inaccurate once an additional pressure measurement device was introduced to the system. This improved with later experiments.

E. EXPERIMENT 4

1. Preparation

Experiment 4 used Sample 4 for its test. Sample 4 was the first sample that used hydrofluoric acid to etch away its nitride layer instead of breaking it with a needle under a microscope. This sample had 24 μm of growth and nice vertical alignment. The sample was prepared with only one strip of Kapton tape as a gap distance standoff. Sample 4 was also the first sample to have the silver epoxy underneath the small wafer to seal and mate to the larger wafer instead of a bead of epoxy around the base on the outside. The sample was placed into vacuum on August 7, 2010.

2. Test Execution and Results

Test parameters for the Fowler-Nordheim characterization for Experiment 4 are shown in Table 14. The initial sign that something might be wrong was that the chamber pressure was only 4.1 x 10^{-7} Torr after six days of vacuuming down. This was not typical behavior for the chamber, which had proven to drop to that pressure in a manner of only hours. However, an attempt was made to try to characterize the sample anyway.

Experiment 4	
Fowler-Nordheim Characterization	
Date	13 August 2010
Initial Chamber Pressure	4.10E-7 Torr
Power Source	Keithley 237
CPA Height	24 μm
Gap Distance	39.5 μm
Compliance Level	2.00E-5 A
Compliance Range	10 μA
Measurements	550
Voltage	Linear stair: 0 V to 550 V

Table 14. Experiment 4 test parameters for Fowler-Nordheim characterization.

The first run went well. There was an odd spike where the sample started field emitting at 250 volts, stopped, and then began again at around 300 volts. However, this is a good turn-on voltage, so all looked well. The second run did not go as well. As soon as voltage was applied, there was an immediate jump to the compliance current. This indicated that there was most likely a short circuit. The sample was pulled to investigate and it was found that a piece of lint lodged itself in the hole. This piece of lint created a short circuit. There was no way to remove it from the hole because it was to small to grab. Table 15 shows the enhancement factors for the one run that was completed.

Experiment 4		
Enhancement Factors		
Sweep	Beta	Gamma
1	3.62E+07	1428

Table 15. Experiment 4 enhancement factor results.

The lint damaged the inside of the hole and appeared to cause a burnout. Figure 45 shows a side-by-side view of the sample before and after the test. Figure 46 shows the burn across the sample and the damage caused by the lint.

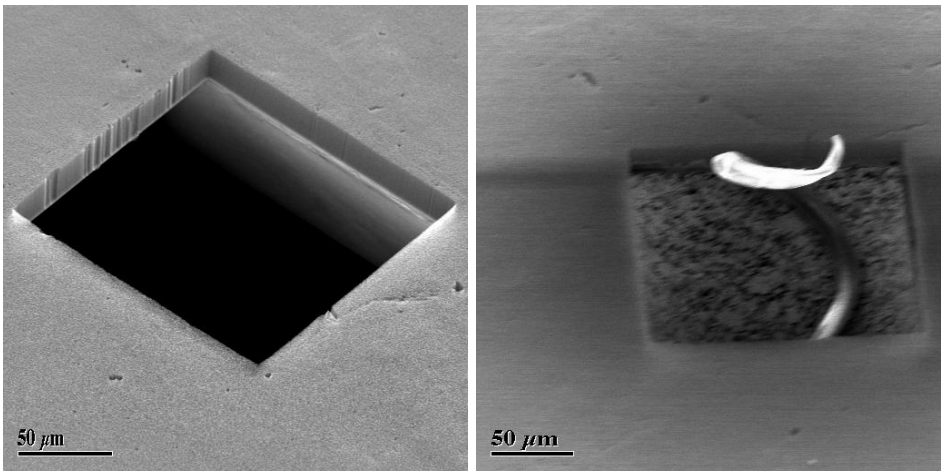

Figure 45. Experiment 4 results. The picture on the left is a picture of the sample prior to testing at 400x magnification. The picture on the right is the sample after testing at 350x magnification.

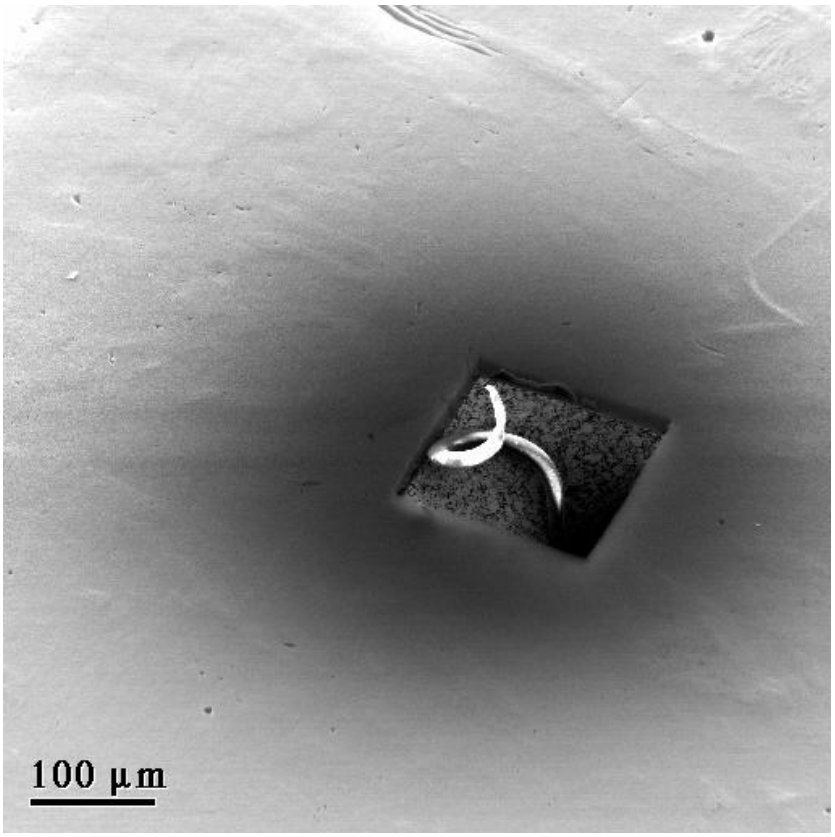

Figure 46. Experiment 4 results. This picture is taken at 150x magnification. Notice the burn across the pillar array as well as the damage caused by the lint.

3. Lessons Learned

The biggest lesson learned during this experiment was the importance of keeping the sample and test area clean. However, during the setup of the next experiment it became apparent that the leak valve was broken. This was the reason the pressure was uncharacteristically high and a possible introduction point for the piece of lint.

F. EXPERIMENT 5

1. Preparation

Once the leak valve was discovered broken, a replacement was immediately purchased to allow for continued testing. This new part was mounted and immediately ready for the Experiment 5 sample the next morning. Experiment 5 used Sample 5, which had a growth of 25.5 μm. The sample was setup similar to Experiment 4 with one piece of Kapton tape as the gap distance standoff. The sample was placed into vacuum on August 14, 2010.

2. Test Execution and Results

The first four runs for the Fowler-Nordheim characterization showed no response. The sample was pulled from the chamber to reveal that the electric leads had snapped off during the loading process. The sample was again loaded and vacuumed down, but the next two runs also showed no response. The sample was pulled out a second time and inspected. After testing the sample with a multi-meter, it became apparent that the piece of silicon with the drilled hole used for mounting the smaller piece of silicon was not the same type used previously. This particular silicon wafer was not conductive, therefore no charge was getting to the CPA. This was remedied by painting a thin layer of silver epoxy to allow for conduction from the retaining clip to the CPA. This repair work is shown in Figure 47.

Figure 47. Thin film of silver epoxy applied to the Experiment 5 sample to allow conduction of the charge from the retaining clip to the CPA.

After ensuring the silver epoxy did work, two pieces of Kapton tape were placed onto the sample as a gap distance standoff. While replacing the sample onto the test base, the electric lead for the cathode bar was moved from the screw and taped to the top of the base instead. This allowed for more even placement of the bar over the test sample. Interestingly enough, this seemed to have an effect of reducing the leakage current. The charge was now going directly to the bar and in no way connected to the screw. Since the leakage current was affected, this indicates that the current was indeed leaking through the ceramic screw. Figure 48 shows an illustration of the new placement for the electric lead.

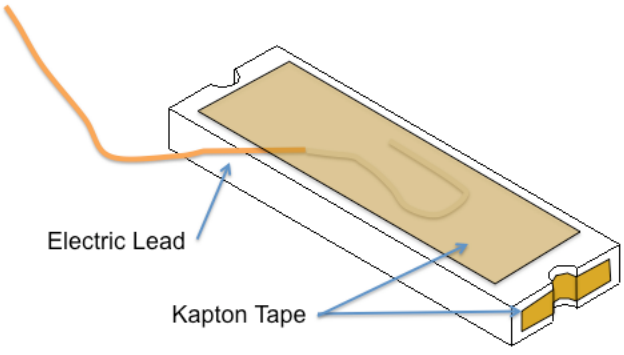

Figure 48. Illustration of the new placement for the electric lead on the bar.

The sample was placed back into the chamber for the third time. Table 16 shows the test parameters for the Fowler-Nordheim characterization runs. Table 17 shows the results. An adjusted average for the Beta and Gamma factors is shown that removes Sweep 1 from the average since it showed signs of conditioning during its first run.

Experiment 5	
Fowler-Nordheim Characterization	
Date	14 August 2010
Initial Chamber Pressure	4.00E-7 Torr
Power Source	Keithley 237
CPA Height	25.5 μm
Gap Distance	101.5 μm
Compliance Level	2.00E-5 A
Compliance Range	10 μA
Measurements	550
Voltage	Linear stair: 0 V to 550 V

Table 16. Experiment 5 test parameters for Fowler-Nordheim characterization. Note: the first sweep stepped to 1100 V instead of 550 V.

Experiment 5		
Enhancement Factors		
Sweep	**Beta**	**Gamma**
1	9.79E+06	994
2	3.41E+07	3463
3	3.64E+07	3690
4	3.48E+07	3529
5	4.42E+07	4483
Average	**3.18E+07**	**3231.8**
Adjusted AVG	**3.74E+07**	**3791.3**

Table 17. Experiment 5 enhancement factor results. An adjusted average is shown that only averages Sweeps 2-5 since Sweep 1 had some conditioning.

The ionization runs began with Run 12. The test parameters for Runs 12-15 are shown in Table 18. These runs showed the typical conditioning shown in the earlier experiments. Early turn-on voltages were seen with an increase to

compliance. Each successive run required more voltage to see excitement take place. Figure 49 shows the graph for these first runs.

Experiment 5	
Argon Ionization Runs 12-15	
Date	14 August 2010
Initial Chamber Pressure	4.40E-7 Torr
Unobstructed Pressure	5.30E-6 Torr
Obstructed Flow Pressure	3.00E-6 Torr
Power Source	Keithley 237
CPA Height	25.5 μm
Gap Distance	101.5 μm
Compliance Level	2.00E-5 A
Compliance Range	100 μA
Measurements	1100
Voltage	Linear stair: 0 V to 1100 V

Table 18. Experiment 5 test parameters for Runs 12-15.

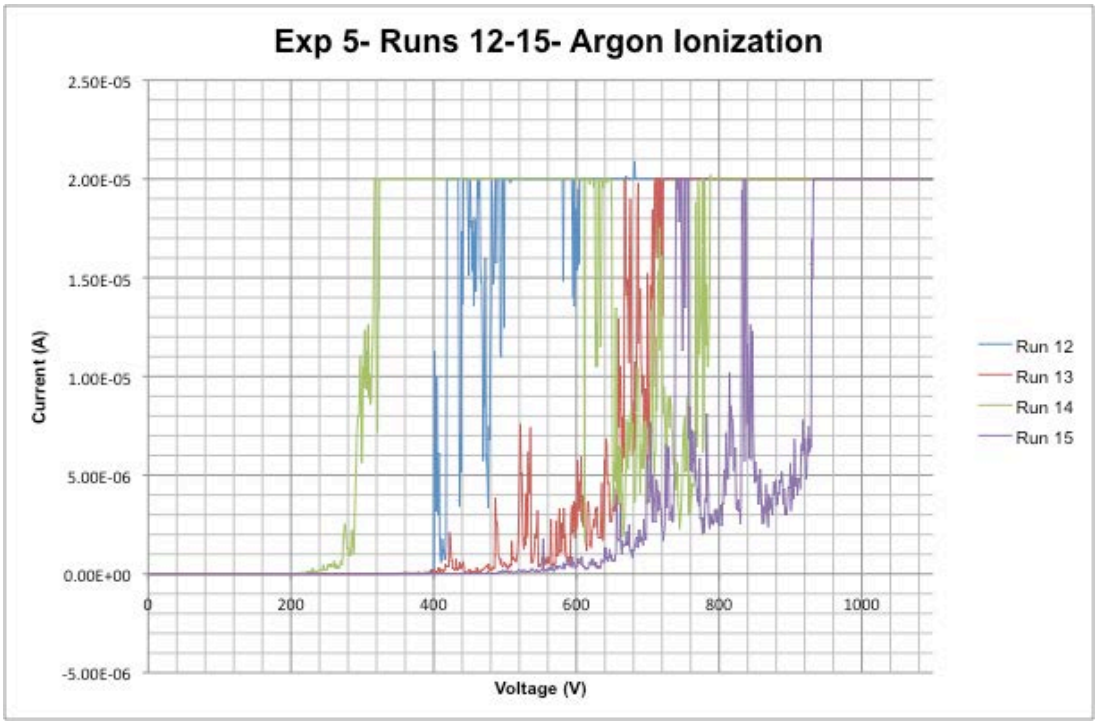

Figure 49. Experiment 5 Argon Ionization Runs 12-15.

Run 16 was conducted with a fixed voltage of 1000 volts. This run had a variable flow rate to see if the current would change based on the flow. The current reacted accordingly, but the data did not save.

Run 17 was similar, but with a fixed voltage of 800 volts. For this run, the chamber was evacuated and brought to a starting pressure of 3.7 x 10^{-7} Torr. Argon was then let into the chamber. The unobstructed flow pressure was 5.3 x 10^{-6} Torr and the obstructed flow pressure was 2.3 x 10^{-5} Torr. The flow was then turned off and the pressure reverted to an unobstructed flow pressure of 3.8 x 10^{-7} Torr. Finally, the flow was turned back on and the obstructed flow pressure was 1.6 x 10^{-5} Torr. Throughout the run, the sample responded appropriately, although the current reached the compliance level. Figure 50 shows the response of the sample during Run 17.

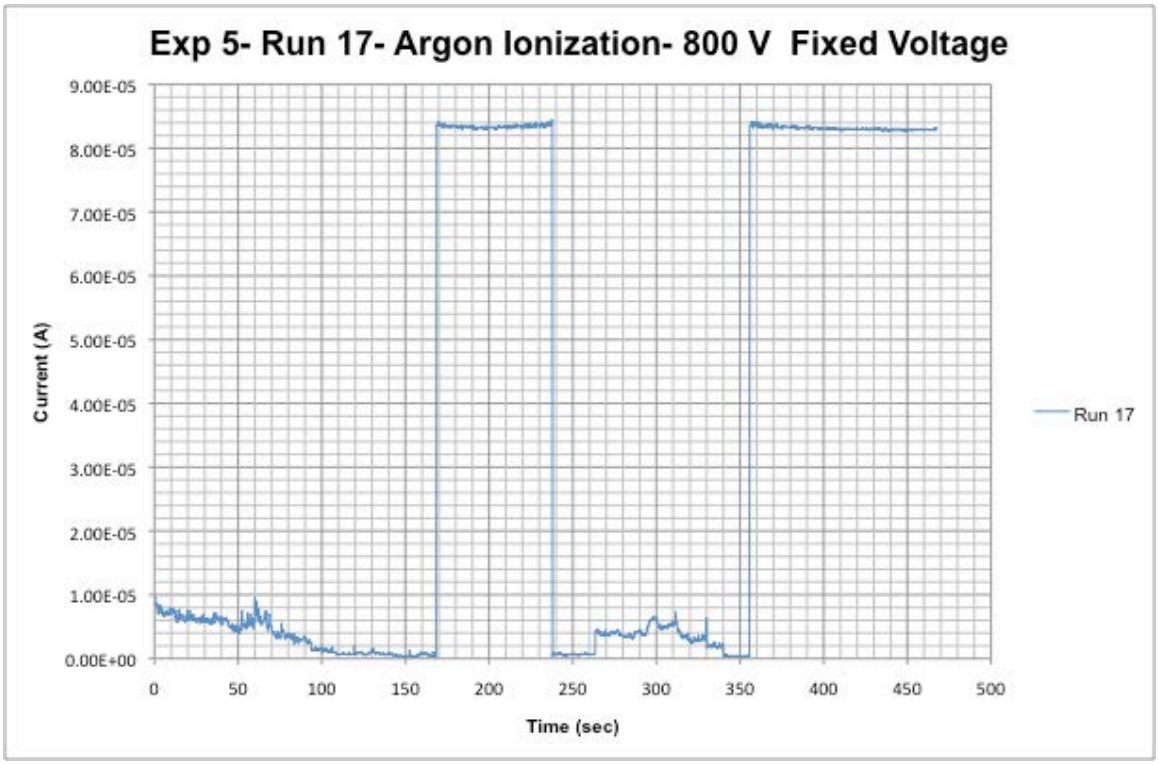

Figure 50. Experiment 5 Argon Ionization Run 17. This run was conducted at a fixed voltage of 800 V with a variable flow rate.

At this point, it appeared that the sample might truly be trying to ionize. Run 18 through Run 23 were each a run varying a specific parameter to try and determine the best way to characterize this sample. The initial compliance value for these runs was 8.00×10^{-5} Amps. The compliance range was 100 μA.

Run 18 focused on a linear voltage step with a higher flow rate represented by a chamber pressure of 5.6×10^{-5} Torr. Run 18 jumped to the compliance current at 350 volts.

Run 19 was the same test but with a low gas flow rate. This particular run jumped to the compliance current at 700 volts.

Run 20 was a repeat of Run 18 with similar results.

Run 21 was a repeat of Run 18, but the compliance value was changed to 1.00×10^{-4} Amps. The current reached the compliance current.

Run 22 was a similar run but the compliance range was changed to 1.00×10^{-3} Amps. The current again reached the compliance current.

Run 23 was a similar run with the compliance value set to 1.00×10^{-3} Amps and the compliance range was changed to 2.0×10^{-3} Amps. This run hit the compliance current at 375 volts.

Runs 24-26 exhibited really nice behavior indicative of ionization. The chamber pressure ranges due to the mass flow rate were on the scale of 4.60×10^{-6} Torr and 2.20×10^{-6} Torr. These runs showed two major plateaus of ionization at approximately 2.50×10^{-5} Amps from 900-1075 Volts and 4.50×10^{-5} Amps from 1075-1100 Volts. Table 19 shows the test parameters for these runs and Figure 51 shows the results.

Experiment 5	
Argon Ionization Runs 24-26	
Date	14 August 2010
Unobstructed Pressure	Variable
Obstructed Flow Pressure	Variable
Power Source	Keithley 237
CPA Height	25.5 μm
Gap Distance	101.5 μm
Compliance Level	2.00E-2 A
Compliance Range	10 mA
Measurements	1100
Voltage	Linear stair: 0 V to 1100 V

Table 19. Experiment 5 test parameters for Runs 24-26.

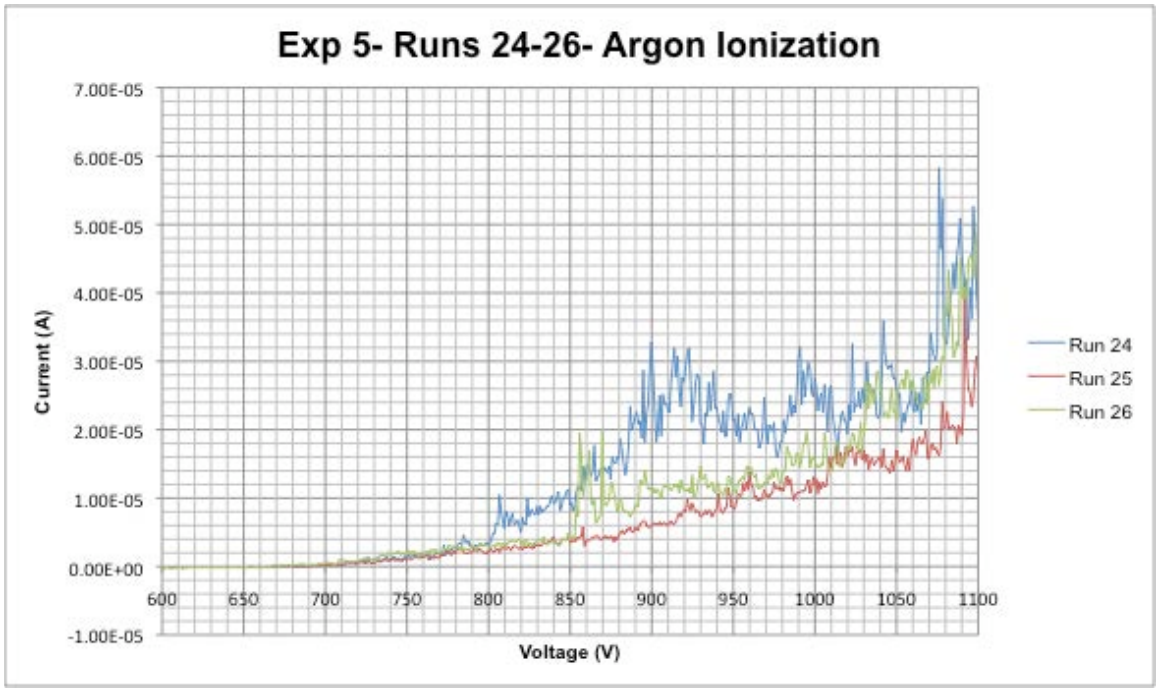

Figure 51. Experiment 5 results for Runs 24-26.

For Runs 27-30, the flow rate was lowered again. This time the chamber pressure was approximately 7.5 x 10^{-7} Torr. Test parameters for these runs were the same as for Runs 24-26. The results showed a similar pattern to Runs 24-26 but more of a gradual slope instead of plateaus. Figure 52 shows the results.

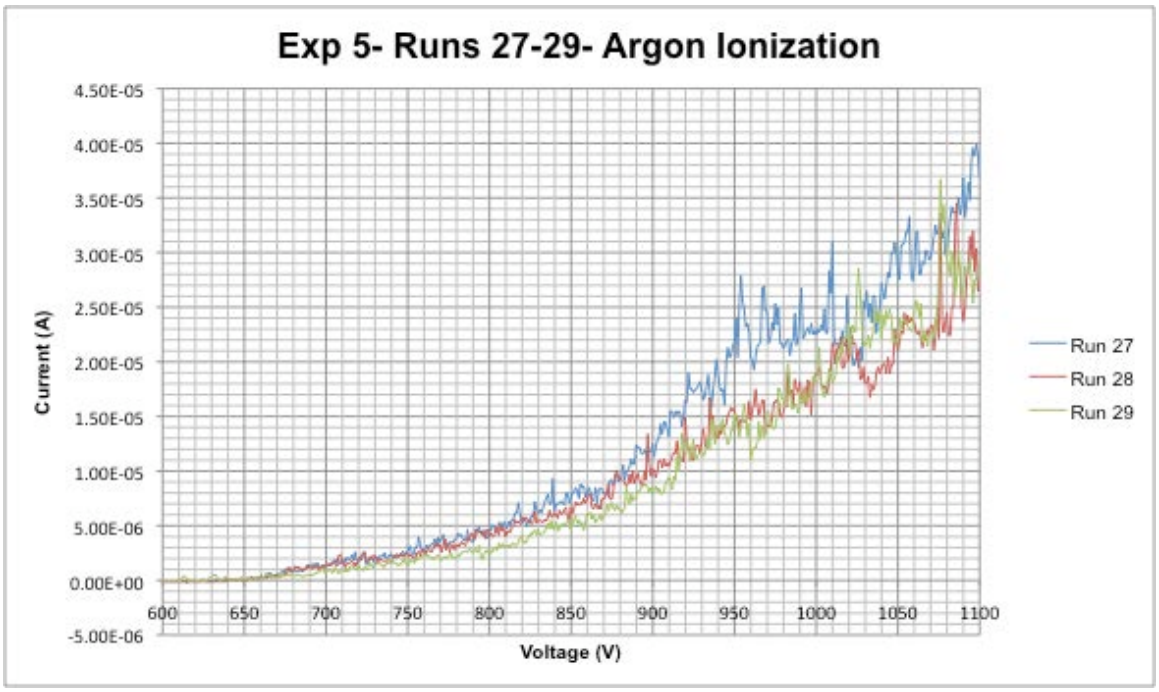

Figure 52. Experiment 5 results for Runs 27-29. These runs were conducted at a lower flow rate than Runs 24-26.

For Runs 30-32, the flow rate was turned off. Based on the results though, there must have been some residual argon left in the chamber. These results are shown in Figure 53.

The peak of almost 4.25 x 10^{-5} Amps prompted the fixed voltage run at 1100 Volts for Run 33. This run showed a steady current of approximately 4.80 x 10^{-5} Amps during a no-flow test. Since this value did not reach the compliance current, it is safe to assume that no arcing took place. It is assumed that residual argon remaining in the chamber was ionized during this test. This test result is shown in Figure 54.

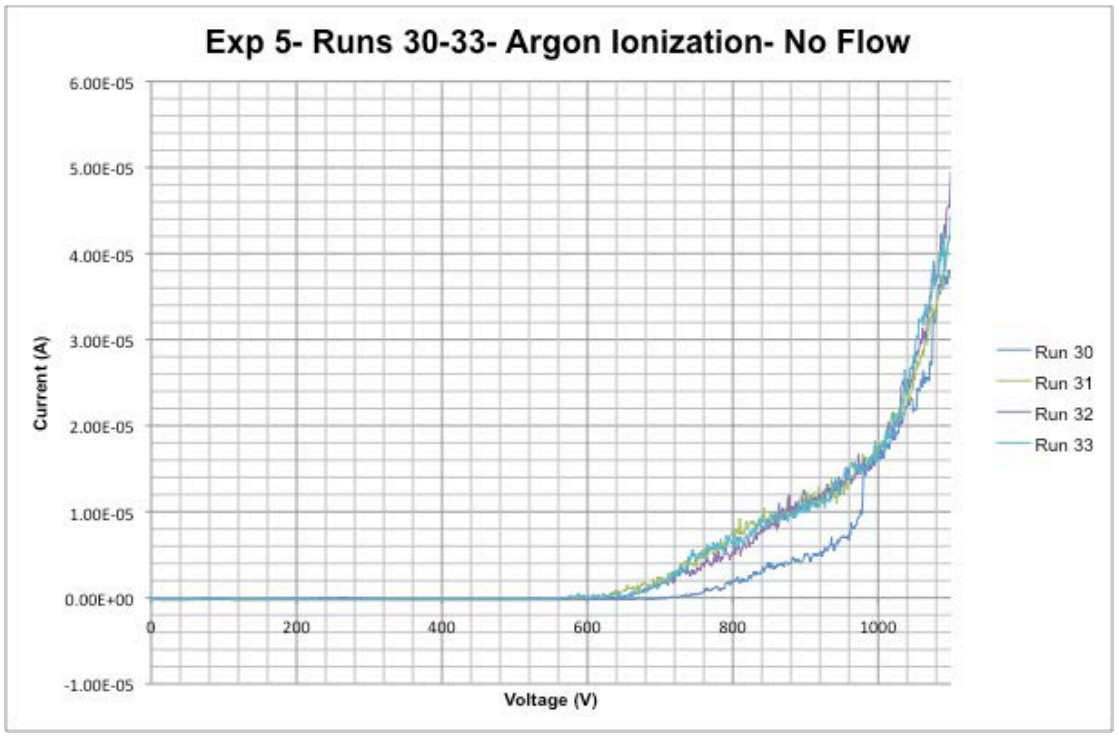

Figure 53. Experiment 5 results for Runs 30-33. These runs were conducted with no flow rate.

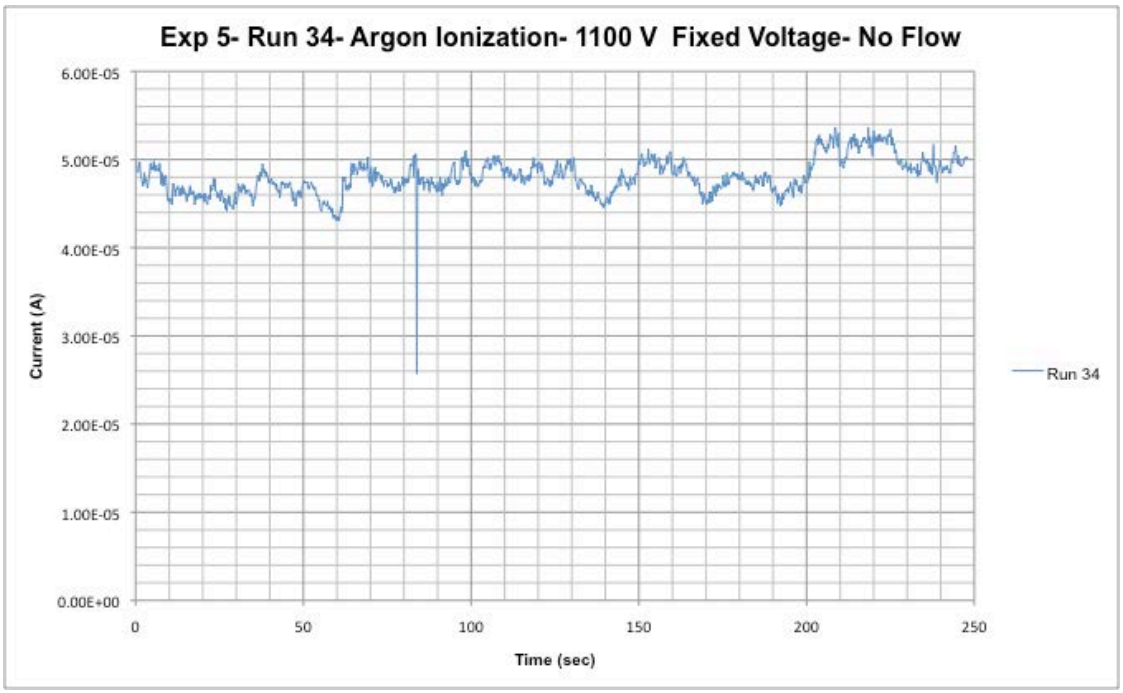

Figure 54. Experiment 5 results for Run 34.

Review of the sample using the SEM showed some damage to the CPA. These areas most likely had CNTs taller than the rest of the array. The areas around the hole showed no damage at all. Figure 55 shows a side-by-side image of the Experiment 5 sample both before and after testing. Figure 56 shows an image of some of the damage done to the array.

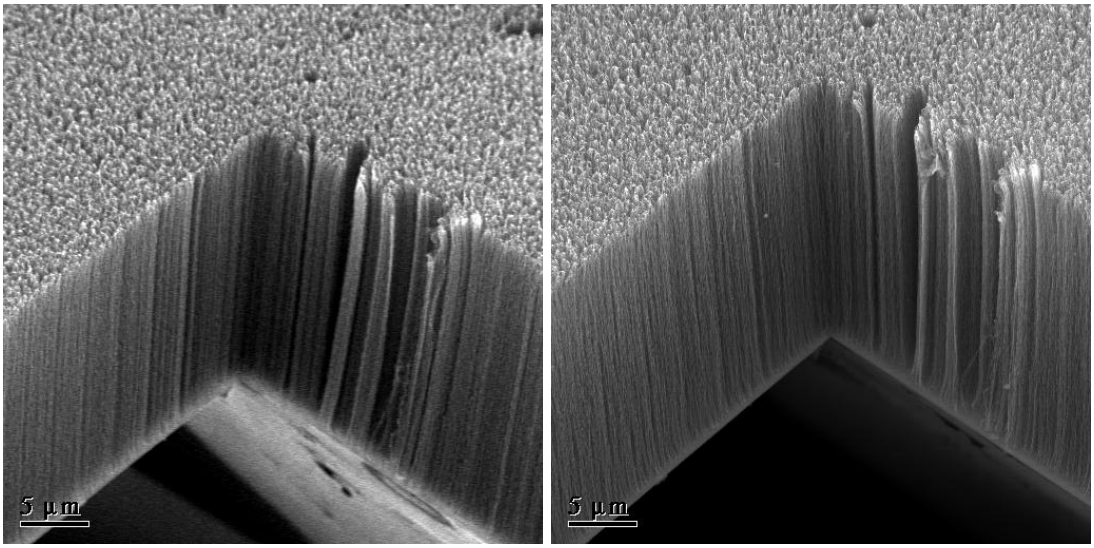

Figure 55. Comparison of the Experiment 5 sample before and after testing. The picture on the left is prior to testing. Both are at 2500x magnification.

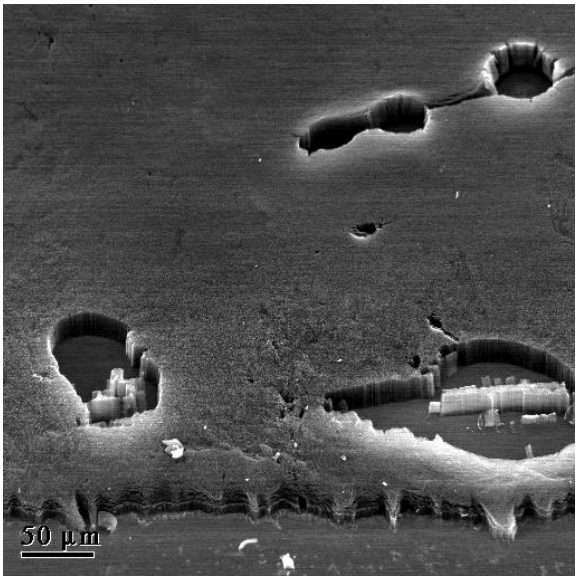

Figure 56. Image showing damage to the Experiment 5 array. These areas most likely had CNTs taller than the rest of the array. Picture is at 250x magnification.

3. Lessons Learned

Attaching the electrode to the top of the bar instead of the screw was beneficial in many ways. It reduced the leakage current exhibited in the system, allowed for better placement of the bar over the substrate, and facilitated easier loading of the system.

G. EXPERIMENT 6

1. Preparation

Attempts were made throughout the course of the experiments to try to characterize the flow rate of the argon in order to determine a mass utilization factor for the samples. This was difficult to do with only one pressure sensor. A new sensor was mounted for this experiment that measured the pressure behind the sample. This new sensor was mounted on a four-way cross directly in between the leak valve and the test base mount. Figure 57 shows the placement of this new device.

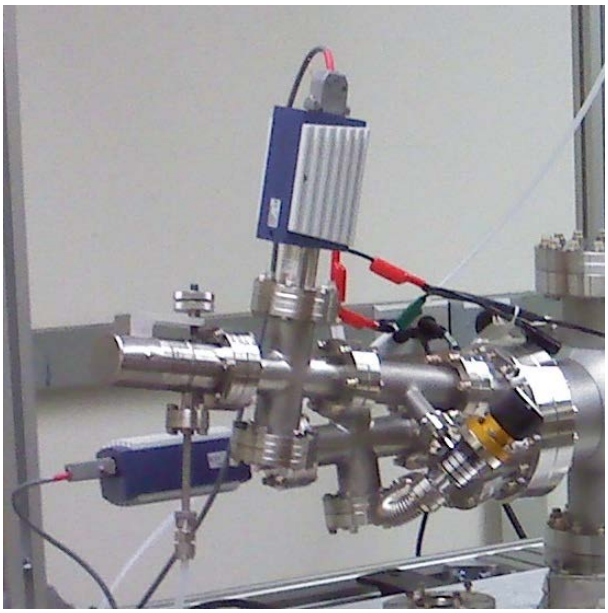

Figure 57. Placement of back pressure sensor. The sensor is the blue and gray box on top of the four-way cross. The chamber sensor can be seen in the background.

To prevent the problems experienced during Experiment 5, the drilled silicon wafer used as the base was first coated with 25 nm of nickel to ensure that the charge would conduct across its surface. Sample 7 was in the process of being mounted on the large wafer when it fell on the floor and scratched its surface. Sample 8 was mounted instead. Sample 8 was a very nice sample with 62.2 μm of growth. A two-strip layer of Kapton tape was used for the gap distance standoff for this experiment. The sample was placed into the chamber and vacuumed down on August 15, 2010.

2. Test Execution and Results

The Fowler-Nordheim characterization runs were the first and only tests conducted on this sample. Table 20 shows the test parameters for these tests. The sample showed very nice, consistent behavior and promised to be one of the best samples yet. The results of the enhancement factor characterization are shown in Table 21.

Experiment 6	
Fowler-Nordheim Characterization	
Date	15 August 2010
Initial Chamber Pressure	1.00E-7 Torr
Initial Back Pressure	7.80E-7 Torr
Power Source	Keithley 237
CPA Height	62.2 μm
Gap Distance	64.8 μm
Compliance Level	2.00E-4 A
Compliance Range	100 μA
Measurements	1100
Voltage	Linear stair: 0 V to 1100 V

Table 20. Experiment 6 test parameters for Fowler-Nordheim characterization.

Experiment 6		
Enhancement Factors		
Sweep	**Beta**	**Gamma**
1	6.47E+07	4191
2	3.82E+07	2475
3	3.89E+07	2521
4	4.86E+07	3149
5	5.98E+07	3878
6	2.53E+07	1640
Average	**5.51E+07**	**3570.8**

Table 21. Experiment 6 enhancement factor results.

With such promising results, Experiment 6 held high hopes for great ionization results. However, when the direction of charge was switched from field emission mode to ionization mode, the sample immediately shorted out. A second attempt gave the same result. The sample worked fine though when the system was put back into field emission mode. Fearing another piece of foreign debris was introduced into the system like Experiment 4, the sample was pulled for inspection.

The sample did indeed have a piece of lint hair caught in the Kapton tape standoff layer. The piece of lint carried a positive charge, so in field emission mode it wanted to stay close to the negatively charged substrate. But, when the leads were switched for ionization mode and the substrate was positively charged, the lint hair was repelled away from the substrate and attracted to the negatively charged bar. This created the short circuit.

The tape was carefully removed and new pieces were cut for replacement, but the surface of the CPA sample was scratched while emplacing the tape. This disturbed the sample to a point that it could no longer be used. Figure 58 shows a picture of the Experiment 6 sample prior to testing.

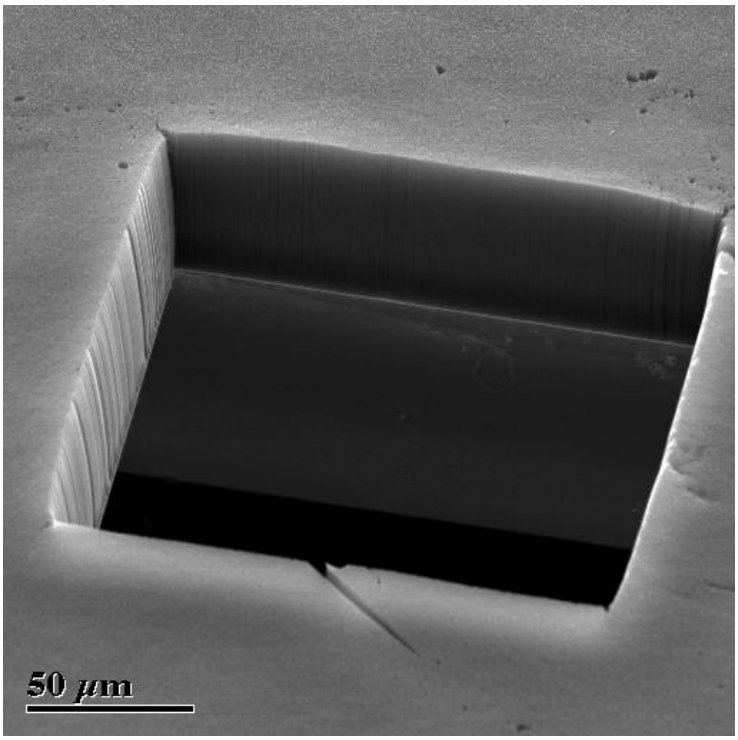

Figure 58. Experiment 6 sample prior to testing. This picture is taken at 450x magnification.

3. Lessons Learned

This was a repeated lesson learned from Experiment 4. Having a clean work area and clean tape would have prevented the need to pull out the sample and risk damage due to handling.

H. EXPERIMENT 7

1. Preparation

Experiment 7 used Sample 6 for its test. This was a nice sample with 26 μm of growth. This sample used two strips of Kapton tape as the gap distance standoff. The sample was placed into vacuum on August 15, 2010.

2. Test Execution and Results

For this experiment, two ion characterization runs were initially conducted with no argon flow. This was followed with six attempted Fowler-Nordheim characterization runs. No significant activity was noticed in any of these runs. A complete checkout of the system showed that the alligator clips connecting the power source to the electric leads uncoupled. This meant no power was getting to the substrate. The problem was fixed and the system was prepared for its Fowler-Nordheim characterization. Table 22 shows the test parameters and Table 23 shows the results for this characterization.

Experiment 7	
Fowler-Nordheim Characterization	
Date	15 August 2010
Initial Chamber Pressure	8.00E-7 Torr
Initial Back Pressure	5.80E-6 Torr
Power Source	Keithley 237
CPA Height	26.0 µm
Gap Distance	101.0 µm
Compliance Level	2.00E-5 A
Compliance Range	100 µA
Measurements	550
Voltage	Linear stair: 0 V to 550 V

Table 22. Experiment 7 test parameters for Fowler-Nordheim characterization.

Experiment 7		
Enhancement Factors		
Sweep	**Beta**	**Gamma**
1	2.23E+07	2249
2	3.19E+07	3219
3	2.84E+07	2867
4	3.48E+07	3513
Average	**2.35E+07**	**2369.6**

Table 23. Experiment 7 enhancement factor results.

The sample showed reasonably nice results for the Beta and Gamma enhancement factors. An ionization characterization run was completed (Run 13) with no flow to observe the behavior of the system prior to flowing the gas in. There was a leakage current present, but nothing else significant to report.

As the argon gas was released into the chamber for the first ionization runs, the pressures were recorded at 60-second intervals. The vacuum remained on during this entire time. Table 24 shows the measured pressures due to flow rates.

Experiment 7		
Flow Measurements		
	Chamber Pressure	Back Pressure
Initial No Flow	5.10E-7 Torr	3.60E-6 Torr
Initial Unobstructed Flow	1.00E-6 Torr	8.90E-5 Torr
Obstructed - 60 sec	5.90E-7 Torr	6.20E-3 Torr
Obstructed - 120 sec	6.90E-7 Torr	9.10E-3 Torr
Obstructed - 180 sec	7.50E-7 Torr	1.10E-2 Torr
Obstructed - 240 sec	7.90E-7 Torr	1.20E-2 Torr
Obstructed - 300 sec	8.10E-7 Torr	1.30E-2 Torr
Obstructed - 360 sec	8.50E-7 Torr	1.40E-2 Torr

Table 24. Experiment 7 measured flow rate pressures.

Runs 14-17 were the first argon ionization runs. These runs were conducted using a linear step of voltage from 0 Volts to 1100 Volts. Throughout the course of these runs, the system never reached a high enough voltage to ionize the argon gas. It is possible that there was a greater gap distance than the measured distance because when the sample was pulled the bar was looser than it should have been. This indicates that if it was not tightened down properly, the distance may have been a few microns more than expected which would have required a greater applied voltage to reach the necessary electric field required for ionization. Table 25 shows the test parameters for these runs. Figure 59 shows the results.

Experiment 7	
Argon Ionization Runs 14-17	
Date	15 August 2010
Initial Chamber Pressure	8.70E-7 Torr
Initial Back Pressure	1.50E-2 Torr
Power Source	Keithley 237
CPA Height	26.0 μm
Gap Distance	101.0 μm
Compliance Level	2.00E-5 A
Compliance Range	100 μA
Measurements	1100
Voltage	Linear stair: 0 V to 1100 V

Table 25. Experiment 7 test parameters for Runs 14-17.

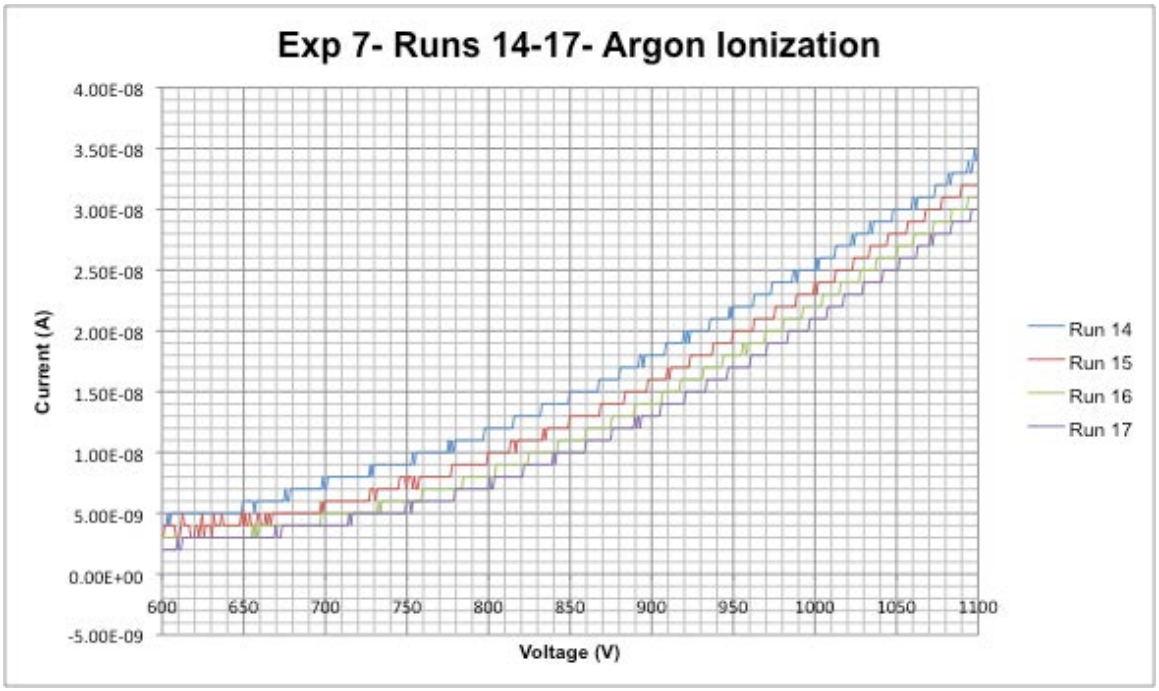

Figure 59. Experiment 7 test results for Runs 14-17.

Since the Keithley power supply was not capable of providing voltages greater than 1100 Volts, we had to move to a different power supply. A Matsusada AU 15R2 15 kV, 2 mA source was used to provide the higher voltages required. The one problem with this is that the Matsusada did not

possess the same level of feedback control capability as the Keithley. When using the Keithley, if the system reached the compliance current, the power source immediately cut the current supply to prevent damage to the structure. The Matsusada does the same thing, but not as quickly, and at much higher voltages. This definitely affected the sample.

Runs 18 and 19 were the only runs conducted using the Matsusada. Table 26 shows the test parameters for these runs. The power supplied to the system ended up destroying the sample. It is possible that the system created a dense argon plasma that ended up sputtering off the CNTs from the substrate. Figure 60 shows the results of the two runs. As can be seen in the graph, Run 19 shows absolutely no activity because the CNTs were removed by that time. Figure 61 shows the extensive damage caused to the sample.

Experiment 7	
Argon Ionization Runs 18-19	
Date	15 August 2010
Initial Chamber Pressure	7.40E-7 Torr
Initial Back Pressure	1.40E-2 Torr
Power Source	Matsusada AU 15R2
CPA Height	26.0 μm
Gap Distance	101.0 μm
Compliance Level	2.00E-5 A
Measurements	700
Voltage (Run 18)	Linear stair: 800-1500 V
Voltage (Run 19)	Linear stair: 1000-1700 V

Table 26. Experiment 7 test parameters for Runs 18-19.

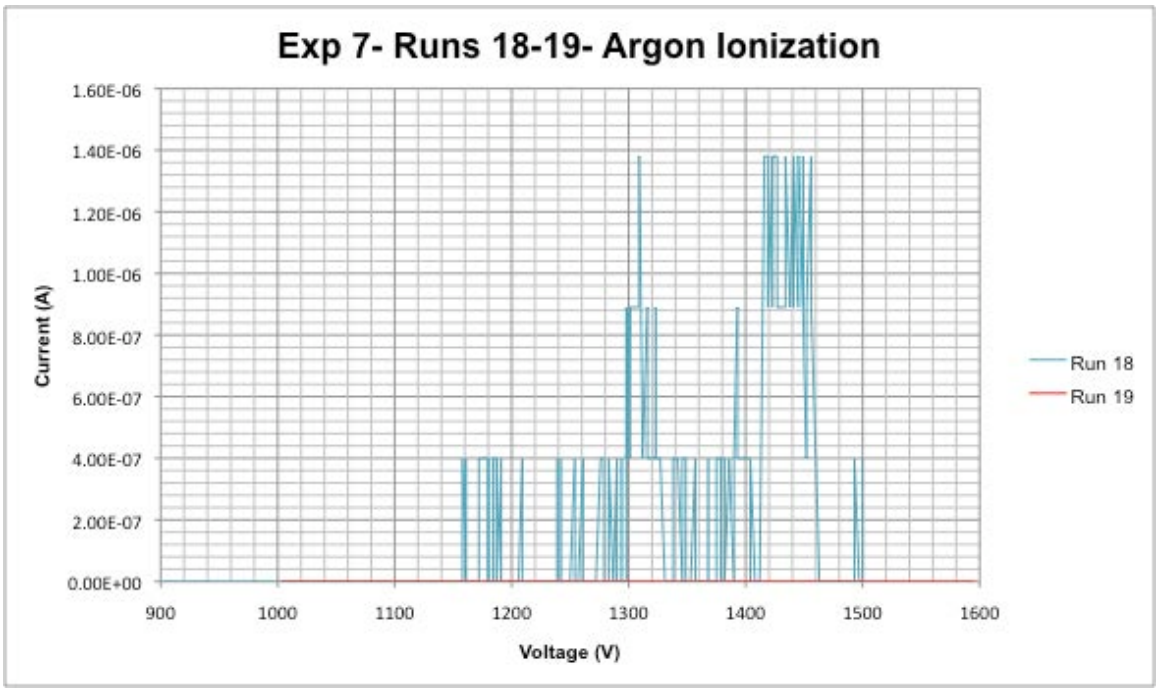

Figure 60. Experiment 7 test results for Runs 18-19.

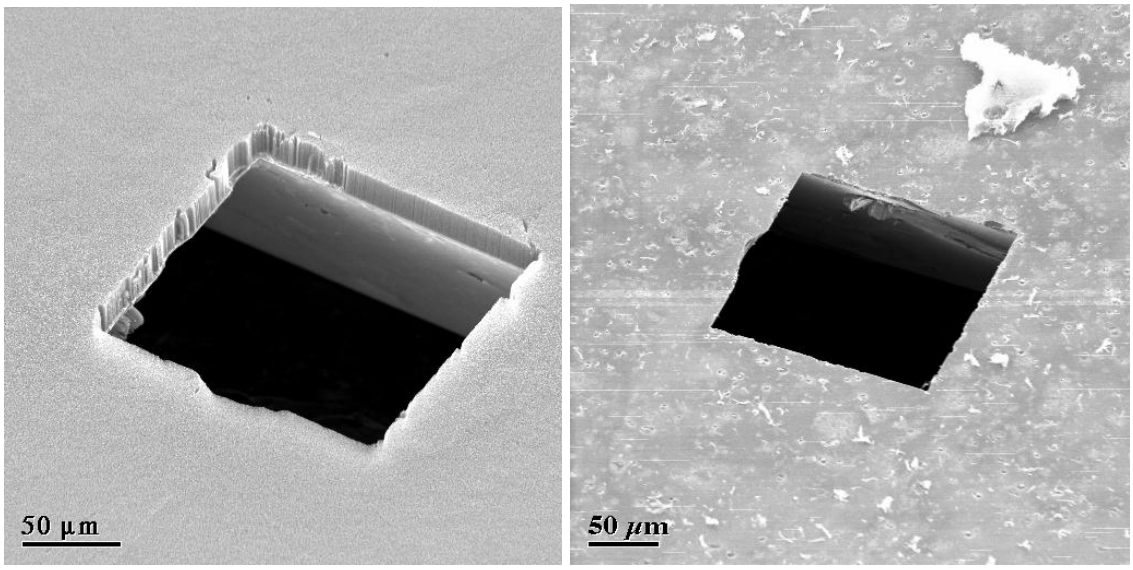

Figure 61. Side-by-side comparison of the Experiment 7 sample. The picture on the left is at 350x magnification. The picture on the right, taken after testing, is at 250x magnification. Note the extensive damage and lack of almost any CNTs remaining on the substrate.

3. Lessons Learned

Control of the applied electric field was the best lesson learned during this experiment. The use of the Matsusada power supply introduced a power system that accounted for no errors. This destroyed the sample. Future space systems that might employ this type of propulsion would need to have feedback mechanisms similar to the Keithley power supply to ensure the propulsion system is not totally destroyed with one surge of power.

I. MASS FLOW RATE CALCULATIONS

The additional pressure sensor was added to the system too late to provide mass flow rate data for the successful experiments. Attempts were made to try and determine the mass flow rate using the pressure change in the chamber when there was one gauge, but this was done while the vacuum was operating, so those values were incorrect.

On September 10, 2010, three more tests were conducted on the system to characterize the coefficient of drag (C_d) for the 200 μm by 200 μm pre-etched hole. With this data, future tests will be able to determine the mass flow rate using the back pressure gauge. The experimentally determined C_d for the 200 μm by 200 μm hole is 2.04.

Knowing the mass flow rate will enable future users to determine what the maximum current should be and ultimately what the achieved propellant utilization factor is. All equations and data for the test are shown in Appendix G.

VI. CONCLUSION AND RECOMMENDATIONS

A. SUMMARY

The first goal of this thesis, to build a device for testing carbon nanotube pillar array samples in a flow, was successfully accomplished. The test device is operational, and was proven over the course of several experiments. It is expandable and was built with the future in mind. Further research efforts will be able to concentrate on building the actual test samples without having to worry about the testing apparatus.

The second goal of this thesis was to master the techniques for and build a carbon nanotube pillar array sample for application as a field ionized ion thruster. This sample had to test the theory that a charge applied to the base of a carbon nanotube pillar array will ionize argon flowing along the length of its tubes. This thesis successfully proved this theory.

The third goal of this thesis was to determine the propellant utilization factor. The thesis did not successfully accomplish that goal. However, components necessary for getting an accurate estimate of the mass flow rate have been added for future experiments. The coefficient of drag was also experimentally determined for the 200 μm by 200 μm hole. This, combined with the added components, sets further research efforts in a position that will allow them to immediately determine the mass flow rate, maximum current expected, and the propellant utilization factor.

B. CONCLUSION

The Fowler-Nordheim plots for all of the samples showed high geometric enhancement factors with averages ranging from 1428 to 5229. This is a testament to the quality of the samples and the growth techniques that developed them. Two of the seven experiments conducted during this thesis produced

meaningful results. Experiments 3 and 5 show that field ionizaton of argon was observed. This was shown in Figures 42 and 51. Future tests to develop an accurate estimate of the propellant utilization factor will establish the efficiencies of this system and hopefully promote field ionization as the next ion generation technique for thrusters.

Several aspects will have to be further investigated before a viable ionization chamber can be developed from this technology. The tests conducted for this thesis had only one hole. Techniques to develop multiple smaller holes are the next step in the development to ensure maximum use of the propellant. Characterization of the best substrate needs to be accomplished as well. Carbon nanotubes are extremely strong, but their weakest point is at the attachment to the substrate. Silicon may not be the answer, but it is useful for test purposes. The connection to the substrate is where all of the damage to the samples generally occurred during handling. Vibration testing will ensure the connections to the substrate can handle the stresses of launch and operation in space.

Overall, the viability of a field-ionized ion thruster appears to be excellent. It should be capable of being miniaturized and offers an efficient, small volume thruster that could be used for cubesat applications.

C. RECOMMENDATIONS

1. Mass Flow Rate

Determination of the mass flow rate through the ionizer is critical for characterizing the propellant utilization factor. The additional pressure sensor added during the last experiments along with the experimentally determined coefficient of drag for the 200 μm by 200 μm hole should enable future users to be able to get a good mass flow rate. However, commercial sensors should be purchased as well.

2. Adapter for Small Wafers

The test base was designed for 1 in^2 test samples. The modification to the test substrates to make the smaller samples fit into the machine was a temporary solution. While the intent for future work is to go back to the 1 in^2 test samples, a small adapter could be built to test smaller samples.

One way to make an adapter would be to machine another test base with a slightly smaller overall diameter, smaller gas port, and sized for a smaller o-ring. The screw holes should remain in the same location though, and two of those holes would go all the way through to allow the adapter test base to screw directly into the existing base. Figure 62 shows an illustration of how the adapter could fit into the existing test base.

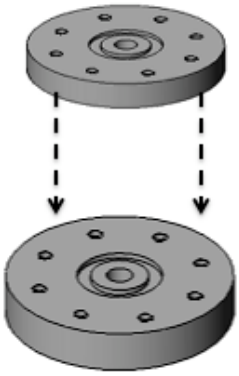

Figure 62. Illustration of a simple test base adapter for smaller substrates. Screw holes would remain in the same location, but the gas port and o-ring would be sized for the smaller substrate and the overall dimension would be slightly smaller.

3. Gap Measurement Device

One problem experienced during testing was the difficulty in measuring a proper gap distance and ensuring the sample was as evenly centered under and separated from the cathode. One way to improve this would be to mount the cathode on a micrometer on one end of a four way cross and the test base on

the opposite end. This would allow for a variance in gap distance without having to remove the sample each time. This would also isolate the two charges, hopefully eliminating any leakage current.

This particular type of setup is similar to the type of gap distance method used at NASA Ames for the argon ionization experiments conducted in a static environment by Troy Hicks in 2008 [13]. The modifications to the current configuration of the test apparatus to make this work would be minor. An illustration of how this would be employed is shown in Figure 63.

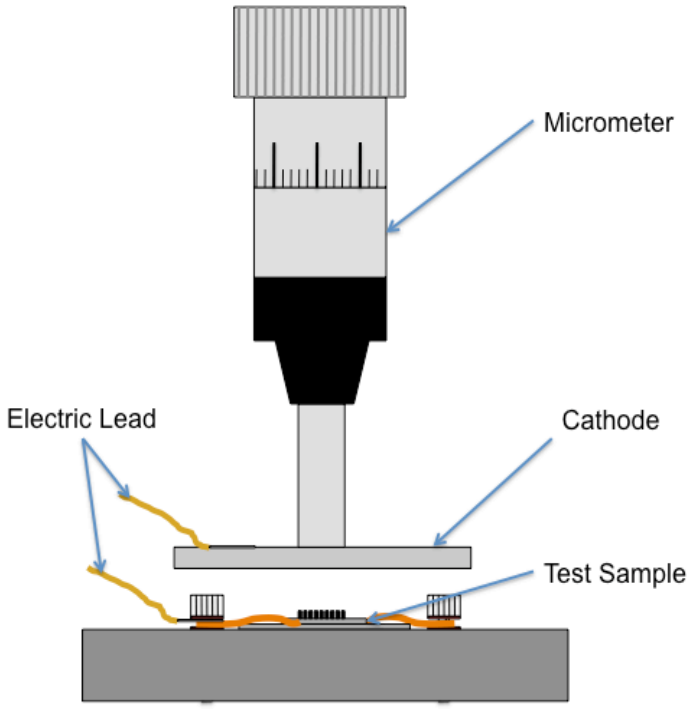

Figure 63. Illustration of micrometer being used to set gap distance.

4. Clean Room

Many of the problems experienced during the course of the experiments were caused by difficulties in keeping the sample clean and free from dust and debris. Preferably, all handling of test samples should be conducted in a clean

room environment or as clean a space as can possibly be accommodated. All samples should be held in sample holders secured with carbon tape to keep them as isolated from debris as possible.

THIS PAGE INTENTIONALLY LEFT BLANK

APPENDIX A. MECHANICAL DRAWINGS

A. TABLE PLATE

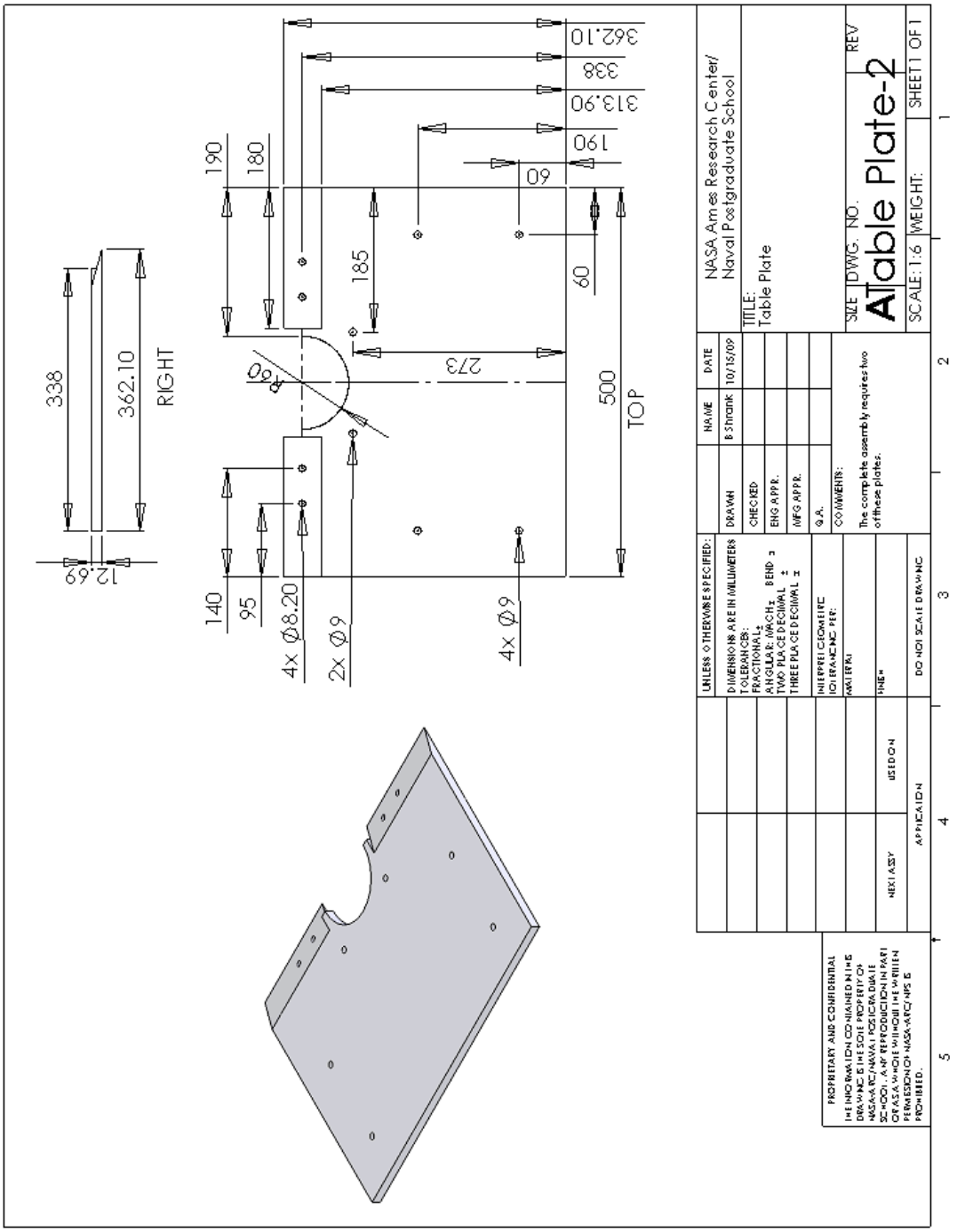

Figure 64. Table plate drawing submitted for machining.

B. TEST BASE

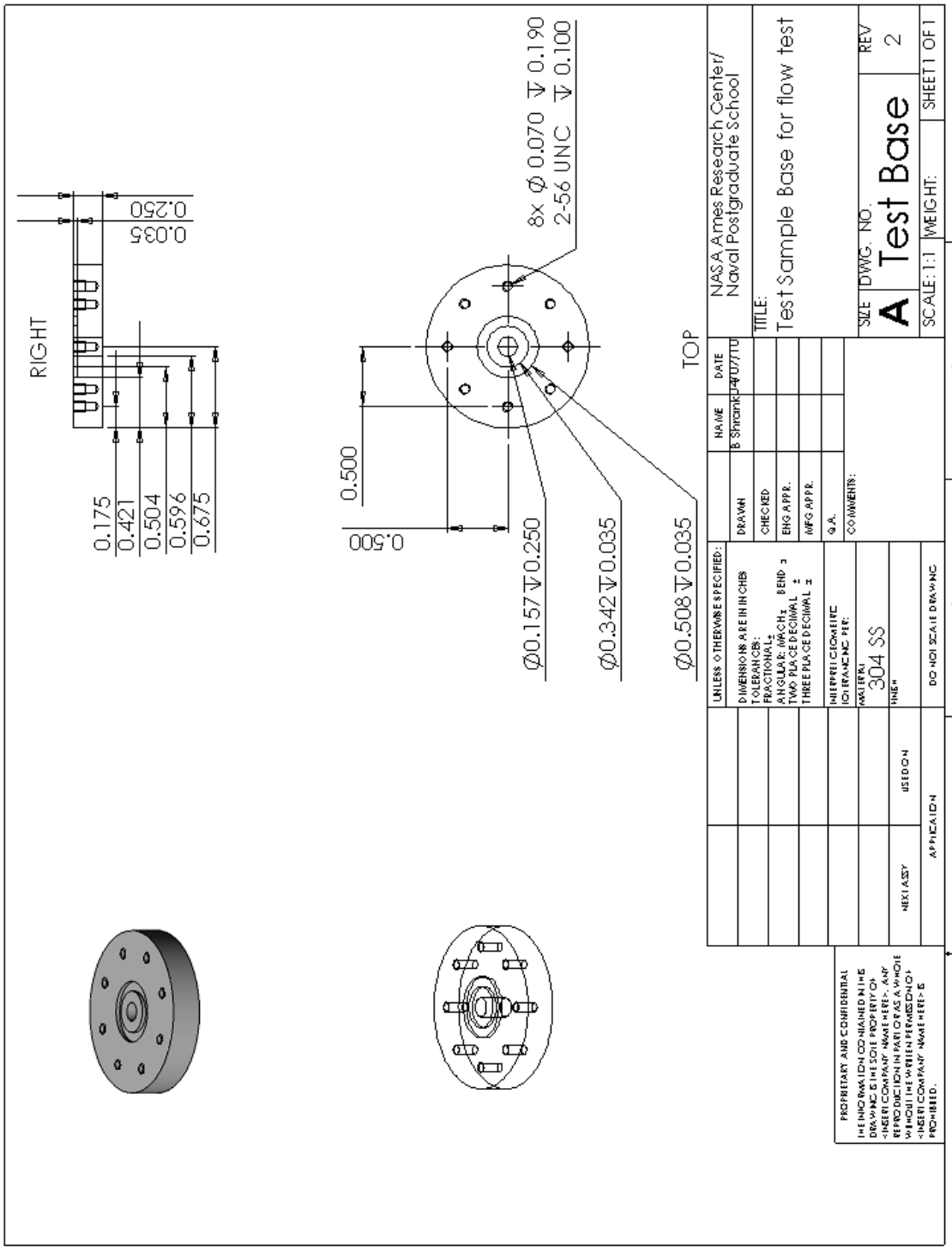

Figure 65. Test base drawing submitted for machining.

C. ANODE/CATHODE

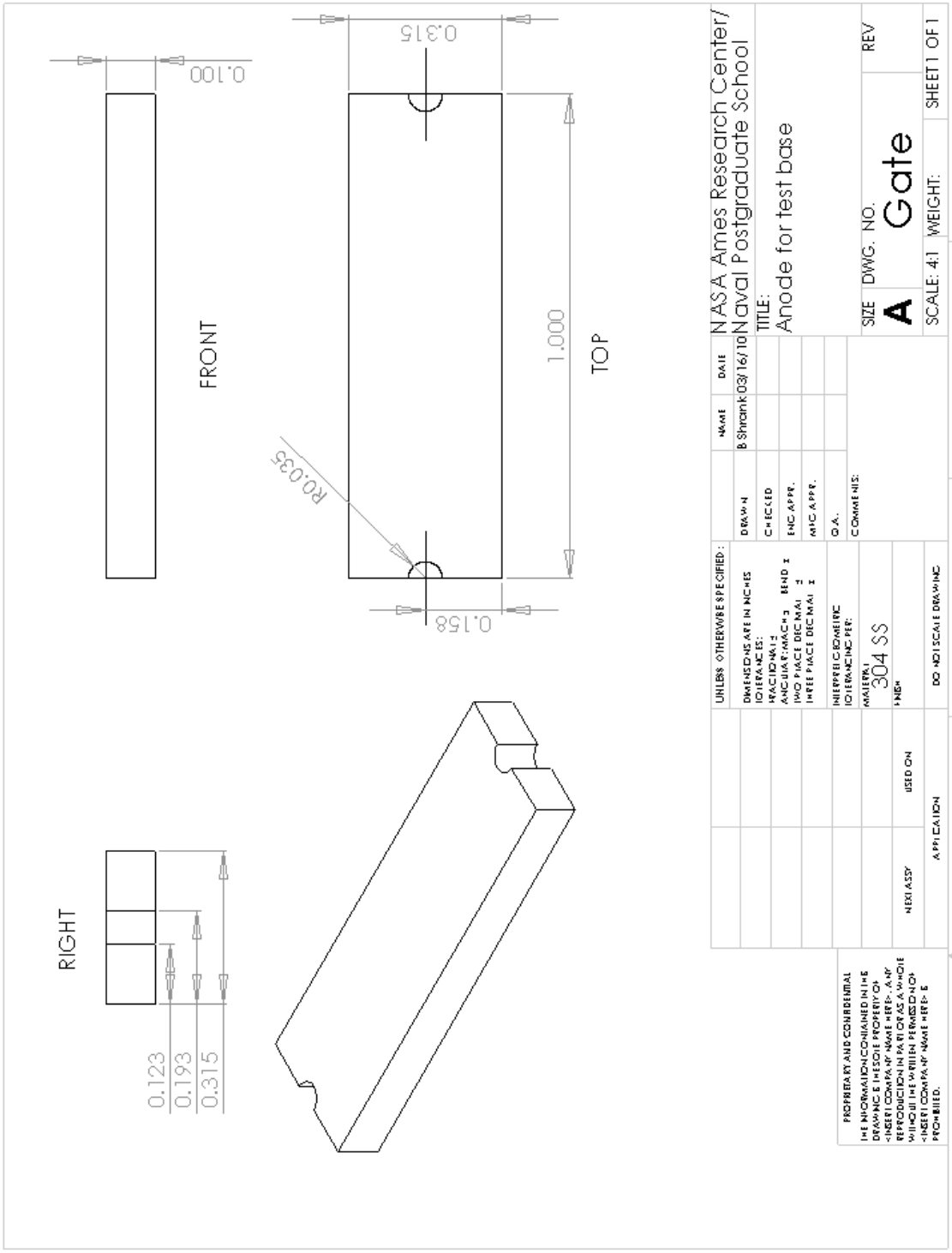

Figure 66. Anode/Cathode drawing submitted for machining.

THIS PAGE INTENTIONALLY LEFT BLANK

APPENDIX B. SPUTTERING PROCEDURES

The following procedures are for use with the IBS/e Ion Beam Sputtering/Etching System made by South Bay Technology, Inc.

1. First ensure that the silicon substrate is clean. While holding the silicon with tweezers, spray it with ethanol and then rinse with de-ionized water. Use compressed air to dry it off.

2. Secure the silicon to the stage with a piece of two-sided carbon tape.

3. Press the vacuum pump on/off button to turn off the vacuum.

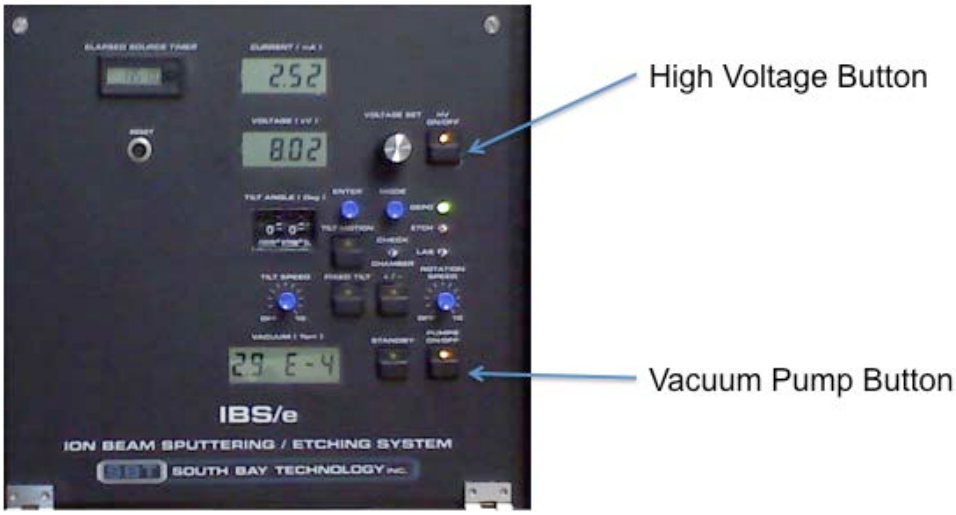

Figure 67. Main Control Panel for the IBS/e Sputterer.

4. Place the stage in the stage mount inside the sputterer.

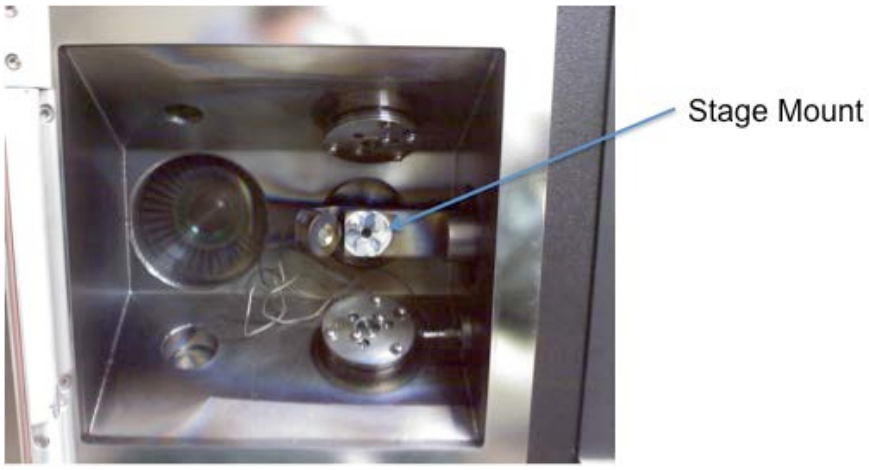

Figure 68. Stage mount inside sputterer.

5. Place the selected target metals in the door mount and screw them into place.

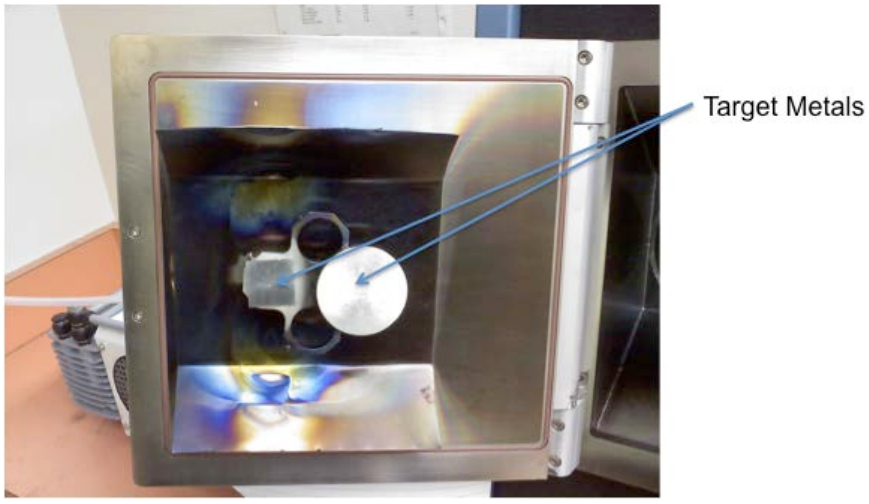

Figure 69. Target metals mounted on the inside of the door.

6. Close the door and hold in place while pushing the vacuum pump on/off button to turn it on. Once the vacuum engages enough to suck in the door, let go of the door. Press zero on the programming panel to start the clock running.

Figure 70. IBS/e Programming Panel.

7. Press the program button and select the code associated with the desired metal using the data up and down keys. Select enter when the appropriate code is reached.

8. Ensure the density shown on the screen is the correct density. If incorrect, adjust with the up and down keys until the appropriate value is reached and then press enter.

9. Ensure the correct Z-factor is shown on the screen. If incorrect, adjust with the up and down keys until the appropriate value is reached and then press enter.

10. Select the appropriate sputter thickness in kilo-Angstroms (kÅ) with the up and down keys and press enter.

11. Select the appropriate end thickness in kilo-Angstroms (kÅ) with the up and down keys and press enter. This should be the same as the sputter thickness.

12. Press program to lock in the selection.

13. After the vacuum has been operating for at least 15 minutes, press the high voltage (HV) button and the zero button. The HV light should turn on. When the selected thickness is reached the HV light should turn off.

14. If another metal needs to be sputtered on, rotate the target wheel to the appropriate position. Repeat steps 7-12 and press the HV button.

15. Once complete, press the vacuum pump on/off button to turn off the vacuum. Remove the sample and the target metals.

16. Hold the door in place and press the vacuum pump on/off button to turn the vacuum back on.

APPENDIX C. CHEMICAL VAPOR DEPOSITION PROCEDURES

1. Take the freshly sputtered substrate and move it to the furnace area. Make sure to use a clean petri dish to transport the substrate.

2. Place the substrate inside the quartz tube. Use a push/pull road to get it to the center of the tube.

3. Place the tube on the furnace. Be sure to position the tube so that the substrate is just beyond the thermocouple.

Figure 71. CVD furnace shown with quartz tube inside.

4. Affix the exhaust attachment onto the exhaust side of the tube and ensure it is aimed into the exhaust tube.

Figure 72. Gas exhaust attachment.

5. Affix the gas inlet attachment onto the inlet side of the tube and ensure it is resting firmly on the jack stand.

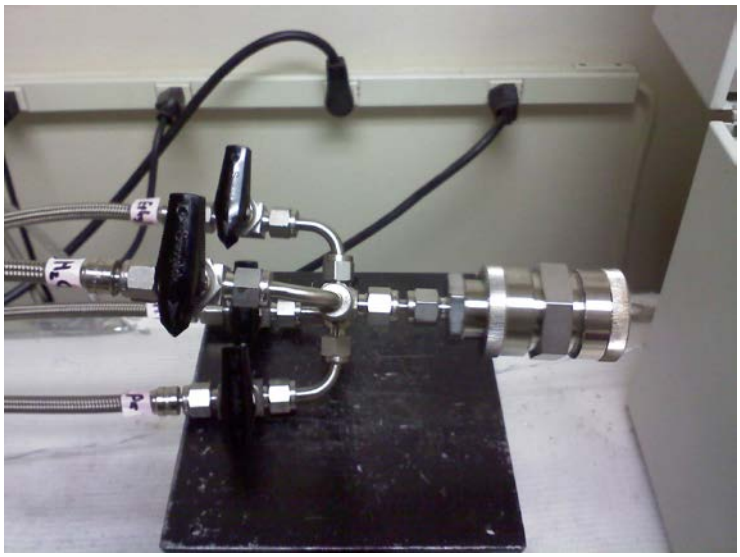

Figure 73. Gas inlet attachment.

6. Close the furnace and lock it.

7. Ensure the argon, hydrogen, and ethylene valves located on the gas inlet attachment are turned to the on position. Check to make sure the gas cylinders are turned on as well.

8. Open the LabVIEW program on the control computer.

Figure 74. Control computer with LabVIEW program.

9. Press the Load button on the graphical user interface and select the appropriate desired recipe. Press enter.

10. Press the start button. Ensure the gases and furnace temperature are behaving according to the recipe.

11. When complete, let the quartz tube cool down. Shut off the valves on the gas inlet valve.

12. When the tube is cool, remove the exhaust attachment and gas inlet valve.

13. Carefully set the quartz tube on the holding rack. Use the push/pull device to pull the sample to the edge of the tube so it can be removed with the tweezers.

14. Place the sample in a petri dish on a piece of double-sided carbon tape to ensure it does not slide around.

THIS PAGE INTENTIONALLY LEFT BLANK

APPENDIX D. SEM OPERATIONS

1. Affix the desired sample to an SEM mount using double-sided carbon tape. Ensure that the sample will not fall off inside of the SEM.

Figure 75. Sample affixed to an SEM mount.

2. Flip the display power switch to the on position. Turn on the computer monitor, the computer/SEM interface, and the specimen chamber monitor as well.

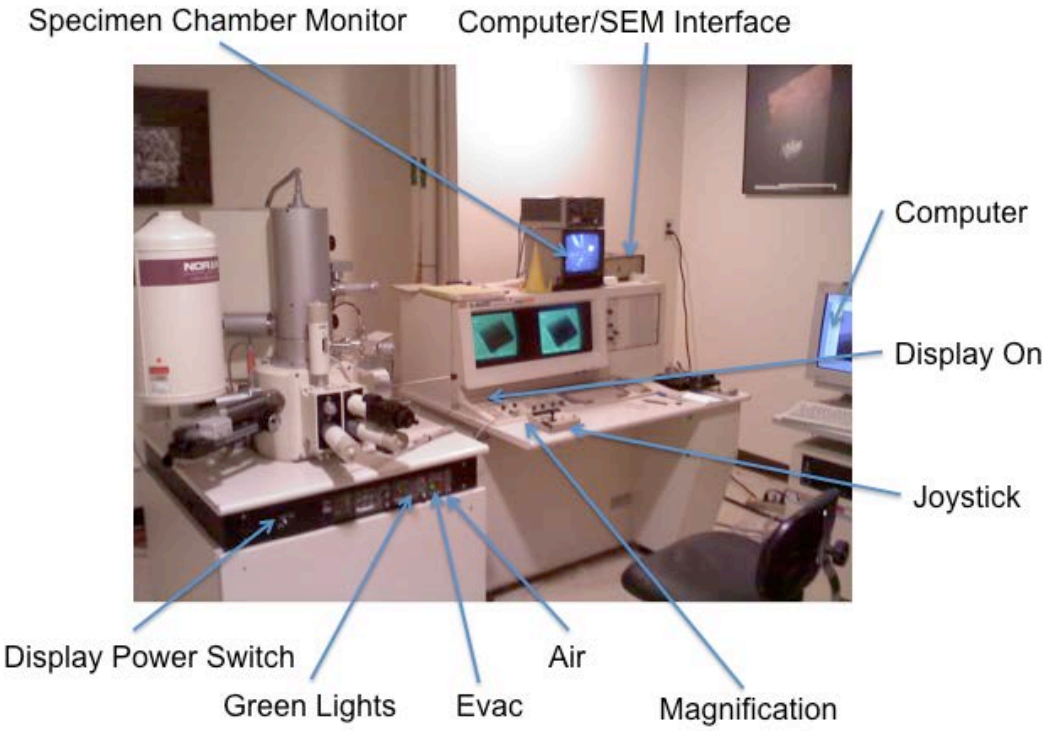

Figure 76. Scanning Electron Microscope (SEM)

3. Press the “Air” button to turn off the vacuum to the specimen evacuation chamber. When the door “falls” open, pull it out.

4. Screw the mount onto the mount pedestal.

5. Close the door and press the “Evac” button to start the vacuum. Hold the door in place until the vacuum sucks it closed.

6. Wait for the two green lights to appear on the panel saying that the chamber is now under high vacuum. Open the chamber door with the lever and use the rod to push the mount into the holding stems. Unscrew the rod and carefully pull it out of the mount. Tap the mount to ensure it is seated correctly then pull back the rod and close the chamber door.

7. Flip the “Lock” switch to lock the chamber door in place.

8. Move to the display screens. Press the power button in the top left corner to turn on the display. Log the V_{ext} into the log book.

9. Use the joystick to move the substrate to the desired viewing position. 45 degrees is the recommended tilt position to get a good measurement.

10. Use the magnification knob to adjust to the desired magnification level and the other knobs to get a clear image.

11. When ready to take a picture, go to the computer and click on the camera icon. Enter in the correct magnification and press enter. Save the image to the desired folder.

12. When complete, move the mount to its original position. Press the exchange button on the joystick and enter to return to the appropriate position.

13. Unlock the chamber door. Open it and use the rod to screw into the mount and pull it back to the specimen exchange chamber. Close the chamber door.

14. Press “Air” to open the door. Pull it back when it “falls” open.

15. Remove the mount, shut the door, and press “Evac” to vacuum the door shut.

16. Once the lights turn green, turn off the display power. Turn off the computer monitor, computer/SEM interface, and specimen chamber monitor as well.

THIS PAGE INTENTIONALLY LEFT BLANK

APPENDIX E. DRILLING THROUGH SILICON WAFERS

1. Prepare the workstation by gathering all of the necessary equipment. Ensure the following is available: Dremel with diamond-tipped bit, full water bottle, Kim-wipes, double-sided carbon tape, small piece of cardboard, scotch tape, silicon wafers, and tweezers.

2. Use the scotch tape to secure the piece of cardboard to the working surface. This will allow the drill to go through the silicon without touching the table.

Figure 77. Secure the cardboard to the working surface with tape and apply a strip of double-sided carbon tape to the center of the cardboard.

3. Place a piece of double-sided carbon tape on the cardboard and affix the silicon wafer to the tape.

4. If possible, have a partner handle the water bottle. Otherwise, grab the Dremel and the water bottle.

Figure 78. Allow the weight of the Dremel to rest on the silicon. Apply a steady stream of water to the silicon while drilling.

5. Turn the Dremel onto its lowest setting. Bring the diamond tip gently down onto the center of the silicon wafer and allow the weight of the Dremel rest onto the silicon, loosely holding it in your hands. DO NOT apply any extra pressure. As the tip touches the silicon, use the water bottle to apply a steady stream of water to the silicon surface.

6. If the slurry makes it to difficult to see, bring a Kim-wipe to the edge of the wafer and allow it to suck up the slurry. Then quickly reapply clean water. Do not stop drilling during this process.

7. Once the drill breaks through the silicon, catch it and lift it away. Controlled careful drilling can continue if a larger hole is desired.

APPENDIX F. TEST DATA

All available test data is provided in this appendix regardless of whether or not it is shown in the body of the thesis. This is to allow for a quick reference to all data without having to jump between the main body of the thesis and the test data appendix to compare the results of various runs.

A. EXPERIMENT 2

Experiment 2		
29 July 2010		
Run	**Type**	**Notes**
1	Fowler-Nordheim / Linear Stair 0-550 V	Field emission achieved.
2	Fowler-Nordheim / Linear Stair 0-550 V	Field emission achieved.
3	Fowler-Nordheim / Linear Stair 0-550 V	Field emission achieved.
4	Fowler-Nordheim / Linear Stair 0-550 V	Field emission achieved.
5	Fowler-Nordheim / Linear Stair 0-550 V	Field emission achieved.
30 July 2010		
1	Argon Ionization / Linear Stair 0-1000 V	Hit compliance current.
2	Argon Ionization / Linear Stair 0-1000 V	Hit compliance current.
3	Argon Ionization / Linear Stair 0-1000 V	Hit compliance current.
4	Argon Ionization / Linear Stair 0-1000 V	Hit compliance current.
5	Argon Ionization / Linear Stair 0-1000 V	Hit compliance current.
6	Breakdown Test / Linear Stair 0-1000 V	Nothing meaningful.
7	Breakdown Test / Linear Stair 0-1000 V	Nothing meaningful.
8	Breakdown Test / Linear Stair 0-1000 V	Nothing meaningful.
9	Argon Ionization / Linear Stair 0-1000 V	Possible small amount of ionization.
10	Argon Ionization / Linear Stair 0-1000 V	Nothing meaningful.
11	Argon Ionization / Linear Stair 0-1000 V	Nothing meaningful.
12	Argon Ionization / Linear Stair 0-1000 V	Possible small amount of ionization.
13	Argon Ionization / Linear Stair 0-1100 V	Nothing meaningful.
14	Argon Ionization / Linear Stair 0-1100 V	Nothing meaningful.
15	Fowler-Nordheim / Linear Stair 0-1100 V	Field emission achieved.
16	Fowler-Nordheim / Linear Stair 0-1100 V	Field emission achieved.

Table 27. Summary of Experiment 2 test runs.

1. Fowler-Nordheim Data

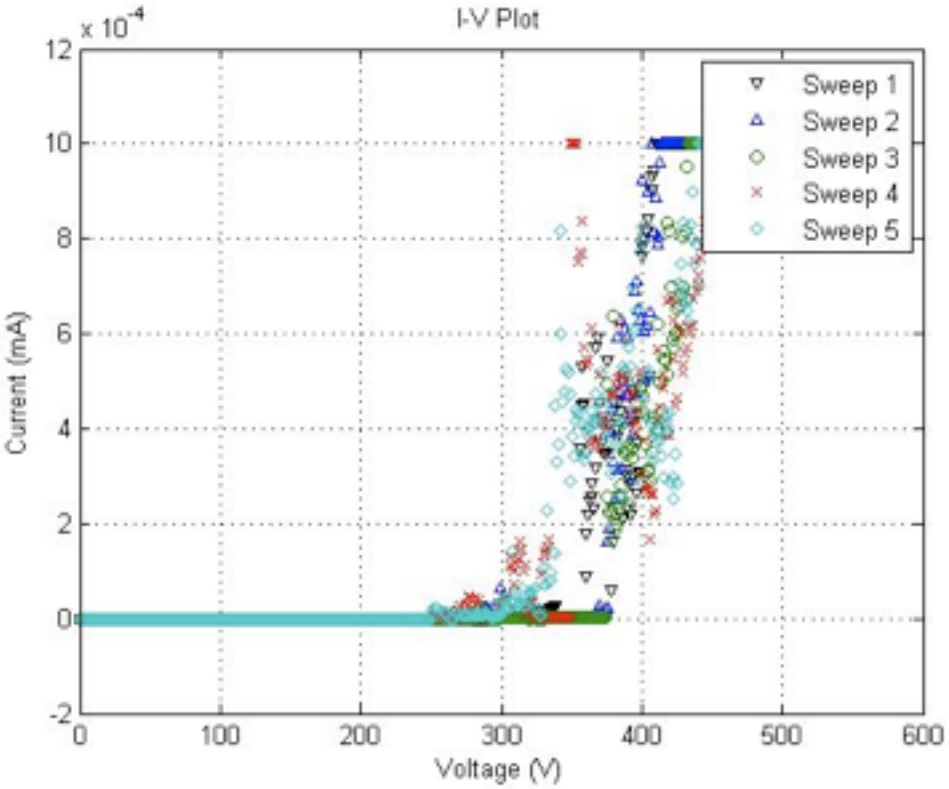

Figure 79. Experiment 2 Current versus Voltage plot for Fowler-Nordheim characterization.

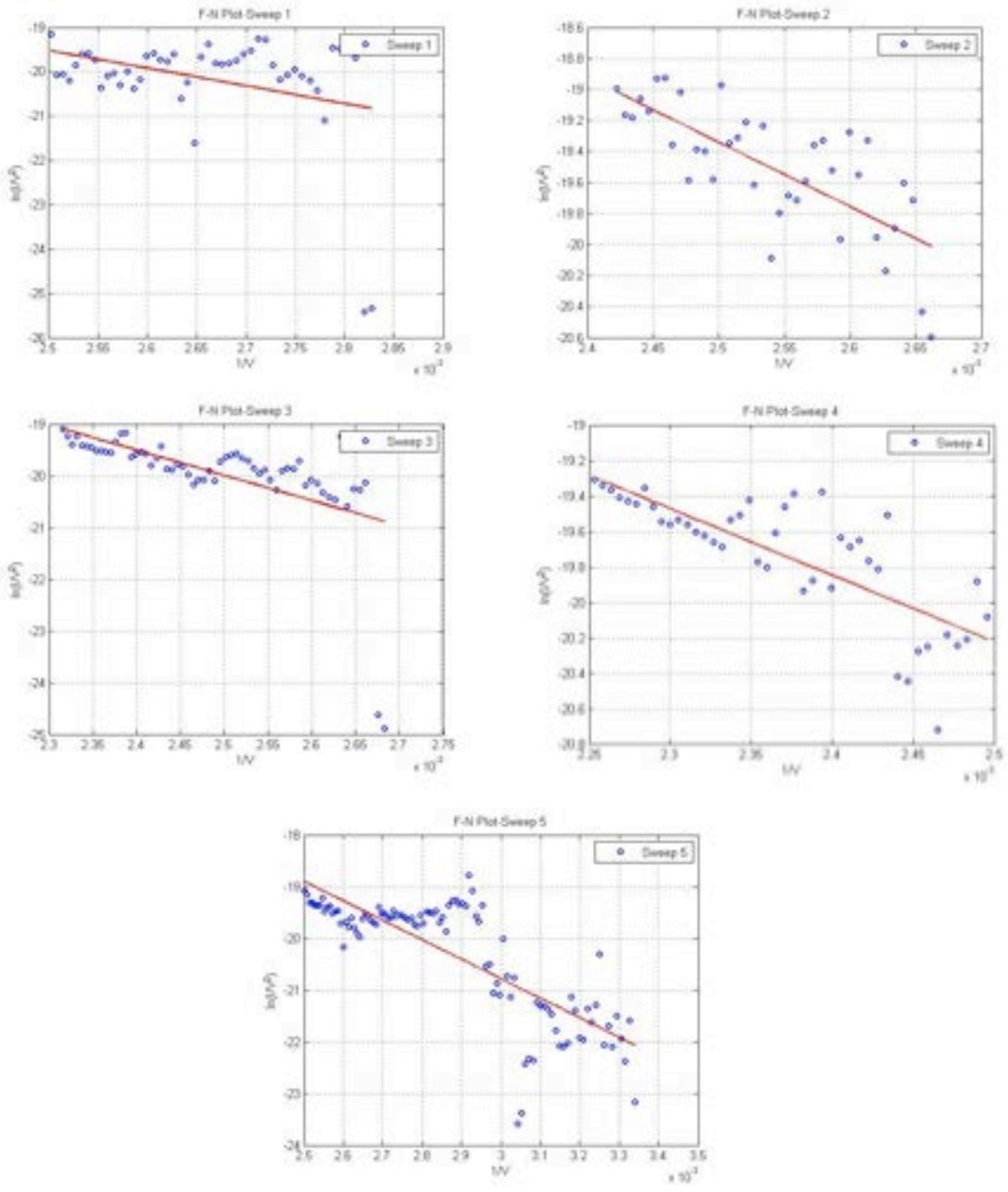

Figure 80. Experiment 2 Fowler-Nordheim plots.

2. Argon Ionization Data

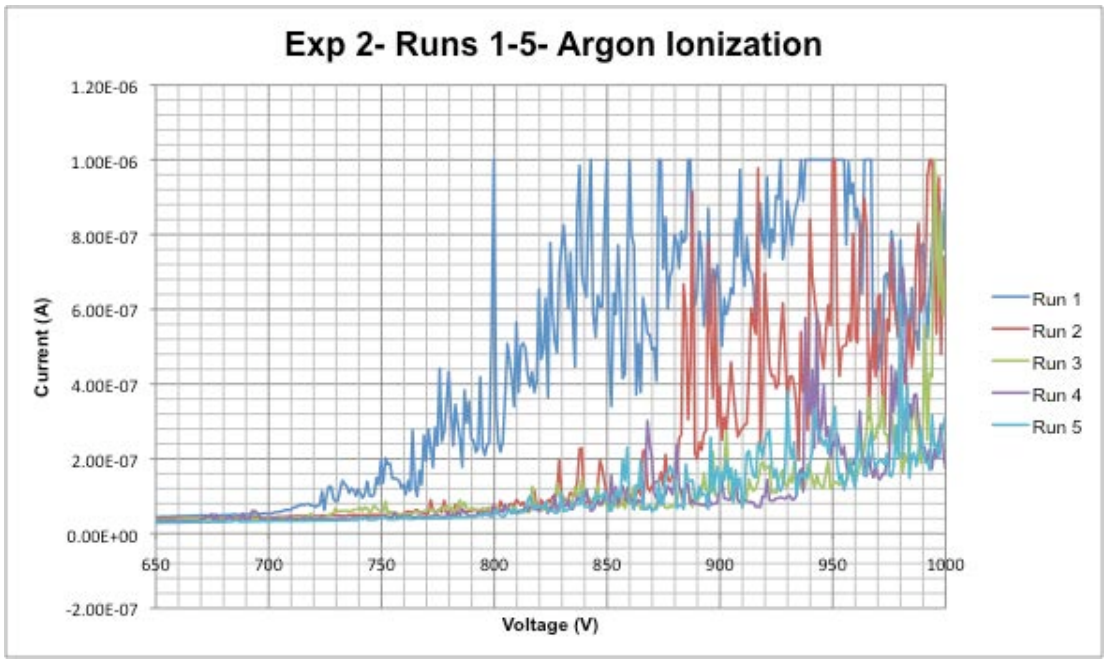

Figure 81. Experiment 2 Argon Ionization Runs 1-5.

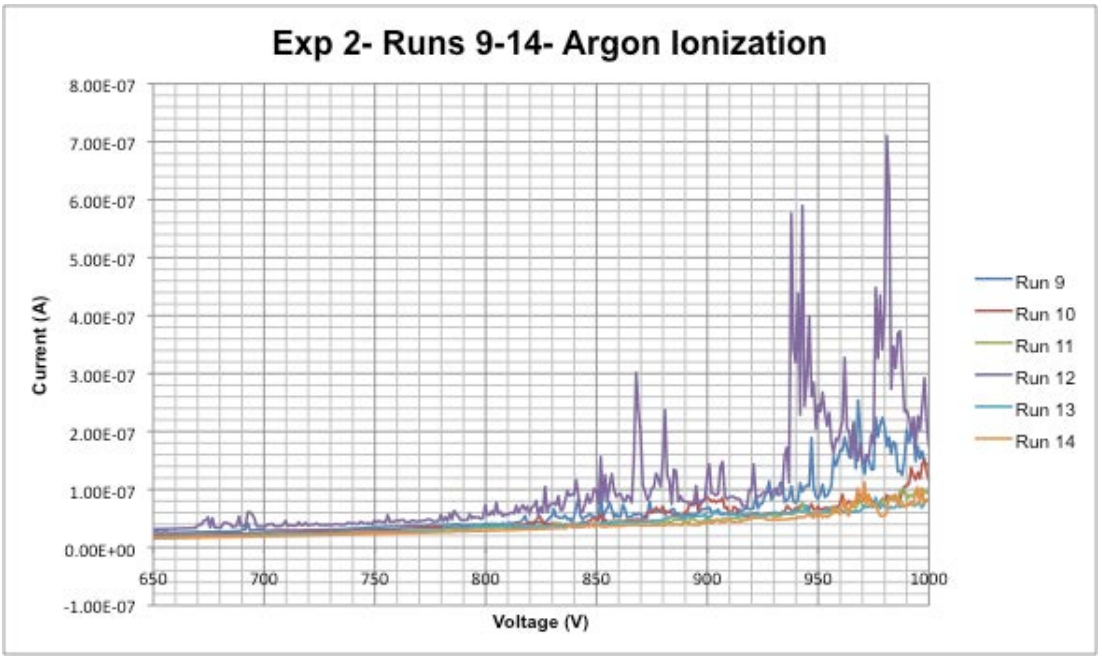

Figure 82. Experiment 2 Argon Ionization Runs 9-14.

B. EXPERIMENT 3

Experiment 3		
7 August 2010		
Run	**Type**	**Notes**
1	Fowler-Nordheim / Linear Stair 0-550 V	Field emission approached.
2	Fowler-Nordheim / Linear Stair 0-550 V	Field emission approached.
3	Fowler-Nordheim / Linear Stair 0-550 V	Field emission approached.
4	Fowler-Nordheim / Linear Stair 0-550 V	Field emission approached.
5	Fowler-Nordheim / Linear Stair 0-350 V	Field emission approached.
6	Fowler-Nordheim / Linear Stair 0-350 V	Field emission achieved.
7	Fowler-Nordheim / Linear Stair 0-350 V	Field emission achieved.
8	Fowler-Nordheim / Linear Stair 0-350 V	Field emission achieved.
9	Fowler-Nordheim / Linear Stair 0-350 V	Field emission achieved.
10	Ionization Char. / Linear Stair 0-550 V	Data did not save.
11	Ionization Char. / Linear Stair 0-550 V	Data did not save.
12	Ionization Char. / Linear Stair 0-550 V	Data did not save.
13	Ionization Char. / Linear Stair 0-900 V	Linear current growth starting at 600 V
14	Ionization Char. / Linear Stair 0-900 V	Data did not save.
15	Ionization Char. / Linear Stair 0-900 V	Data did not save.
16	Ionization Char. / Linear Stair 0-900 V	Data did not save.
17	Ionization Char. / Fixed Voltage 750 V	Steady current at 2E-6; Odd spike from 400-600 s.
18	Argon Ionization / Linear Stair 0-900 V	Possible Ionization.
19	Argon Ionization / Linear Stair 0-900 V	Possible Ionization.
20	Argon Ionization / Linear Stair 0-900 V	Possible Ionization.
21	Argon Ionization / Linear Stair 0-1100 V	Nothing meaningful.
22	Argon Ionization / Linear Stair 0-1100 V	Nothing meaningful.
23	Argon Ionization / Linear Stair 0-1100 V	Possible Ionization.
24	Argon Ionization / Linear Stair 0-1100 V	Nothing meaningful.
25	Argon Ionization / Fixed 1000 V / Adj. Flow	Ionization-Steady current at 2.2E-5.
26	Argon Ionization / Fixed 1000 V / Adj. Flow	Hit compliance current but turned on and off.
27	Argon Ionization / Linear Stair 0-1100 V/ Adj	Nothing meaningful.
28	Argon Ionization / Linear Stair 0-1100 V/ Adj	Possible small amount of ionization.
29	Argon Ionization / Linear Stair 0-1100 V/ Adj	Nothing meaningful.
30	Argon Ionization / Fixed 1050 V / Adj. Flow	Incomplete test. Noisy then stopped.

Table 28. Summary of Experiment 3 test runs.

1. Fowler-Nordheim Data

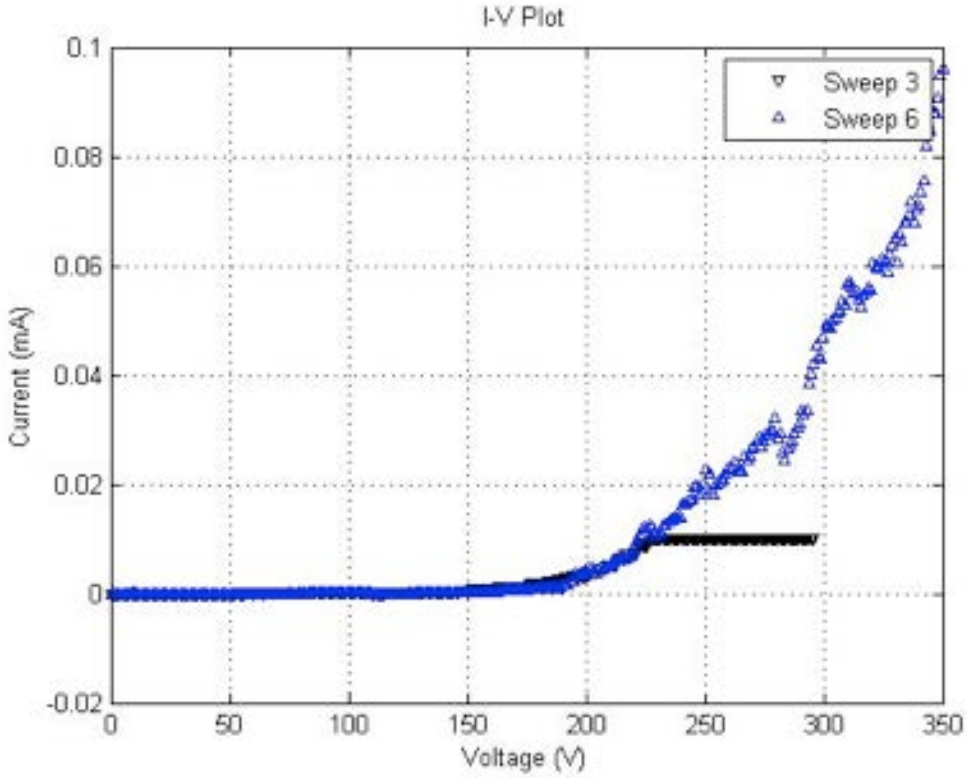

Figure 83. Experiment 3 Current versus Voltage plot for Fowler-Nordheim characterization.

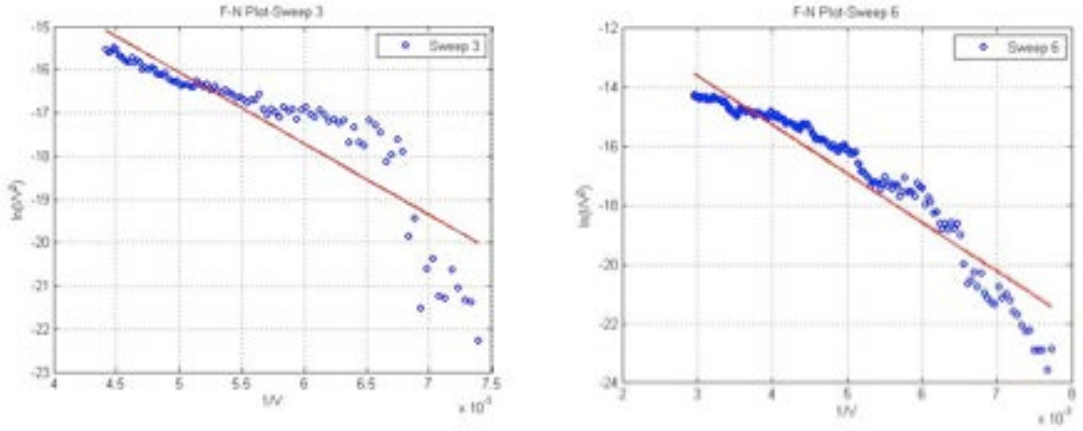

Figure 84. Experiment 3 Fowler-Nordheim plots.

2. Argon Ionization Data

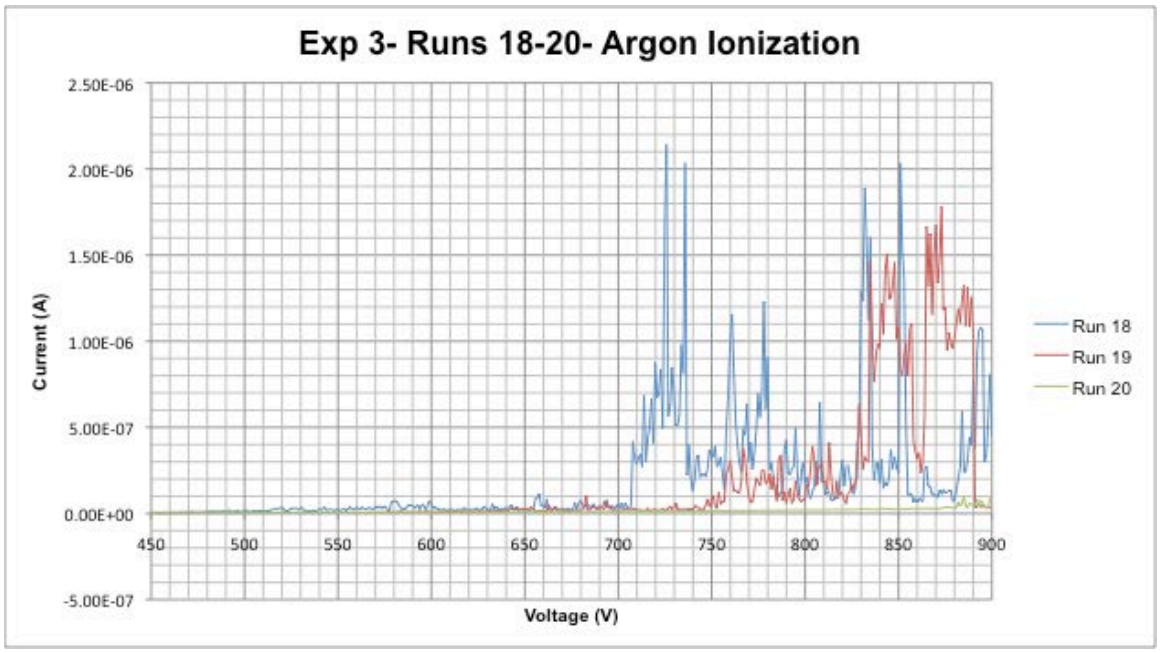

Figure 85. Experiment 3 Argon Ionization Runs 18-20.

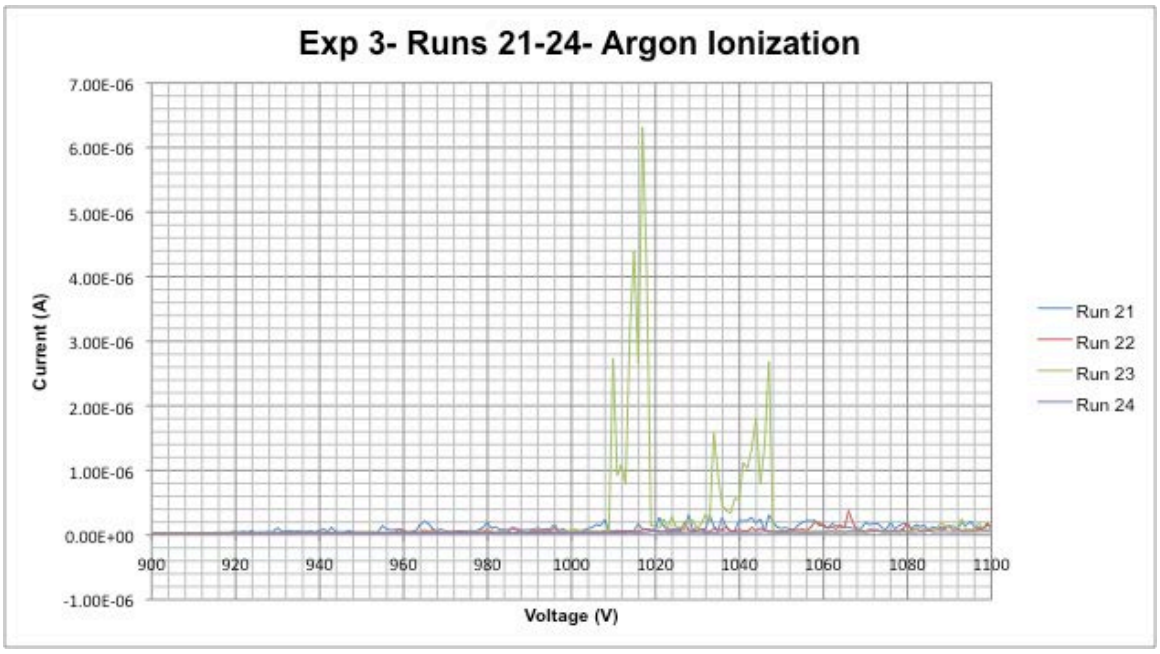

Figure 86. Experiment 3 Argon Ionization Runs 21-24.

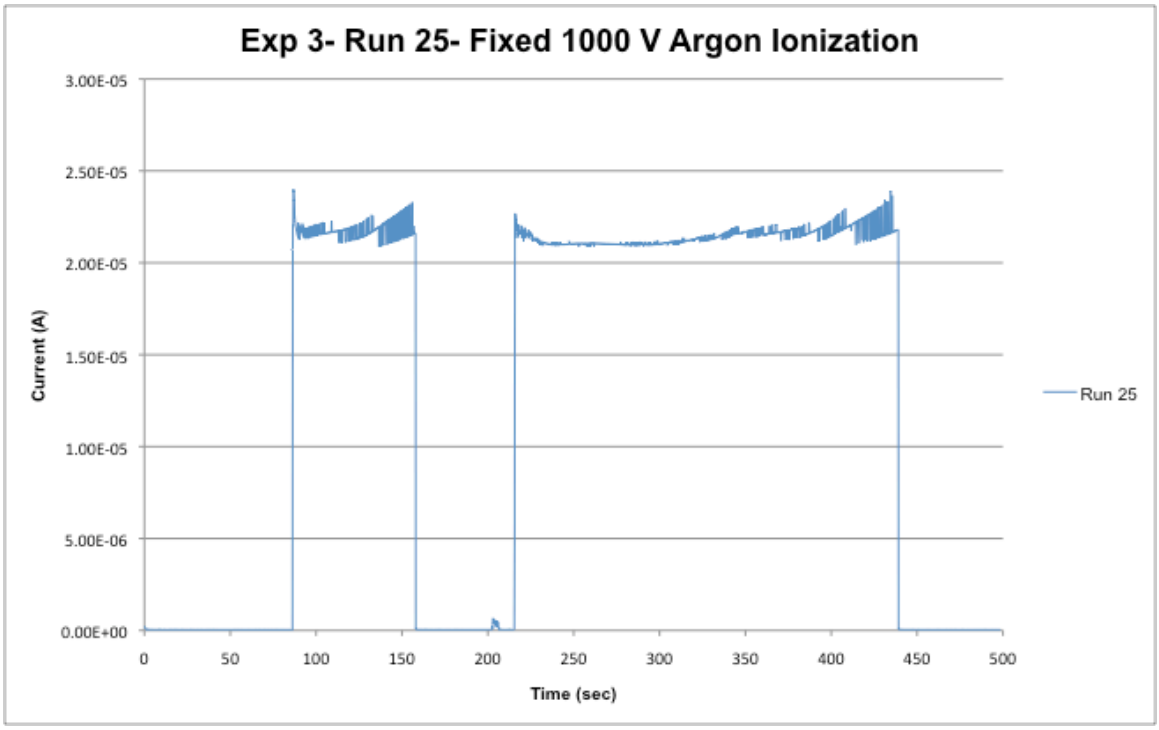

Figure 87. Experiment 3 Argon Ionization Run 25.

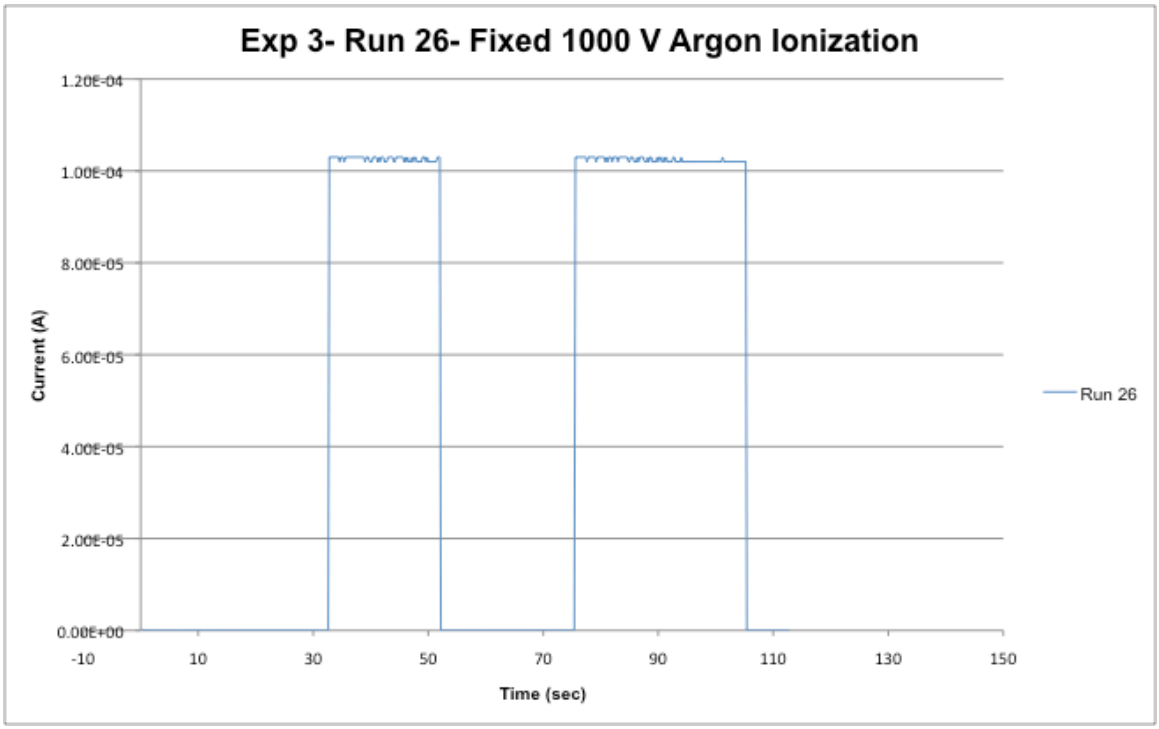

Figure 88. Experiment 3 Argon Ionization Run 26.

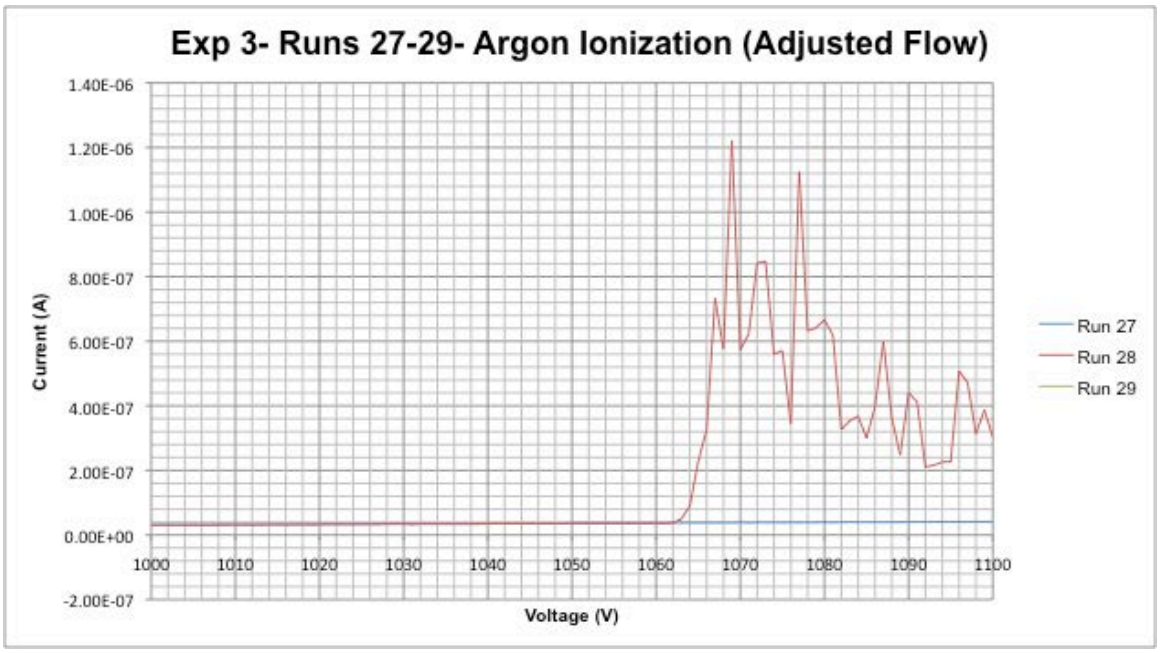

Figure 89. Experiment 3 Argon Ionization Runs 27-29.

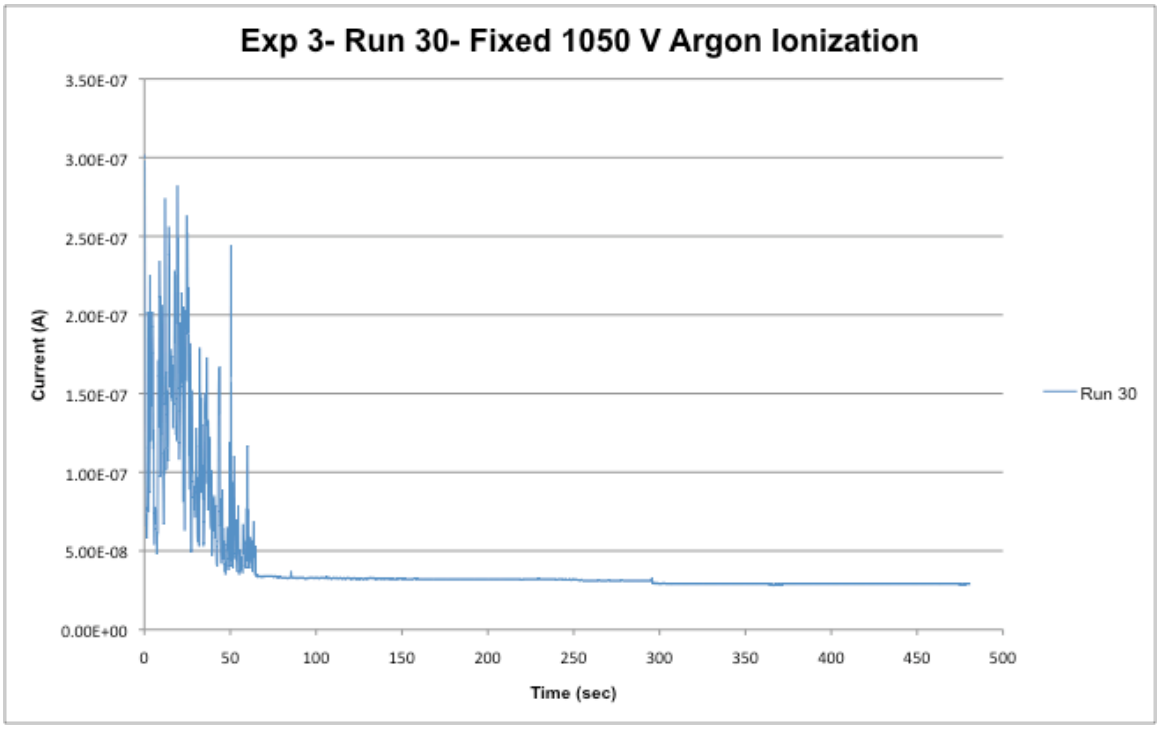

Figure 90. Experiment 3 Argon Ionization Run 30.

C. EXPERIMENT 4

Experiment 4		
13 August 2010		
Run	**Type**	**Notes**
1	Fowler-Nordheim / Linear Stair 0-1100 V	Field emission achieved.

Table 29. Summary of Experiment 4 test runs.

1. Fowler-Nordheim Data

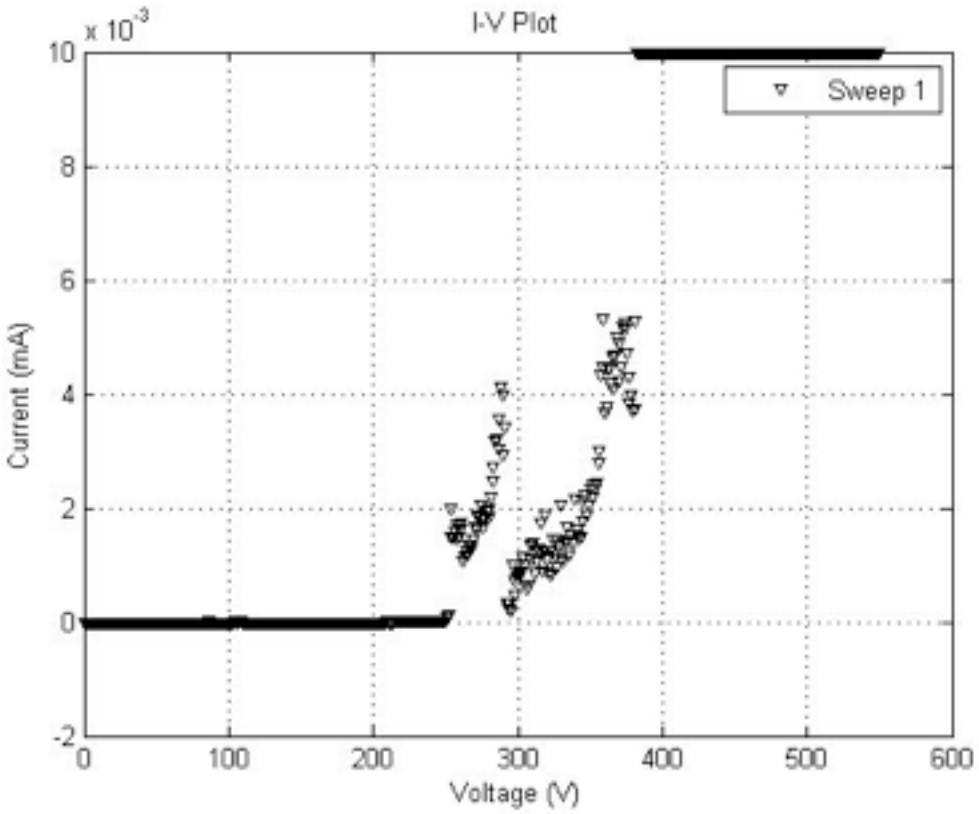

Figure 91. Experiment 4 Current versus Voltage plot for Fowler-Nordheim characterization.

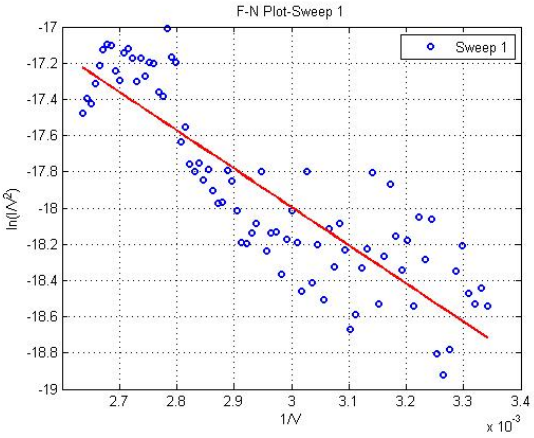

Figure 92. Experiment 4 Fowler-Nordheim plot.

D. EXPERIMENT 5

Experiment 5		
14 August 2010		
Run	**Type**	**Notes**
1	Fowler-Nordheim / Linear Stair 0-1100 V	No emission. Electric leads snapped.
2	Fowler-Nordheim / Linear Stair 0-1100 V	No emission. Electric leads snapped.
3	Fowler-Nordheim / Linear Stair 0-1100 V	No emission. Electric leads snapped.
4	Fowler-Nordheim / Linear Stair 0-1100 V	No emission. Electric leads snapped.
5	Fowler-Nordheim / Linear Stair 0-1100 V	No emission. No transmission of charge.
6	Fowler-Nordheim / Linear Stair 0-1100 V	No emission. No transmission of charge.
7	Fowler-Nordheim / Linear Stair 0-1100 V	Field emission achieved.
8	Fowler-Nordheim / Linear Stair 0-550 V	Field emission achieved.
9	Fowler-Nordheim / Linear Stair 0-550 V	Field emission achieved.
10	Fowler-Nordheim / Linear Stair 0-550 V	Field emission achieved.
11	Fowler-Nordheim / Linear Stair 0-550 V	Field emission achieved.
12	Argon Ionization / Linear Stair 0-1100 V	Hit compliance current.
13	Argon Ionization / Linear Stair 0-1100 V	Hit compliance current.
14	Argon Ionization / Linear Stair 0-1100 V	Hit compliance current.
15	Argon Ionization / Linear Stair 0-1100 V	Hit compliance current.
16	Argon Ionization / Fixed 1000 V / Adj. Flow	Data did not save. Hit compliance but turned on and off.
17	Argon Ionization / Fixed 800 V / Adj. Flow	Hit compliance but turned on and off.
18	Argon Ionization / Linear Stair 0-1100 V	Higher flow. Hit compliance.
19	Argon Ionization / Linear Stair 0-1100 V	Data did not save. Lower flow. Spike at 700 V.
20	Argon Ionization / Linear Stair 0-1100 V	Higher flow. Hit compliance.
21	Argon Ionization / Linear Stair 0-1100 V	Higher flow. Hit compliance.
22	Argon Ionization / Linear Stair 0-1100 V	Higher flow. Hit compliance.
23	Argon Ionization / Linear Stair 0-1100 V	Higher flow. Hit compliance.
24	Argon Ionization / Linear Stair 0-1100 V	Medium flow. Ionization.
25	Argon Ionization / Linear Stair 0-1100 V	Medium flow. Ionization.
26	Argon Ionization / Linear Stair 0-1100 V	Medium flow. Ionization.
27	Argon Ionization / Linear Stair 0-1100 V	Lower flow. Possible Ionization.
28	Argon Ionization / Linear Stair 0-1100 V	Lower flow. Possible Ionization.
29	Argon Ionization / Linear Stair 0-1100 V	Lower flow. Possible Ionization.
30	Argon Ionization / Linear Stair 0-1100 V	No flow. Possible ionization of residual argon.
31	Argon Ionization / Linear Stair 0-1100 V	No flow. Possible ionization of residual argon.
32	Argon Ionization / Linear Stair 0-1100 V	No flow. Possible ionization of residual argon.
33	Argon Ionization / Linear Stair 0-1100 V	No flow. Possible ionization of residual argon.
34	Argon Ionization / Fixed 1100 V	No flow. Possible ionization of residual argon.

Table 30. Summary of Experiment 5 test runs.

1. Fowler-Nordheim Data

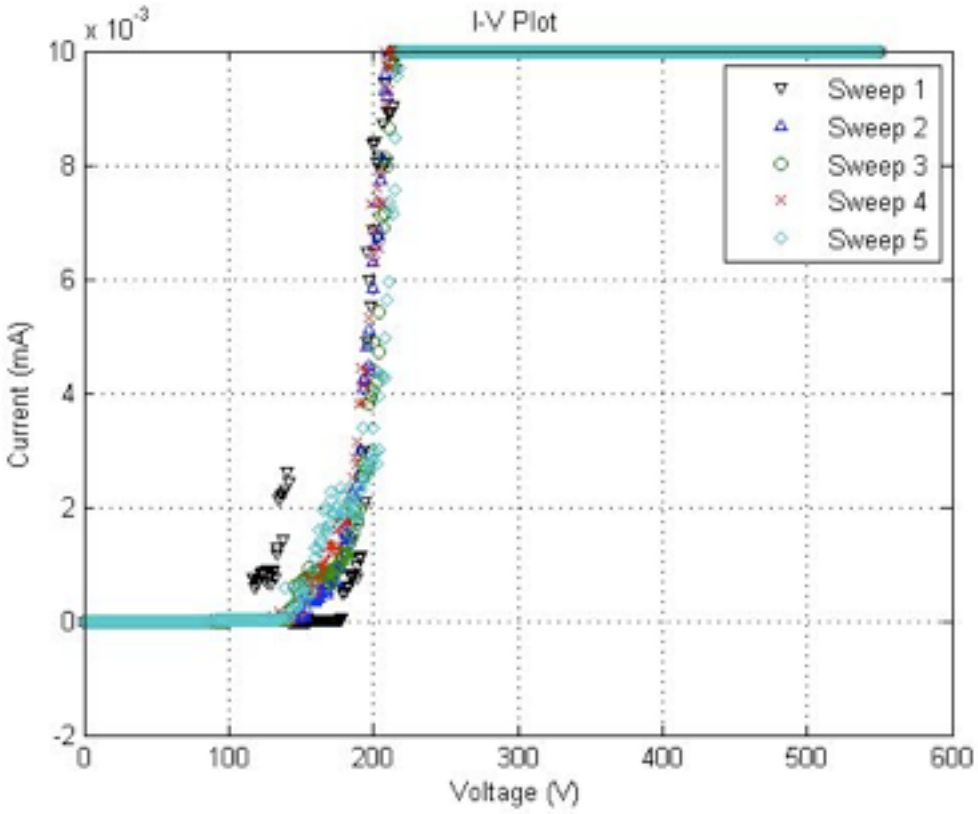

Figure 93. Experiment 5 Current versus Voltage plots for Fowler-Nordheim characterization.

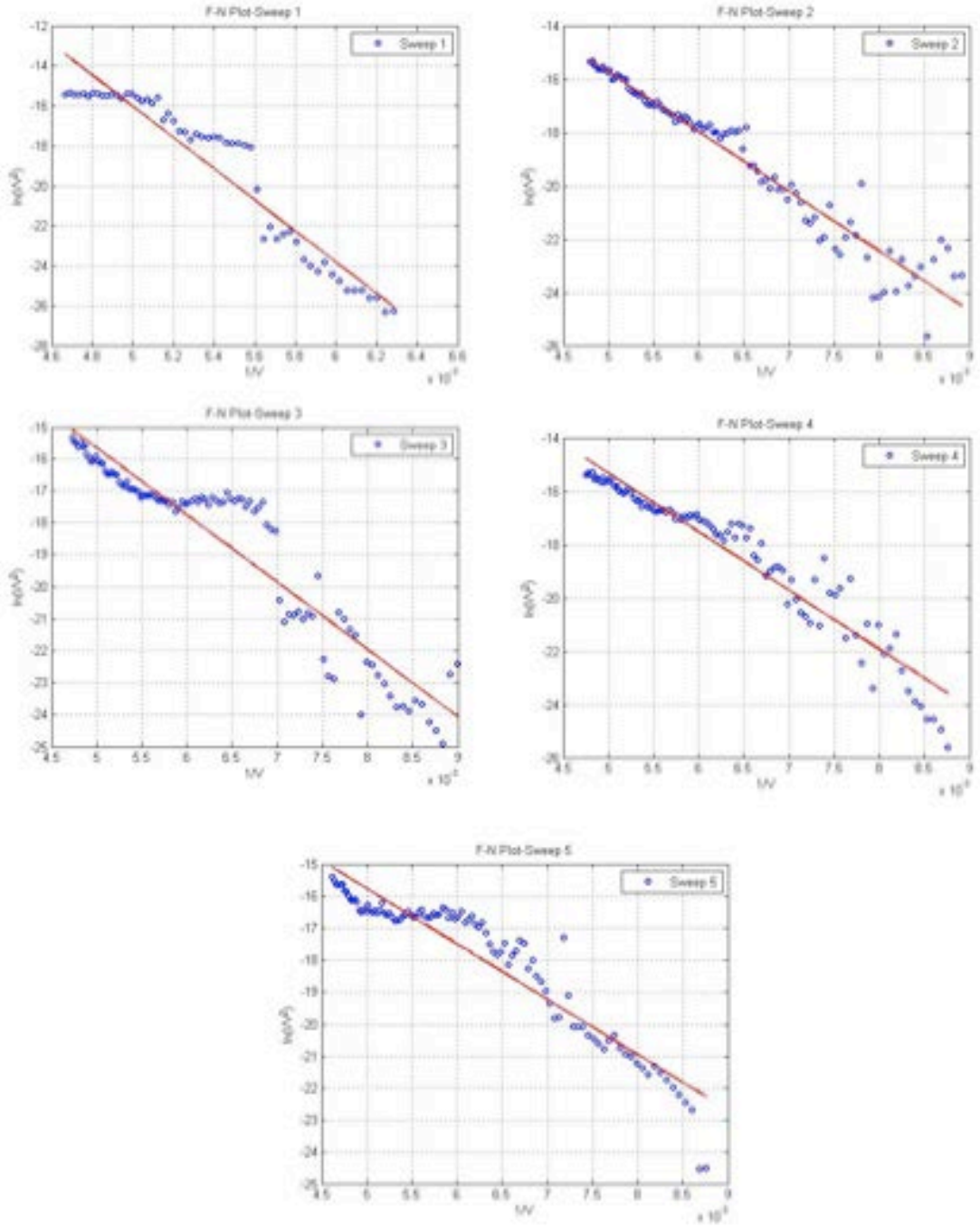

Figure 94. Experiment 5 Fowler-Nordheim plots.

2. Argon Ionization Data

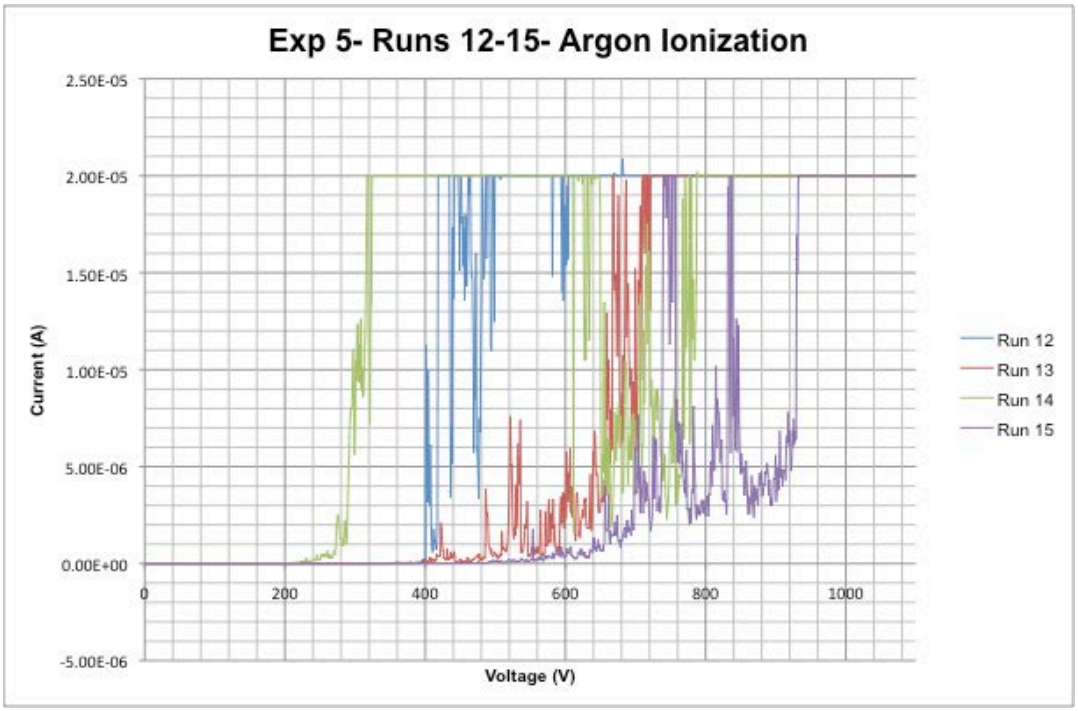

Figure 95. Experiment 5 Argon Ionization Runs 12-15.

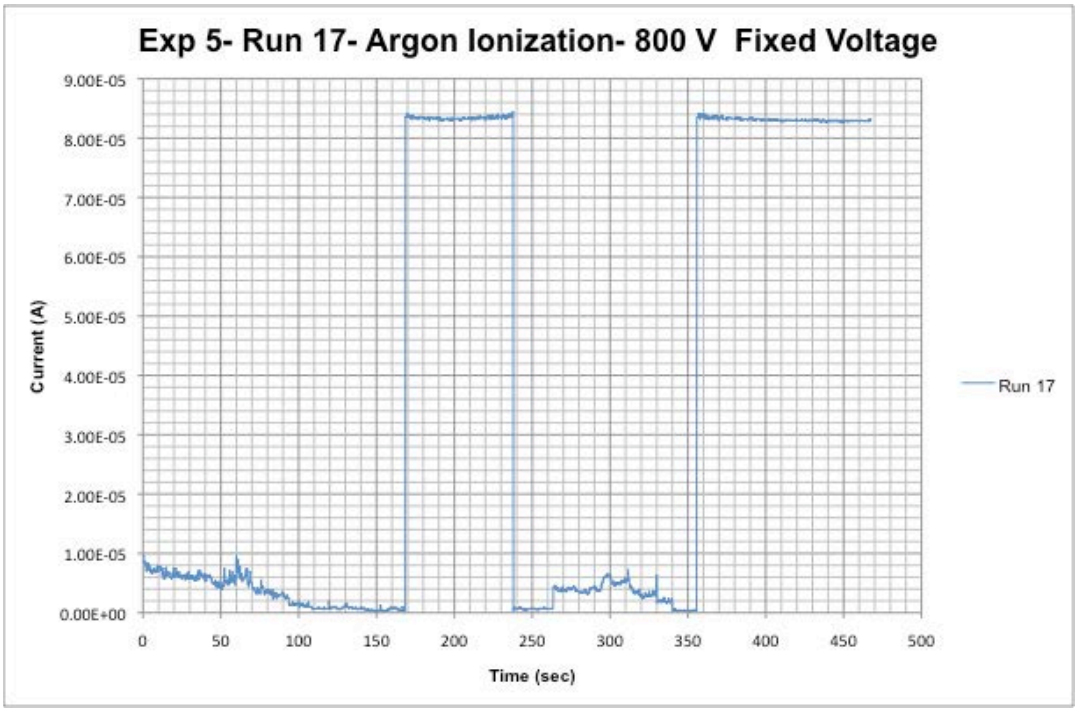

Figure 96. Experiment 5 Argon Ionization Run 17.

Figure 97. Experiment 5 Argon Ionization Runs 18-23.

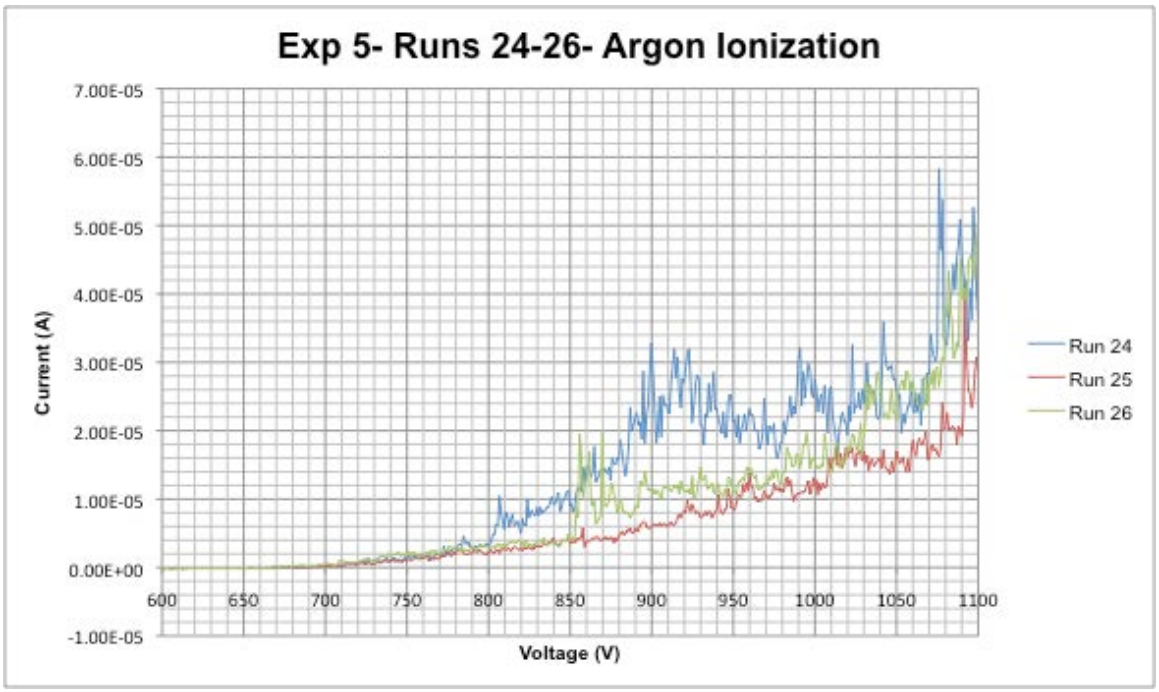

Figure 98. Experiment 5 Argon Ionization Runs 24-26.

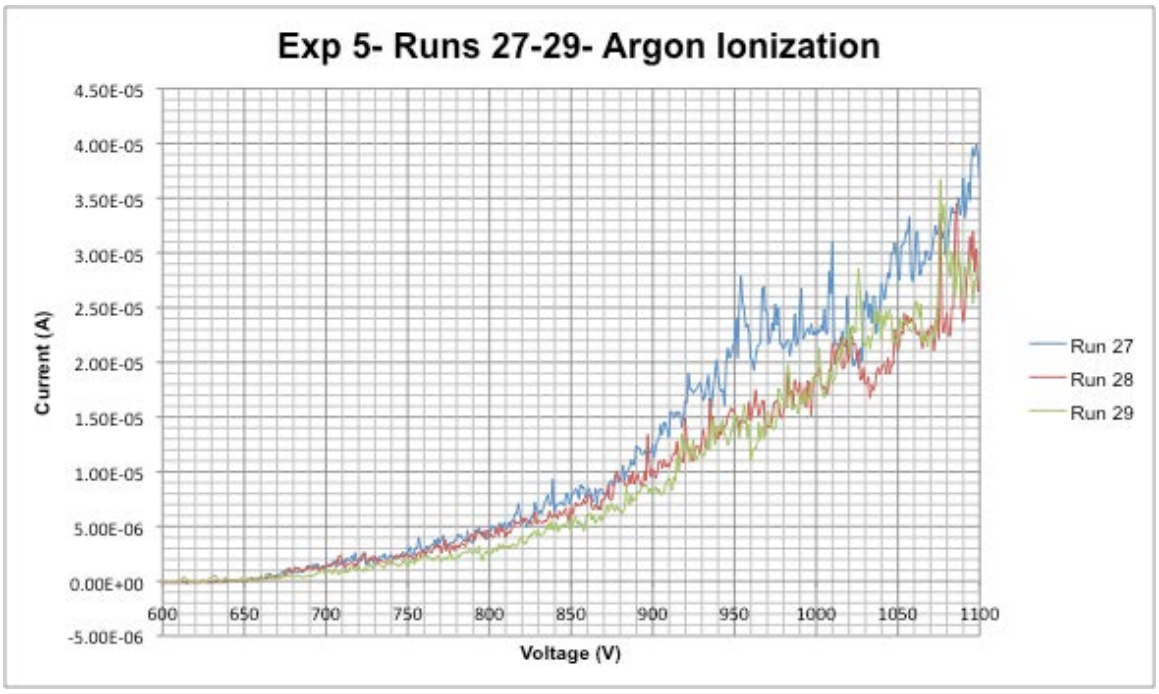

Figure 99. Experiment 5 Argon Ionization Runs 27-29.

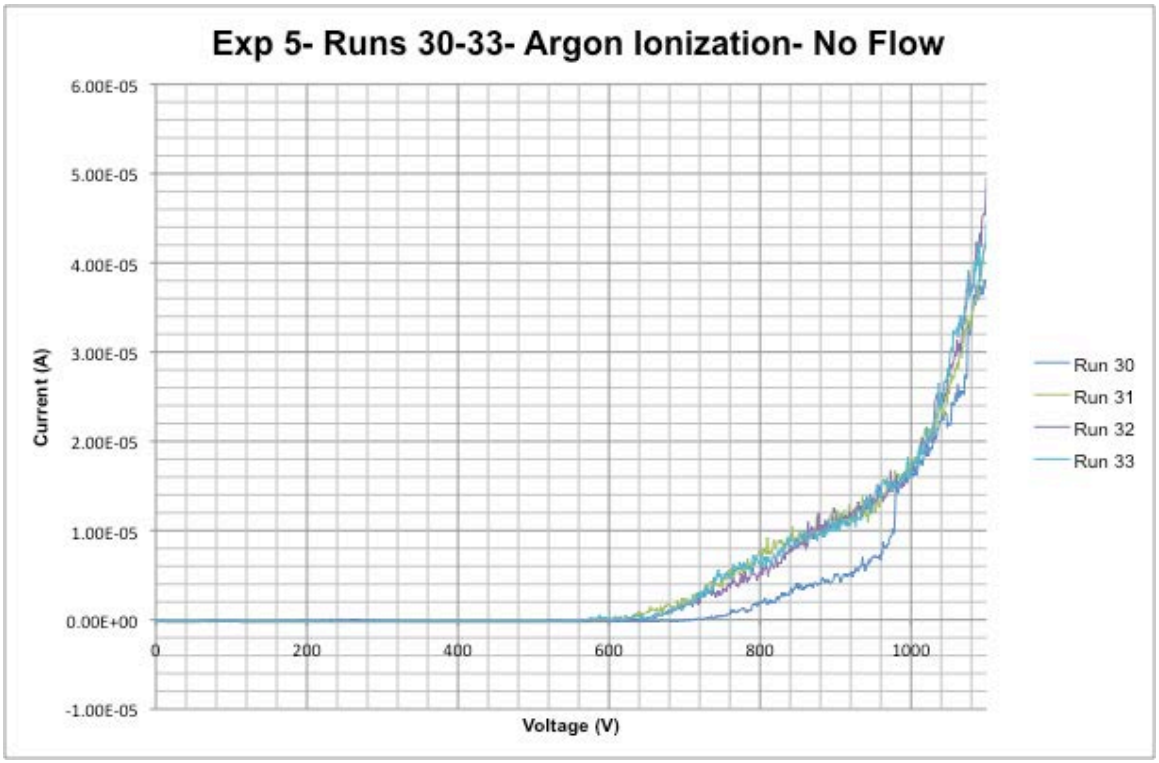

Figure 100. Experiment 5 Argon Ionization Runs 30-33.

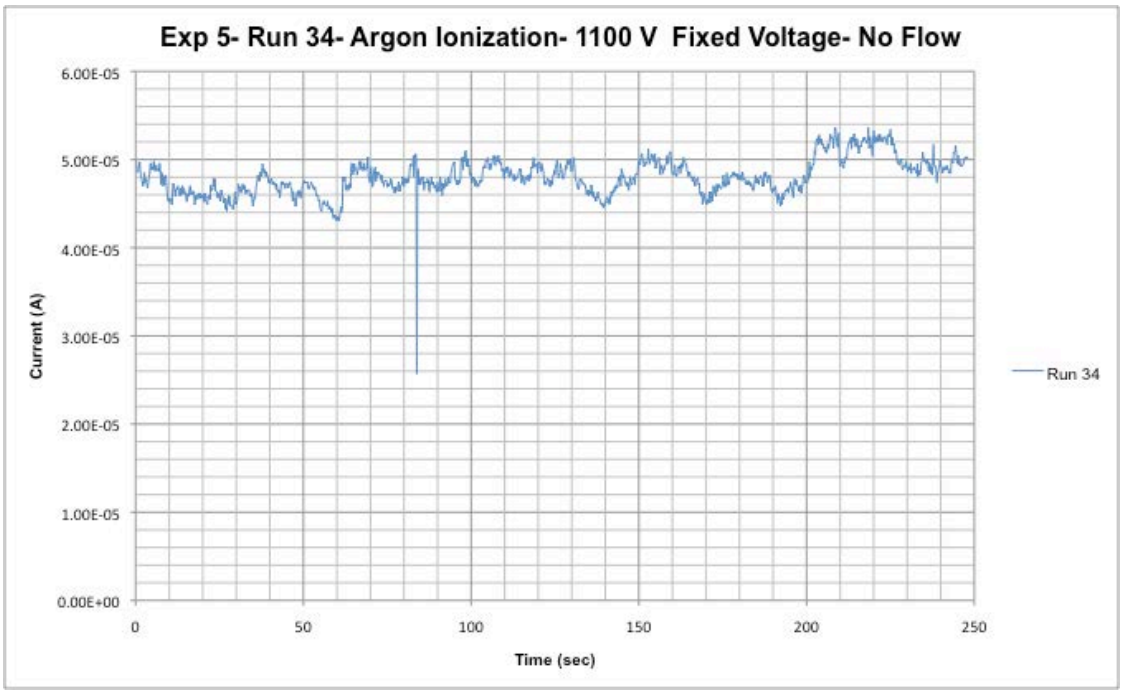

Figure 101. Experiment 5 Argon Ionization Run 34.

E. EXPERIMENT 6

Experiment 6		
15 August 2010		
Run	**Type**	**Notes**
1	Fowler-Nordheim / Linear Stair 0-1100 V	Field emission achieved.
2	Fowler-Nordheim / Linear Stair 0-1100 V	Field emission achieved.
3	Fowler-Nordheim / Linear Stair 0-1100 V	Field emission achieved.
4	Fowler-Nordheim / Linear Stair 0-1100 V	Field emission achieved.
5	Fowler-Nordheim / Linear Stair 0-1100 V	Field emission achieved.
6	Fowler-Nordheim / Linear Stair 0-1100 V	Field emission achieved.

Table 31. Summary of Experiment 6 test runs.

1. Fowler-Nordheim Data

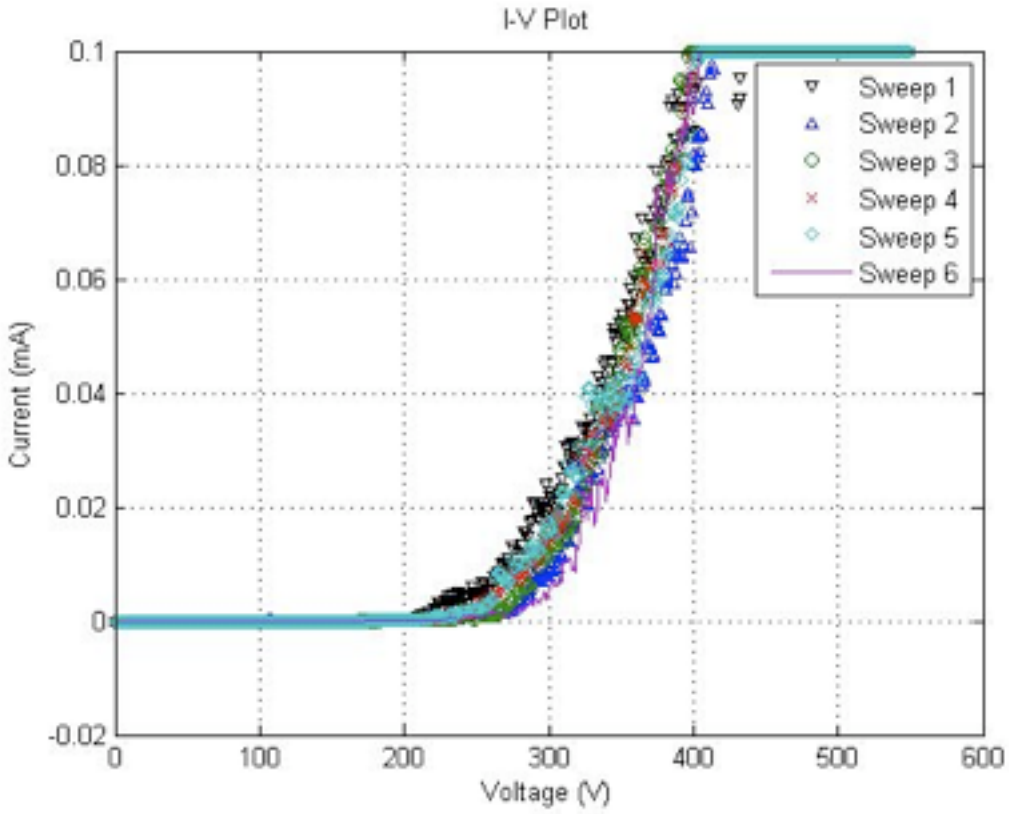

Figure 102. Experiment 6 Current versus Voltage plot for Fowler-Nordheim characterization.

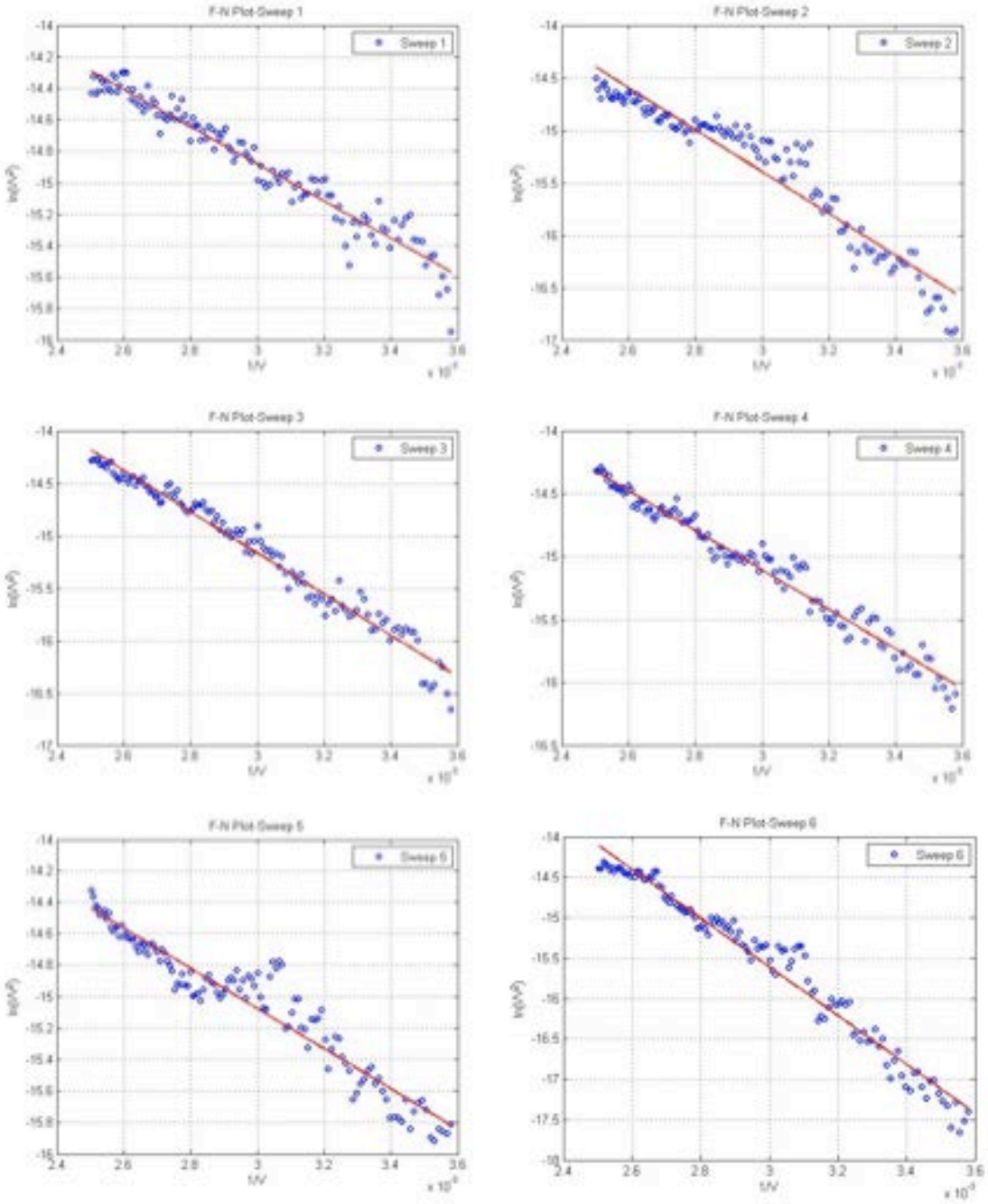

Figure 103. Experiment 6 Fowler-Nordheim plots.

F. EXPERIMENT 7

Table 32. Summary of Experiment 7 test runs.

1. Fowler-Nordheim Data

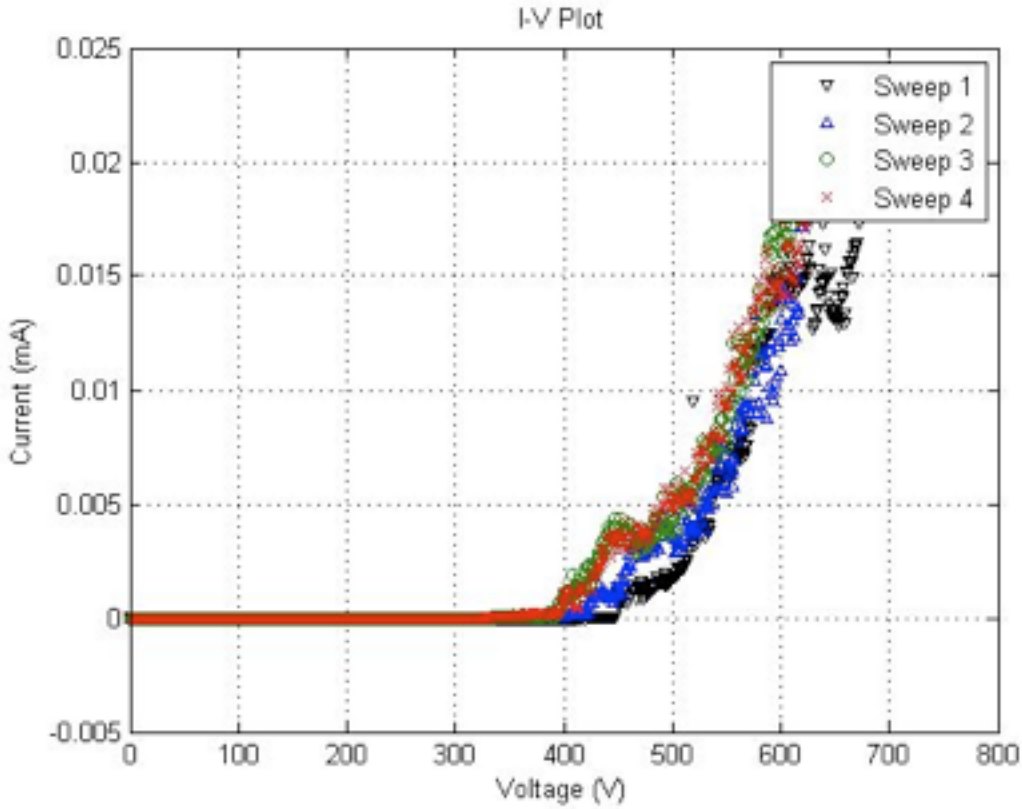

Figure 104. Experiment 7 Current versus Voltage plot for Fowler-Nordheim characterization.

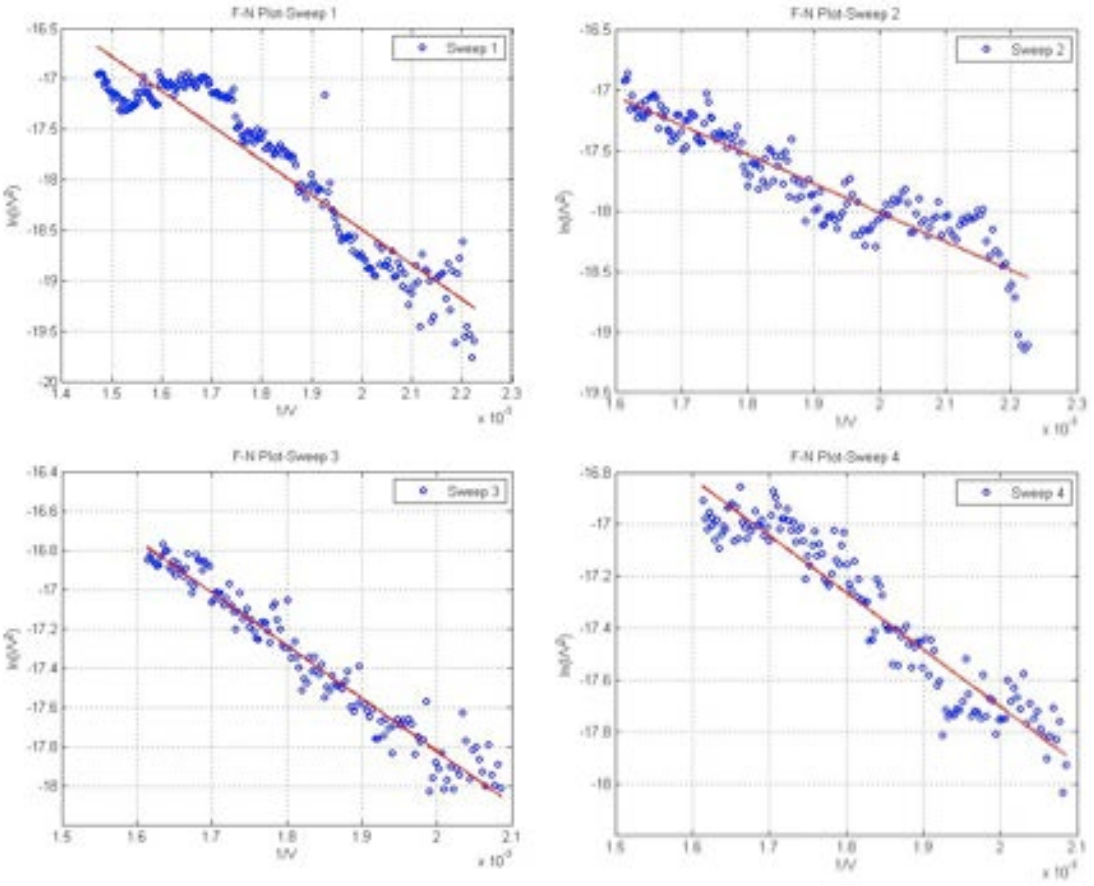

Figure 105. Experiment 7 Fowler-Nordheim plots.

2. Argon Ionization Data

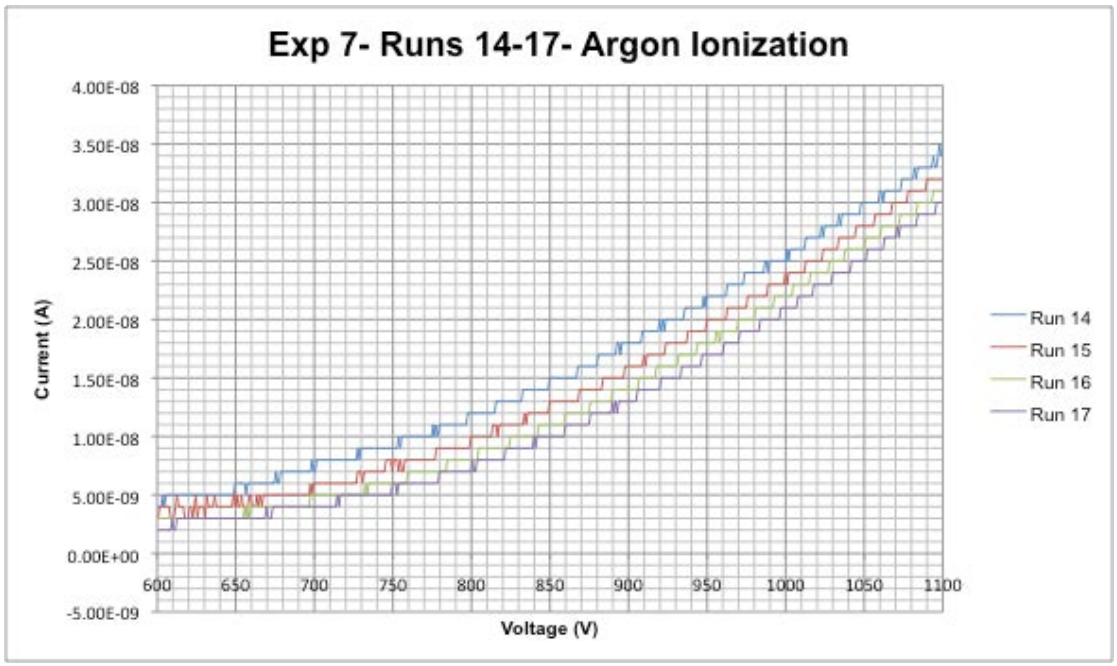

Figure 106. Experiment 7 Argon Ionization Runs 14-17.

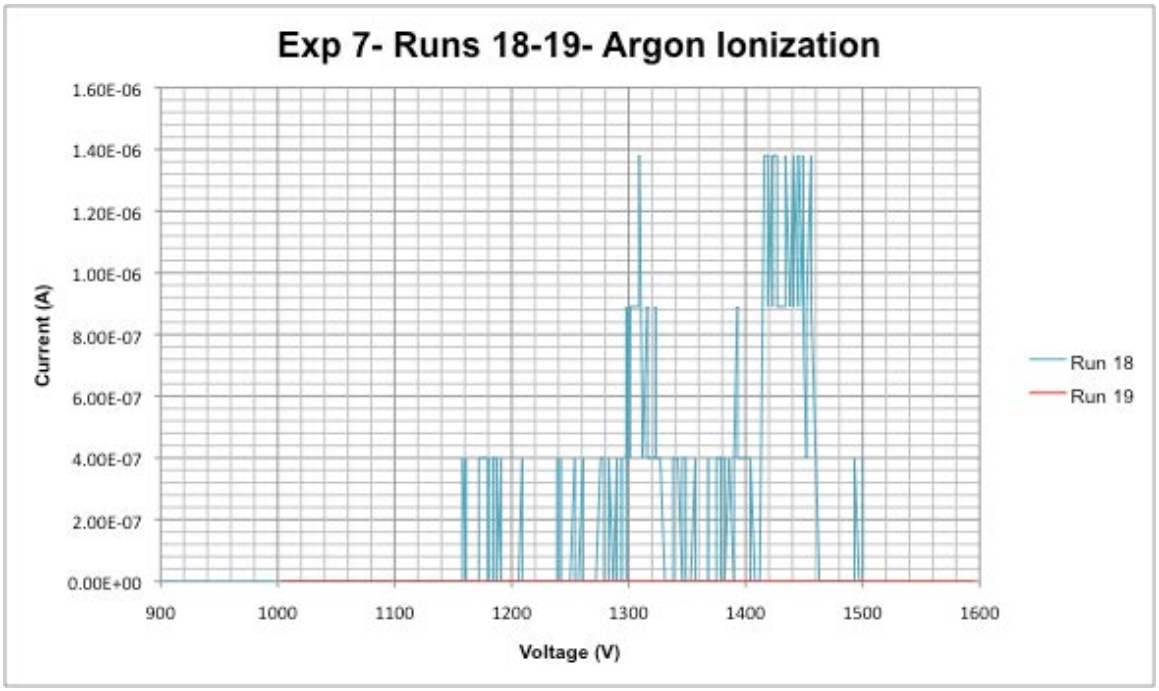

Figure 107. Experiment 7 Argon Ionization Runs 18-19.

THIS PAGE INTENTIONALLY LEFT BLANK

APPENDIX G. MASS FLOW RATE AND MAX CURRENT

A. MASS FLOW RATE CALCULATIONS

Three test runs were conducted on September 10, 2010 to determine the coefficient of drag (C_d) of the single 200 μm by 200 μm pre-etched hole. This was accomplished by first placing a sample into the chamber and letting it vacuum down. Argon was released into the chamber with the back pressure valve closed to ensure all flow was directed through the hole. The vacuum valve was then shut closed and the change in chamber pressure was recorded over the first few seconds of flow. The vacuum valve was then reopened, the argon turned off, and the vacuum allowed to run for a few minutes to try and evacuate the chamber prior to conducting the next iteration.

The second test did not get good data because the valve covering the vacuum did not close off quickly enough. Due to this, that particular set of data is not reported.

The readings for Runs 1 and 3 are shown in Table 33.

Run	Back Pressure (Torr)	Back Pressure (Pa)	Chamber Δp (Torr)	Chamber Δp (Pa)	Time (s)
1	5.10E-05	6.80E-03	4.40E-07	5.87E-05	4.4
3	5.10E-05	6.80E-03	3.00E-07	4.00E-05	2.7

Table 33. Pressure and time readings for the mass flow rate tests.

Now that the changes in pressure were recorded, it was possible to determine the amount of mass pushed through the hole during the given time using the equation:

$$m = \frac{\Delta PV}{RT} \tag{7}$$

This equation was used to solve for the mass and was then divided by the time observed to determine the mass flow rate. The values for volume, argon gas constant, and temperature are shown with the results in Table 34.

Known Parameters:		
V	7.07E-03	m^3
R	208.12807	J/kg-K
T	295	K
Run	**mass (kg)**	**mass flow (kg/s)**
1	6.75E-12	1.54E-12
3	4.61E-12	1.71E-12

Table 34. Mass and mass flow rate results for Runs 1-3.

Using these results, the following equation was used to determine the C_d for each run [25]:

$$C_d = \frac{\dot{m}}{P_{in} A \left(\frac{\alpha}{\sqrt{RT}} \right)} \tag{8}$$

Where the value, α, is a function of the specific heat ratio of argon (k_{Ar}). The specific heat ratio of argon is 1.667.

$$\alpha = \sqrt{k_{Ar} \left(\frac{2}{1 + k_{Ar}} \right)^{\left(\frac{k_{Ar}+1}{k_{Ar}-1} \right)}} \tag{9}$$

The calculated coefficients of drag were then averaged. The result is the C_d for the 200 μm by 200 μm pre-etched hole. The results are shown in Table 35.

Run	**Cd**
1	1.93
3	2.14
Average C_d	2.04

Table 35. Calculated and average C_d for the 200 μm by 200 μm pre-etched hole.

If Equation 8 is rearranged, the following equation can be used for all future tests with the 200 μm by 200 μm pre-etched hole to determine the mass flow rate based off of the back pressure value.

$$\dot{m} = C_d P_{in} A \left(\frac{\alpha}{\sqrt{RT}} \right) \tag{10}$$

B. MAX CURRENT CALCULATIONS

Once the mass flow rate is determined, it is fairly easy to determine the max current that the system should be capable of producing. This equation uses the mass of the argon ion (μ_{Ar}) which is equal to 6.68178 x 10^{-26} kg and the charge of an electron (e) which is equal to 1.6021176 x 10^{-19} C.

$$I_{\max} = \dot{m} \left(\frac{e}{\mu_{Ar}} \right) \tag{11}$$

C. PROPELLANT UTILIZATION FACTOR

Once the max current is solved for, the propellant utilization factor (PUF) is solved for using the following equation:

$$PUF = \frac{I_{measured}}{I_{\max}} \tag{12}$$

THIS PAGE INTENTIONALLY LEFT BLANK

APPENDIX H. MATLAB CODE

A. MATLAB CODE FOR FOWLER-NORDHEIM PLOTS

The following code was modified from a code presented in a thesis by Troy Hicks [12]. It was modified for the purposes of this thesis.

```
clc
clear all

%Fowler Nordheim Fitting
%Experiment 4
%Gap Distance:  39.5 um
%Test:  13 August 2010

gap=39.5e-6;

%Sweep 1
[x1,TXT,RAW]=xlsread('Data_Characterization','Exp 4 FN Fitting',...
    'b39:b588');
[y1,TXT,RAW]=xlsread('Data_Characterization','Exp 4 FN Fitting',...
    'c39:c588');
y1=y1/1e-3;

x11=1./x1;
y11=log(y1./(x1.^2));
p1=polyfit(x11(300:380),y11(300:380),1);
y111=p1(1).*x11+p1(2);
beta(1)=-6.831e9*5^1.5/p1(1);

gamma=beta*gap;

fprintf('\nResults for Sweep 1: Beta %5.0f Gamma %5.0f\n', beta(1),...
    gamma(1))


%I-V Plot
figure(1),
plot(x1,y1,'kv','markersize',5);

grid on
xlabel('Voltage (V)')
ylabel('Current (mA)')
title('I-V Plot')
legend('Sweep 1');

%F-N Plot
```

```
%Sweep 1 Plot
figure(11),
plot(x11(300:380),y11(300:380),'o',...
    x11(300:380),y111(300:380),'r','markersize',5,'linewidth',2);

grid on
xlabel('1/V')
ylabel('ln(I/V^2)')
title('F-N Plot-Sweep 1')
legend('Sweep 1');
```

LIST OF REFERENCES

[1] NASA, “Deep Space 1.” [Online]. Available: http://nmp.jpl.nasa.gov/ds1/. [Accessed: June 8, 2009].

[2] NASA, “Dawn.” [Online]. Available: http://dawn.jpl.nasa.gov/mission/index.asp. [Accessed: June 9, 2009].

[3] Georgia State University, “Ionization Energy,” February 3, 2002. [Online]. Available: http://hyperphysics.phy-astr.gsu.edu/HBASE/CHEMICAL/ionize.html. [Accessed: June 9, 2009].

[4] P. Hill and C. Peterson, *Mechanics & Thermodynamics of Propulsion*. Reading, MA: Addison-Wesley Publishing Company, 1992, p. 658.

[5] R. Jahn, *Physics of Electric Propulsion*. New York: McGraw-Hill Book Company, 1968.

[6] E. Stuhlinger, *Ion Propulsion for Space Flight*. New York: McGraw-Hill Book Company, 1964.

[7] A. T. Forrester and R. C. Speiser, “Cesium Ion Propulsion,” *Astronautics*, p. 18, October 1959.

[8] NASA, “Dawn Ion Propulsion Timeline.” [Online]. Available: http://dawn.jpl.nasa.gov/DawnClassrooms/2_ion_prop/briefing/2_sis_timeline.pdf. [Accessed: June 17, 2009].

[9] NASA Glenn Research Center, “Glenn Research Center Fact Sheet: Innovative Engines.” [Online]. Available: http://www.nasa.gov/centers/glenn/about/fs08grc.html. [Accessed: June 17, 2009].

[10] G. Sutton and O. Biblarz, Rocket Propulsion Elements, 7th Ed. New York: John Wiley and Sons, Inc., 2001.

[11] D. Tenenbaum, “Keeping an eye on ions.” [Online]. Available: http://whyfiles.org/shorties/ion_thruster.html. [Accessed: June 9, 2009].

[12] B. Halpern and R. Gomer, “Field Ionization in Liquids,” *Journal of Chemical Physics*, vol. 51, no. 11, p. 1055, July 2004.

[13] T. Hicks, “A Carbon Nanotube Pillar Array Ionizer for Miniature Ion Engine Applications,” M.S. thesis, Naval Postgraduate School, Monterey, California, 2008.

[14] D. Niemann, “Experimental and Theoretical Investigations of Field Emission in Carbon Nanotubes and their Multiscale Integrated Systems,” Doctoral Thesis, Santa Clara University, Santa Clara, California, June 2008.

[15] R. Reilly, “Carbon Nanotubes: Potential Benefits and Risks of Nanotechnology in Nuclear Medicine,” *Journal of Nuclear Medicine*, vol. 48, No. 7, p. 1039, 2007. [Online]. Available: http://jnm.snmjournals.org/cgi/content/full/48/7/1039#FIG1. [Accessed: August 23, 2010].

[16] M. Yu, O. Lourie, M. Dyer, K. Moloni, T. Kelly, and R. Ruoff, “Strength and Breaking Mechanism of Multiwalled Carbon Nanotubes Under Tensile Load,” *Science*, Vol. 287, No. 5453, pp. 637–640, January 2000. [Online]. Available: http://www.sciencemag.org/cgi/content/abstract/287/5453/637. [Accessed: September 13, 2010].

[17] B. Demczyk, Y. Wang, J. Cummings, M. Hetman, W. Han, A. Zettl, and R. Ritchie, “Direct Mechanical Measurement of the Tensile Strength and Elastic Modulus of Multiwalled Carbon Nanotubes,” *Materials Science and Engineering A*, Vol. 334, No. 1-2, pp. 173–178, June 2002. [Online]. Available: http://www.sciencedirect.com/science?_ob=ArticleURL&_udi=B6TXD-4625DK9-1J&_user=3326500&_coverDate=09%2F01%2F2002&_rdoc=1&_fmt=high&_orig=search&_origin=search&_sort=d&_docanchor=&view=c&_acct=C000060280&_version=1&_urlVersion=0&_userid=3326500&md5=d5d384ea5c3ebbcfb34cde7ee5fc69e2&searchtype=a. [Accessed: September 13, 2010].

[18] P. Collins and P. Avouris, “Nanotubes for Electronics,” *Scientific American*, Vol. 283, No. 62, pp. 67–69, December 2000. [Online]. Available: http://www.sciamdigital.com/index.cfm?fa=Products.ViewIssuePreview&ARTICLEID_CHAR=DE3A5CCE-263F-44B5-AD3F-C880AAA7A6D. [Accessed: September 13, 2010].

[19] S. Hong and S. Myung, “Nanotube Electronics: A Flexible Approach to Mobility,” *Nature Nanotechnology*, Vol. 2, No. 4, pp. 207–208, 2007. [Online]. Available: http://www.nature.com/nnano/journal/v2/n4/full/nnano.2007.89.html. [Accessed: September 13, 2010].

[20] R. Doak, “The assessment of field ionization detectors for molecular beam use,” *Journal of Physics: Condensed Matter*, Vol. 16, pp. S2683–S2869, July 2004.

[21] Y. Feng and J. Verboncoeur, “A model for effective field enhancement for Fowler-Nordheim field emission,” *Physics of Plasmas*, Vol. 12, No. 10, pp. 103301–103301-6, July 2005.

[22] DCL Vacuum Coating Corporation, “Ion Beam Sputtering,” dclvacuum.com. [Online]. Available: http://www.dclvacuum.com/tech-3.asp. [Accessed: August 28, 2010].

[23] South Bay Technology, Inc., “Model IBSe Ion Beam Sputter Deposition and Etching System,” southbaytech.com. [Online]. Available: http://www.southbaytech.com/shop/ibse/shtml. [Accessed: August 28, 2010].

[24] A. Henning, et al., “Microfluidic MEMS for Semiconductor Processing,” *IEEE Transactions on Components, Packaging, and Manufacturing Technology-Part B*, Vol. 21, No. 4, pp. 329–337. November 1998.

THIS PAGE INTENTIONALLY LEFT BLANK

INITIAL DISTRIBUTION LIST

1. Defense Technical Information Center
   Ft. Belvoir, VA

2. Dudley Knox Library
   Naval Postgraduate School
   Monterey, CA

3. Professor Oscar Biblarz
   Department of Mechanical and Aerospace Engineering
   Naval Postgraduate School
   Monterey, CA

4. Professor Marcello Romano
   Department of Mechanical and Aerospace Engineering
   Naval Postgraduate School
   Monterey, CA

5. Dr. Cattien V. Nguyen
   NASA Ames Research Center
   Moffett Field, CA

6. Dr. Darrell L. Niemann
   NASA Ames Research Center
   Moffett Field, CA